

University of Nevada, Reno

# **The Mineralogy, Paragenesis and Alteration of the Camino Rojo Deposit, Zacatecas, Mexico**

A thesis submitted in partial fulfillment of the requirements for the degree  
of Master of Science in Geology

by  
Saige Sanchez

Dr. Greg Arehart/ Thesis Advisor

May, 2017



THE GRADUATE SCHOOL

We recommend that the thesis  
prepared under our supervision by

**SAIGE SANCHEZ**

Entitled

**The Mineralogy, Paragenesis And Alteration Of The Camino Rojo Deposit,  
Zacatecas, Mexico**

be accepted in partial fulfillment of the  
requirements for the degree of

MASTER OF SCIENCE

Dr. Greg Arehart, Advisor

Dr. John Muntean, Committee Member

Dr. Scott Mensing, Graduate School Representative

David W. Zeh, Ph.D., Dean, Graduate School

May, 2017

## ABSTRACT

The Camino Rojo Zn-Pb-Ag-Au deposit, located in north-central Mexico, has characteristics of intermediate to low sulfidation epithermal deposits, skarns, and carbonate replacement deposits. Mineralization is hosted in sulfide-rich vein networks and manto-style replacements within calcareous, Cretaceous sedimentary rocks. U-Pb and fission track dating of zircon grains from a mineralized dike constrained the maximum age of the deposit to about 73Ma.

Primary sulfides at the deposit include pyrite, sphalerite, arsenopyrite, galena, marcasite, chalcopyrite, electrum, acanthite, pyrargyrite, and tennantite-tetrahedrite. The deposit veins and manto replacement bodies are composed of massive-textured, intergranular sulfides and are concentrated in the carbonaceous siltstone and sandstone of the Caracol Formation. Disseminated sulfides commonly spread outward along bedding planes. Gangue mineralogy includes calcite and potassium feldspar, with lesser amounts of quartz, sericite, and fluorite.

Two stages of mineralization were identified using optical petrography. Stage 1 mineralization consists of extensive pyrite-sphalerite-arsenopyrite-galena- chalcopyrite deposited as veins and mantos. Stage 2 mineralization was further divided into two parts: (2a) includes electrum± galena± chalcopyrite± acanthite filling fractures within stage 1 sulfides; and (2b) includes calcite, galena, pyrargyrite, acanthite, and argentiferous tennantite-tetrahedrite within veins which can cross-cut stage 1 mineralization. Over 80% of the electrum at the deposit formed during Stage 2a. Stage 2a and 2b have not been observed to be temporally or spatially associated.

Three alteration events were recognized at Camino Rojo. First, early potassic metasomatism and decarbonization bleached and hardened the sedimentary host rocks through K-feldspar flooding of the host matrix. Second, an ore-stage calcite -sericite± pyrite ± quartz alteration overprinted the potassic metasomatism. The final alteration stage is characterized by late calcite dissemination and multiple generations of cross-cutting calcite veins and veinlets. Hornfels texture within the host rocks indicates proximity to a deeper intrusion. Skarn formed within the limestone units underlying the bulk of deposit mineralization. The Camino Rojo deposit is likely part of a larger porphyry system, and the veining and manto replacement which host mineralization may be a transition between distal skarn and the epithermal environment.

## **ACKNOWLEDGMENTS**

The research presented in this Master's Thesis would not have been possible without the assistance, support, and encouragement of many individuals.

I would like to give many thanks to Goldcorp Inc. for their financial contribution. In addition, the individuals involved with Goldcorp's Camino Rojo project provided assistance and gave access to the property in order to collect hand samples and review core logs, assay data, and cross sections. In particular, Brendan Scorrar provided advice and support in the early drafts of this thesis.

I would also like to thank Dr. Greg Arehart, my MS thesis advisor, for his direction, support, and contributions to the manuscript. Dr. Arehart was very patient with my pacing, and never discouraged my research. Acknowledgment and thanks also goes to Dr. John Muntean and Dr. John McCormick, who provided insightful questions which helped direct my study.

Special thanks to Steven Weiss for his insights and assistance in writing and editing. Without his guidance and knowledge, this work would not have been possible.

As well, to all family and friends who supported me in obtaining my MS in geology: thank you.

## TABLE OF CONTENTS

Abstract.....	i
Acknowledgments.....	ii
Table of Contents.....	iii
List of Tables .....	v
List of Figures .....	vi
1 Introduction .....	1
1.1 Rationale for Study .....	1
1.1.1 Thesis Objectives.....	1
1.2 Deposit History.....	2
1.3 Methods of Study.....	3
2 Regional and Deposit Scale Geology.....	5
2.1 Regional Geology .....	5
2.2 Structural Setting .....	9
2.3 Geology of Camino Rojo .....	11
2.3.1 Cretaceous Sedimentary Host Lithologies .....	12
2.3.2 Intermediate Composition Dikes .....	15
3 Mineralization at Camino Rojo .....	19
3.1 Mineralization Style (Vein vs Manto).....	20
3.1.1 Vein Sulfides and Textures.....	21
3.1.2 Manto (Replacement) Sulfides and Textures.....	24
3.2 Mineral and Sulfide Petrography and Paragenesis.....	27
3.2.1 Calcite Petrography.....	32
3.2.2 Quartz Petrography.....	34
3.2.3 Pyrite and Marcasite Petrography .....	37
3.2.4 Sphalerite Petrography .....	39
3.2.5 Arsenopyrite Petrography.....	40
3.2.6 Chalcopyrite and Galena Petrography .....	42
3.2.7 Tetradymite ( $\text{Bi}_2\text{Te}_2\text{S}$ ).....	46

3.2.8	Electrum Petrography .....	48
3.2.9	Petrography of Silver Minerals .....	49
4	Hydrothermal Alteration at Camino Rojo .....	54
4.1	Potassic Metasomatism .....	57
4.2	Calcite- Sericite- $\pm$ Pyrite $\pm$ Quartz Alteration.....	61
4.2.1	Illite/ Muscovite and smectite as part of ore-related alteration .....	65
4.3	Late, Overprinting Calcite $\pm$ Pyrite .....	67
4.4	Contact Metamorphism, Skarn and Recrystallization at Camino Rojo .....	68
5	Assay Correlations and Spatial Trends.....	70
5.1	Spatial trends of gold, silver, lead, and arsenic at Camino Rojo.....	72
6	Geochronology of a Mineralized (Pre-Ore) Dike .....	73
7	Summary, Conclusions, and Discussion .....	76
7.1	Mineralization at Camino Rojo .....	76
7.2	Hydrothermal Alteration at Camino Rojo .....	80
7.3	Timing of Camino Rojo Mineralization and Deeper Magmatic Activity.....	81
7.4	Overview of Epithermal, Skarn, and Carbonate Replacement Deposit Models .....	82
7.5	Comparison of Camino Rojo to Other Deposit Types .....	85
7.5.1	Camino Rojo Compared to Mexican Epithermal Deposits.....	86
7.6	Future Research .....	92
8	References .....	94
9	Appendix A: Selected thin section petrography and photomicrographs. ....	100
10	Appendix B: Zircon U-Pb and FT data .....	136

**LIST OF TABLES**

<b>Table 4.1:</b> Description of alteration stages at Camino Rojo .....	54
<b>Table 5.1:</b> Correlation Coefficients of Au, Ag, As, Pb, and Cu Assay data from Camino Rojo drill core. ....	70
<b>Table 6.1:</b> Zircon U-Pb and ZFT analyses of a pre-mineralization dike.....	74
<b>Table 7.1 :</b> Summary of mineralization characteristics in polymetallic veins, manto-replacement, and skarn at Camino Rojo .....	77

## LIST OF FIGURES

<b>Figure 1:</b> Map of the major physiographic provinces of Mexico, showing the location of Camino Rojo in northern Zacatecas, on the edge of the Mesa Central province.....	3
<b>Figure 2:</b> Map of the regional geology surrounding Camino Rojo in Northern Zacatecas. Modified from Weiss et al, 2011). .....	9
<b>Figure 3:</b> Schematic cross section of the three identified zones at Camino Rojo: the Represa, the West Extension, and the Don Julio prospect. ....	12
<b>Figure 4:</b> The stratigraphic section of Camino Rojo.....	15
<b>Figure 5:</b> Photomicrograph examples of the three intrusive types present at Camino Rojo.....	18
<b>Figure 6:</b> Schematic map of planar dike trends at Camino Rojo, with general, >1ppm Au mineralization trends projected to the surface. The planar arrays, likely faults, are oriented NE and dip at 80°. Mineralized zones become deeper to the SW; this study focuses on the highlighted West Extension zone.....	19
<b>Figure 7:</b> A visual comparison of vein- vs manto-style mineralization in core .....	21
<b>Figure 8:</b> Photographs depicting sulfide vein mineralogy, texture and structure at Camino Rojo	24
<b>Figure 9:</b> (A) Photograph of thin manto-replacement lense within the sedimentary Caracol Formation; and (B) photomicrograph of brecciated pyrite cemented by calcite, a texture unique to manto-mineralization .....	26
<b>Figure 10:</b> Paragenesis of vein and manto mineralization at Camino Rojo. ....	28
<b>Figure 11:</b> Photomicrographs depicting pre-ore, post-ore, and ore stage mineralization at Camino Rojo.....	31
<b>Figure 12:</b> Photomicrographs of calcite textures at Camino Rojo.....	33
<b>Figure 13:</b> Photomicrographs of quartz occurrence and textures at Camino Rojo .....	36
<b>Figure 14:</b> Photomicrographs of pyrite and marcasite textures at Camino Rojo. ....	39
<b>Figure 15:</b> Photomicrographs of arsenopyrite and sphalerite textures at Camino Rojo.....	41
<b>Figure 16:</b> Photomicrographs of galena and chalcopyrite textures within veins and mantos. ....	43
<b>Figure 17:</b> Photomicrograph and SEM analysis of stage 2a galena associated with electrum.....	46
<b>Figure 18:</b> Photomicrograph and SEM analysis of late-stage tetradymite. ....	47
<b>Figure 19:</b> Photomicrographs of electrum within sulfide veins and mantos at Camino Rojo. ....	49
<b>Figure 20:</b> Photographs of silver-rich samples at Camino Rojo. ....	53



<b>Figure 21:</b> Generalized schematic long-section with spatial relationships of the three alteration types at Camino Rojo. The Au>1ppm shell is used as a proxy to estimate the calcite-sericite alteration geometry. ....	56
<b>Figure 22:</b> North-south cross section along ~243700 E in the West Extension zone. The gradational change of the potassic alteration within the Caracol Formation is illustrated. The Indidura Formation has been recrystallized. ....	58
<b>Figure 23:</b> Photomicrographs of potassic metasomatism in the sedimentary host rocks at Camino Rojo. ....	60
<b>Figure 24:</b> Breccia sample composed of potassically altered, rounded clasts cemented by ore-related calcite- sericite ± pyrite± quartz alteration. ....	62
<b>Figure 25:</b> Photomicrographs of the ore-related sericite-calcite ±quartz ± pyrite alteration affecting the sedimentary host rocks. ....	64
<b>Figure 26:</b> Presence of illite/muscovite clays are determined from reflected light spectroscopy	66
<b>Figure 27:</b> Photographs of late-stage calcite-pyrite flooding and veining at Camino Rojo	68
<b>Figure 28:</b> A schematic cross section through the West Extension zone of Camino Rojo showing soft shells of Au, Ag, As, and Pb assay data. The section is cut along a parallel to the planar dike trends (Figure 6). ....	71
<b>Figure 29:</b> Comparison of zircon ages (Ma): U-Pb vs FT. U-Pb ages do not vary greatly from a late Cretaceous age for dike emplacement . ....	75
<b>Figure 30:</b> Map of Mexico depicting Ag-Au, Ag-Pb-Zn, or Ag-Pb-Zn (Cu) epithermal vein and carbonate replacement deposits. The basin and range, Middle Tertiary ignimbrites, and the Mexican volcanic belt provinces are also marked. ....	89
<b>Figure 31:</b> Ages and locations of dated epithermal deposits in northern and central Mexico. The location of Camino Rojo is identified by a red star. The trend of deposits surrounding Camino Rojo range from 36-27 Ma. ....	92

## **1 INTRODUCTION**

### **1.1 Rationale for Study**

World-class ore deposits are found throughout Mexico. The Camino Rojo deposit, located on the outskirts of the small town of San Tiburcio in the state of Zacatecas, Mexico, has undeveloped yet significant silver and gold resources. Combined, proven and probable reserves and measured and indicated resources are estimated to be nearly 100 million ounces (Moz) silver at roughly 10 grams/ metric tonne (g/ton) and 9 Moz gold at roughly 0.8 g/ton (Anonymous, 2015). The deposit also contains zinc and lead resources.

Though drilling of the deposit has defined significant amounts of gold and silver, there have been few studies to define and understand the characteristics of mineral formation and associated hydrothermal alteration. This descriptive study of the mineralogy and paragenesis of the hydrothermal mineralization and alteration of Camino Rojo will be an important resource for geologists and metallurgists working on Camino Rojo in the future.

#### **1.1.1 Thesis Objectives**

The main objectives of this research are to provide a basic understanding of the nature and style of mineralization and alteration at Camino Rojo. Identifying the hydrothermal mineralogy and patterns associated with mineralization is important for future exploration, metallurgical processing, and mine planning.

Three main topics are addressed:

- (1)** Identification of primary sulfides and paragenetic relationships, especially as they relate to electrum formation and to the host and intrusive rocks;

(2) Determination of alteration styles and patterns, and relative timing of alteration events in relation to mineralization;

(3) Determination of the relationship of Camino Rojo to the regional geologic history through geochemical analysis, geochronological data, and review of published data.

## **1.2 Deposit History**

Camino Rojo is located in central Mexico, in the northern Mesa Central province (Figure 1). The deposit site was discovered in June 2007, when exploration geologists working in the region identified red, oxidized, road ballast on a dirt road leading from a main highway. All 16 initial samples collected from the quarry where the road ballast was excavated contained silver, gold, arsenic, zinc and lead concentrations that were significantly higher than the background. Gold contents ranged from 0.22 g/ton to 1.58 g/ton. As a result of the assay data, a rapid, reverse-circulation (RC) drilling program began in November 2007. Within a year and a half the Represa resource, the initial, near-surface oxidized discovery, was outlined with mineral resources containing an estimated 3.45 Moz of gold and 60.7 Moz of silver, as well as significant amounts of lead and zinc (Blanchflower, 2009). Since early 2011, over 100,000 meters of diamond core drilling has been conducted to expand and better define the Camino Rojo deposit.

A single, small exposure of the oxidized part of the deposit is present through post-mineralization cover in the gravel pit that was excavated for the road ballast. No previous mining or exploration workings are present in the immediate area. A mineral deposit completely covered by Quaternary alluvium is unusual in Mexico, and highlights how underexplored the country is. No previous government or academic studies have been

conducted at Camino Rojo, though there have been company reports (for example, Blanchflower, 2009).



**Figure 1:** Map of the major physiographic provinces of Mexico, showing the location of Camino Rojo in central Mexico, on the edge of the Mesa Central province. Modified from Rhoda and Burton, 2010.

### 1.3 Methods of Study

An initial, two-week visit to the Camino Rojo project in Zacatecas, Mexico occurred from December 2012 to January 2013. A second visit was made in the summer of 2013, when nearly eight weeks were spent at the project location. Both visits allowed for the examination of whole and half cut drill core, with samples collected based on visible alteration changes and assay

values, with a preference for strongly mineralized samples. Ninety-three hand samples were collected from Camino Rojo drill core; of these, 63 specimens which appeared to represent the alteration, mineralization, and host rock types were made into polished thin sections.

Optical petrography was the primary method used in this study, and examination of Camino Rojo thin sections began in August of 2013. Before microscopic examination, hand samples were examined with the aid of a 10x hand lens to determine overall rock texture and structure. All samples were stained with sodium cobaltinitrite to visually estimate the amount of potassium feldspar. Each thin section was studied using an Olympus BX53 microscope in both transmitted and reflected light. Digital photomicrographs were taken using an Infinity2 camera.

For selected samples, the scanning electron microscope (SEM) at the University of Nevada, Las Vegas, was used to further study textures, paragenetic relations, and to identify fine-grained sulfide minerals associated with gold mineralization. The SEM has a resolution of 1  $\mu\text{m}$  and a magnification range from x35 to x100,000. Both scanning-electron and backscatter-electron images were captured. Seven thin sections were examined with the SEM, five of which were mineralized samples with clear electrum deposition.

The three-dimensional modeling software Leapfrog was used to spatially model and visualize lithology, field alterations, and assay data from 22 drill holes. Zonation patterns and trends were viewed from many angles and cross-sectional views. Cross-sections in this paper were produced with the Leapfrog modeling software, and are in Universal Transverse Mercator (UTM) coordinates from the 1927 North American Datum, zone 11. Easting labels and elevation above sea level (ASL) are indicated. There is no vertical exaggeration in any of the cross-section figures presented.

Zircon separation and isotopic analyses were conducted by Apatite to Zircon Inc., in Viola, Idaho. The zircon fission track (ZFT) analyses were performed by embedding zircon grains in FEP Teflon, polishing the grains to expose internal grain surfaces, and etching the polished grains in a eutectic melt of NaOH-KOH at approximately 230°C for 24 to 72 hours (Donelick and Donelick, 2012-2013). ZFT ages were determined following the methods of Donelick and Donelick, 2012-2013. The etched zircon grains were also analyzed by the laser-ablation inductively-coupled-plasma mass-spectrometry (LA-ICP-MS) method, from which were derived uranium-lead (U-Pb) ages.

## **2 REGIONAL AND DEPOSIT SCALE GEOLOGY**

### **2.1 Regional Geology**

Mexico's diverse geologic history includes the formation of a variety of ore deposit types, including abundant epithermal and porphyry-related deposits, skarns, polymetallic carbonate replacement deposits and volcanigenic massive sulfides. In the northern half of Mexico, the three most important physiographic provinces, with respect to mineralization, are the western Sierra Madre Occidental (SMO), the eastern Sierra Madre Oriental (SMOr), and the Mesa Central (Figure 1). These provinces formed as the result of broad Mesozoic sedimentation and periods of volcanism.

The SMO is a large volcanic mountain range in western Mexico, trending southeast from the US-Mexico border and ending at the volcanic axis in the center of the country (Figure 1). Cretaceous to Cenozoic magmatic and tectonic events, the result of the subduction of the Farallon plate beneath North America, formed the SMO and were contemporaneous with the

formation of many epithermal ore deposits across Mexico (Camprubi and Albinson, 2007; Ferrari et al., 2007). The SMO province is made up principally of pyroclastic tuffs and ignimbrites.

The SMO is composed of two aerially extensive sequences of upper Mesozoic and Tertiary igneous rocks. The lower sequence, known as the Lower Volcanic Series (100-45 Ma), is dominantly andesitic flows and large calc-alkaline intrusions of intermediate to felsic composition. The overlying sequence, the Upper Volcanic Series (34-27 Ma), is primarily composed of rhyodacitic ash-flow tuffs. From about 12 Ma onward, thin, minor basalt flows locally covered the Upper Volcanic Series (Clark et al., 1982). During the late eruption stages of the Upper Volcanic Series, silicic ignimbrites within the SMO were emplaced during two pulses, with transitional basaltic-andesitic lavas erupted at the end of each ignimbrite pulse (Ferrari et al., 2007). Post-subduction volcanism consisting of alkaline basalts and silicic ignimbrites began around 12 Ma.

The SMOr province (Figure 1) is an eastern Mexican mountain range formed by compressional tectonics of the Laramide Orogeny. Folded, Cretaceous sedimentary units make up much of the SMOr, and were deposited on a passive margin, which included earlier, Late Triassic-Middle Jurassic basinal rocks and Early Cretaceous platform carbonates (Eguiluz de Antuñano et al., 2000, Nieto-Samaniego et al., 2007).

The Mesa Central is a relatively flat, high plateau located in central Mexico (Figure 1). The Mesa Central is composed chiefly of Mesozoic marine sedimentary rocks over a Paleozoic and Precambrian basement, and covered by Quaternary conglomerates and alluvium (Mixon et al., 2004). The southern end of the province is an elevated plateau with immature stages of erosion (Nieto-Samaniego et al., 2007). In contrast, the flatter and less elevated northern portion of the Mesa Central shows advanced stages of erosion, with large alluvial and lacustrine continental

basins (Nieto-Samaniego et al., 2007). Along the western edge of this province, the broadly distributed volcanic units of the SMO unconformably overlie the Mesozoic sedimentary sequence of the Mesa Central (Moller et al, 2001).

A Paleozoic age has been suggested for the base of the stratigraphic section in the region, based on the presence of Pennsylvanian spores and fossil plants. More likely, the oldest sedimentary units in the Mesa Central are Upper Triassic in age (Nieto-Samaniego et al., 2007). There is a lack of recent publications addressing the age and composition of the basement rocks in the Mesa Central, though some authors have reported Paleozoic muscovite schist at the edges of the Mesa Central. In Zacatecas, the oldest exposed units are Triassic, clastic sedimentary rocks with low metamorphic degrees. Phyllite and schist interbedded with conglomerate and sandstone are common toward the base of the rock sequence, and are overlain by phyllite with sandstone and marble (Nieto-Samaniego et al., 2007).

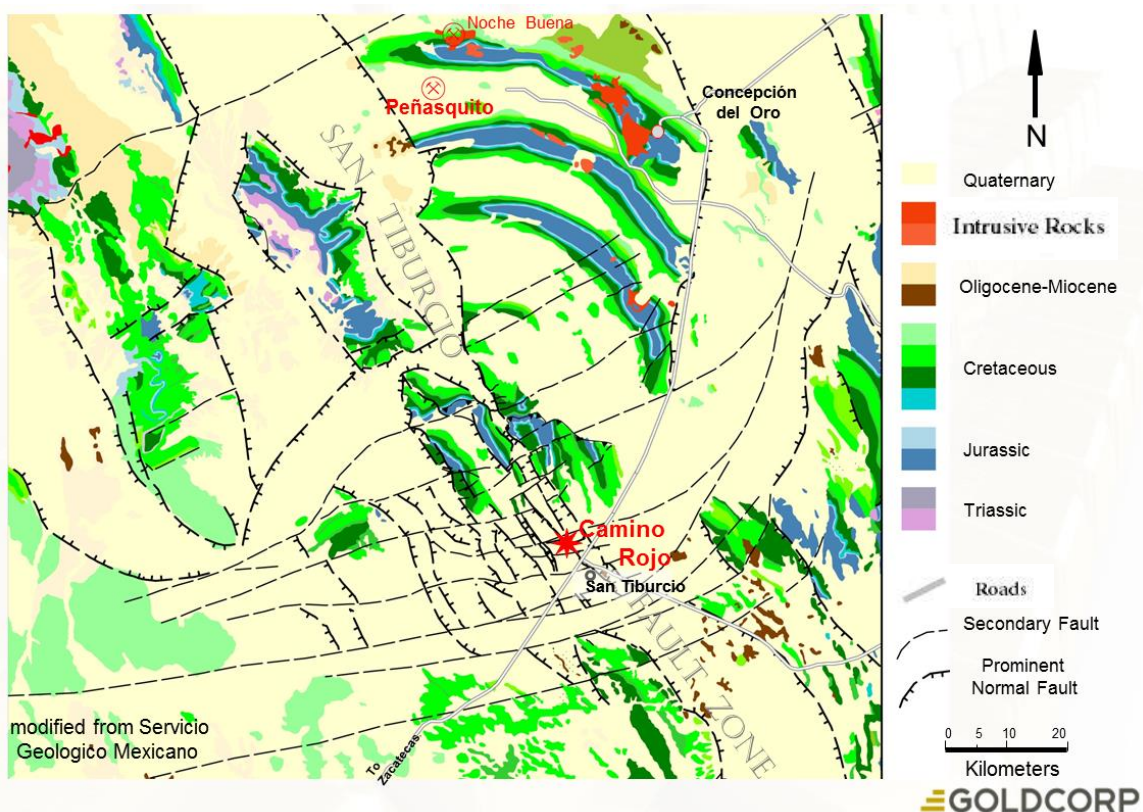
At the top of the Triassic meta-sedimentary rocks is a regionally extensive unconformity over which lie sandstone, conglomerate, and volcanic rocks deposited from the early to middle Jurassic. These continental fluvial, alluvial, and volcanic sediments formed red beds (the Huizachal Group) which underlie a widespread unconformity and late Jurassic, calcareous, marine rocks of platform limestone and calcareous mudstone (Salvador, 1987). This second unconformity marks the transition from a continental to a marine environment, which prevailed from the upper Jurassic through the Cretaceous (Nieto-Samaniego et al., 2007). The marine environment was present for almost 100 million years.

An influx of detrital sediments from uplift to the west began in the late Cretaceous, and changed the regimen of sedimentation in central Mexico (Nieto-Samaniego et al., 2007). As the sea retreated eastward, limestones and shales of the Indidura Formation were deposited.



Lithologies vary laterally within the Indidura Formation at the same stratigraphic horizon. The Indidura was followed by the deposition of interbedded shales and sandstones of the Caracol Formation (Moràn-Zenteno, 1994). These two sedimentary formations are the principal host rocks at Camino Rojo. Cretaceous units younger than the Caracol Formation are not present in the northern Mesa Central where Camino Rojo is located. This was due to a decrease in sediment accumulation and greater amounts of erosion during the early Tertiary as a result of the gradual retreat of the marine environment (Moràn-Zenteno, 1994; Nieto-Samaniego et al., 2007). Throughout north-central Mexico, the permeable rocks of the Caracol Formation are important host rocks for mineral deposits.

Dominantly Tertiary-age intermediate to felsic plutons, stocks, and dikes occur throughout the Mesa Central (Nieto-Samaniego et al., 2007). These include late Eocene to early Oligocene stocks and plutons in the Camino Rojo region (Figure 2).



**Figure 2:** Map of the regional geology surrounding Camino Rojo in Northern Zacatecas. Modified from Weiss et al, (2011). The geology of the region surrounding Camino Rojo has been mapped and described in four geo-quadrangle maps by the Servicio Geológico Mexicano (Gonzalez-Arroyo, et al., 1998; Gonzalez-Arroyo, et al., 1999; Montanez-Castro, et al., 2000; Moreira-Rivera, et al., 1996). In Figure 2, these maps have been simplified to the immediate region surrounding Camino Rojo.

## 2.2 Structural Setting

Active subduction of the Farallon plate under western Mexico began in the late Triassic. This produced a convergent margin and magmatic arc of Andean type in the present site of the SMO (Morán-Zenteno, 1994). Beginning in the late Cretaceous (around 70 Ma) and ending in the Eocene (between 35 and 55 Ma), the subduction of the Farallon plate resulted in the Laramide Orogeny, a major compressional deformation event throughout western North America. The Laramide Orogeny produced faults and folds which host porphyry copper deposits

(Ferrari et al., 2007), as well as polymetallic skarns, and replacement and diatreme-hosted deposits such as Concepcion del Oro and Peñasquito (Figure 2).

The thrusting and shortening of the Laramide Orogeny affected the Camino Rojo region and the SMOr around 65 Ma (Dickinson and Lawton, 2001, Goldhammer, 1999). Laramide deformation and regional shortening was stronger in the SMOr than in the Mesa Central and SMO (Moran-Zenteno, 1994). The Jurassic to Cretaceous sedimentary formations in the SMOr were deformed in E-W and NW-SE folds, and faulted in accordance with the Laramide stresses. Narrow folds within the Mesa Central follow the general strike of the NW-SE SMOr mountain range (Moran-Zenteno, 1994).

In the early Tertiary, a change in the movement of the North American and Farallon plates produced open N-NW trending folds in the SMO. This was followed by block faulting, erosion, and volcanism (Cserna, 1976; Coney, 1983). In the Oligocene, grabens bounded by high-angle normal faults formed in the eastern portion of the SMO.

In the northern Mesa Central, the San Tiburcio Fault Zone (Figure 2) also formed during this time, with splays that accommodated minor, late Tertiary extension. Mitre-Salazar (1989) defined the San Tiburcio lineament through interpretation of satellite images and geologic maps in the state of Zacatecas, and concluded that the San Tiburcio lineament corresponded to a left-lateral fault as evidenced by right-lateral Riedel shears. In opposition to this conclusion, Goldcorp geologists have observed that fold patterns and Jurassic-Cretaceous stratigraphic units match up well on both sides of the San Tiburcio fault zone, with little or no lateral displacement (Figure 2). Drilling in the broad valley west of Peñasquito allowed Goldcorp geologists to observe thick sequences of graben fill within the San Tiburcio fault zone, which are consistent with an extensional fault setting (S.I. Weiss, personal communication, 2015). Locally and regionally, the

San Tiburcio fault zone appears to have normal movement, and has overprinted the Laramide fold and thrust architecture.

### 2.3 Geology of Camino Rojo

Camino Rojo is situated in a low-relief alluvial valley on the northern edge of the Mesa Central province (Figure 1), and is almost completely masked by post-mineralization alluvial cover. The deposit is hosted in Cretaceous marine sedimentary rocks, and is located between segments and cross faults of the NW trending San Tiburcio Fault Zone (Figure 2). Two continuous areas of mineralization within the deposit have been identified:

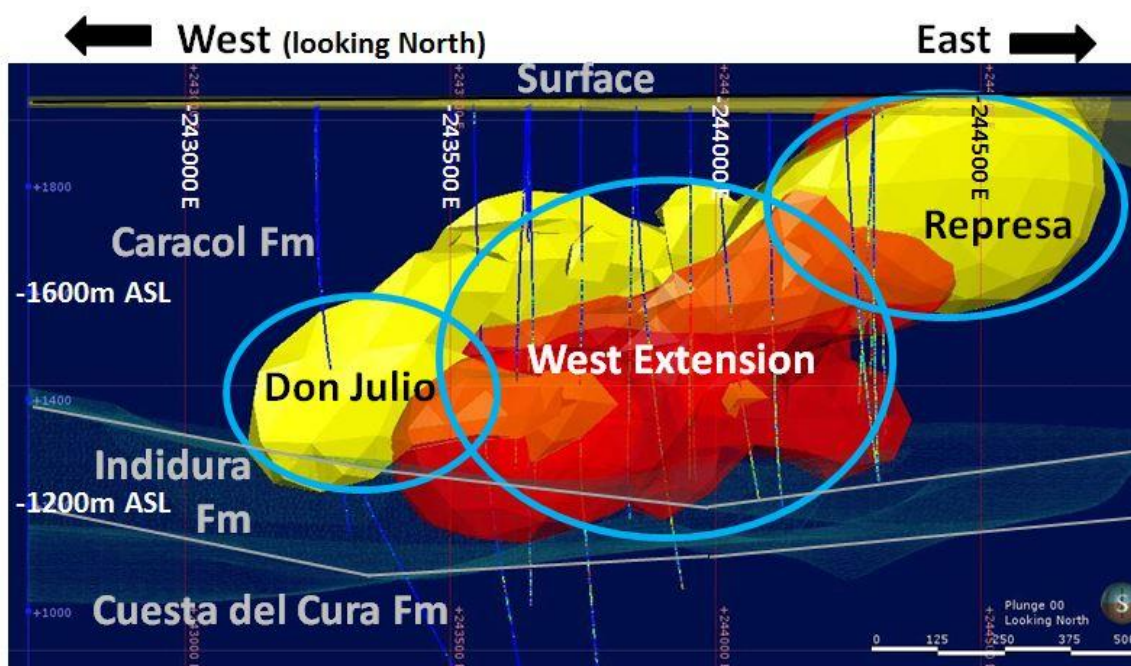
(1) **Represa zone** – consists of near-surface, oxidized, potential ore extending to just over 400m below alluvial cover (Figure 3), and comprising all of the probable mineral reserves at Camino Rojo.

(2) **West Extension zone** – located west of and below the Represa zone; consists of weakly and unoxidized, deeper potential ore extending to roughly 800m below the surface (Figure 3), and comprising the majority of the measured and indicated mineral resources.

A separate, third area to the west, with limited extent, has also been identified, and is known as the **Don Julio** prospect. This westernmost zone does not occur until nearly 400m below the surface, and consists of scattered intervals of weak mineralization spanning roughly 200m in vertical extent (Figure 3).

This study focuses on the West Extension zone at Camino Rojo (Figure 3). Due to extensive drilling, consistent gold and silver mineralization have been identified in the West

Extension zone. Oxidation is weak or absent in the rocks and veins of the West Extension, allowing for the determination of original mineralogy and paragenesis. Hand samples for this study were collected almost entirely from drill core from the West Extension zone (Figure 3).



**Figure 3:** Schematic cross section of the three identified zones at Camino Rojo: the Represa, the West Extension, and the Don Julio prospect. The yellow horizontal layer at the surface indicates Quaternary alluvium; the other three stratigraphic units are labeled. Intraformational folds within the Caracol Formation are not shown. The blue lines extending from the surface are the subset of 22 drill holes used to make the Au and Ag assay shells in this study. The yellow shell represents Ag >10ppm; the red shell represents Au >1ppm and extends to the surface in the Represa zone, but is hidden by the silver grade shell. The orange color is an overlap of the yellow and red shells.

### 2.3.1 Cretaceous Sedimentary Host Lithologies

Mineralization at Camino Rojo is primarily hosted in the Caracol Formation and the Indidura Formation, the two uppermost Cretaceous sedimentary units in the northern Mesa Central region. Though mineralization has also been observed in the underlying Cuesta del Cura Formation, underlying carbonaceous units have not been drilled extensively. The Caracol and

Indidura Formations consist of interstratified shales and sandstones, and are underlain by the limestone of the Cuesta del Cura Formation (Figure 3, Figure 4). The sandstone beds are calcareous, and commonly massive to finely laminated and cross stratified. Small-scale scour and fill textures indicate the sandstone beds were deposited by turbidity flows.

The host formations are flat-lying, though the rocks are internally folded. In particular, the Caracol Formation has many undefined, intraformational folds, which have not yet been mapped and do not appear to direct or concentrate mineralization. The host formations are described below, from oldest to youngest.

***Cuesta Del Cura Formation (Mid-Cretaceous– thick limestone unit)***

The Cuesta del Cura Formation (Figure 4) is composed of resistant dark gray limestone, with persistent thin- to medium-bedded wavy stratification. Black shale partings and elongate lenses of black chert occur along limestone beds, and are more abundant in the lower portion of the formation. The upper contact with the Indidura Formation is defined by the change from wavy-bedded limestone to medium-bedded and increasingly shaly limestone. Elsewhere in northern Mexico, the formation is estimated to have an average thickness of 270m (Bartolini et al., 1990, Rogers et al., 1956). At Camino Rojo, the deeper exploration drill holes mainly terminate in the Cuesta del Cura Formation, where skarn features and occasional mineralization have been penetrated. The thickness of this lower stratigraphic unit at Camino Rojo is estimated to be 250m, based on the average thicknesses from surrounding regions. A minimum thickness based on drilling is not available.

***Indidura Formation (Early Upper-Cretaceous–shaly unit)***


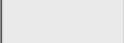





The Indidura Formation (Figure 3, Figure 4) is composed of grey, evenly stratified, thin calcareous shale beds with grey shaly limestone and siltstone. The lower contact is distinct due to the contrast between the laminar shaly beds of the Indidura Formation and the underlying limestone of the Cuesta del Cura Formation. The upper contact with the Caracol Formation is defined by the change from regularly bedded, shaly limestone to an irregular mix of gray sandy beds with interbedded dark shale. The upper (roughly 50m) portion of the Indidura is composed of homogeneous, fissile, dark-gray calcareous shale. An average thickness of 190m has been calculated in other locations (Bartolini et al., 1990), and at Camino Rojo the Indidura Formation is consistently about 200m thick. The altered Indidura is recrystallized at Camino Rojo.

***Caracol Formation (Upper Cretaceous– interbedded calcareous shale and sandstone)***

The majority of mineralization at Camino Rojo is hosted in the upper Cretaceous Caracol Formation (Figure 4), which is made up of interbedded, dark gray, carbonaceous, calcareous siltstone and lighter grey, finely bedded, calcareous sandstone. The shale beds are dominant, and the color of the Formation varies from the light gray sandstone to the dark gray, carbon-rich shales. The lower boundary with the Indidura Formation is defined by the lowest occurrence of sandstone. The upper boundary in the West Extension zone is an erosional unconformity with overlying Quaternary gravels; in the eastern Represa zone, the Caracol is overlain by Oligocene ash flow tuff. The age of the Caracol Formation based on fossil evidence ranges from Turonian to Santonian (Diaz-Salgado, et al., 2006), or as young as the early Campanian (Lawton, 2012).

Based on drill core at Camino Rojo, the Caracol Formation ranges from about 600m to just over 800m thick (Figure 3). A minimum of 800m is mapped elsewhere in the Zacatecas

region, though the Caracol thickness varies due to irregular deposition in synclinal valleys (Bartolini et al, 1990, Moran-Zenteno, 1994, Rogers et al, 1956). The calcareous sandstone beds contain angular to moderately rounded feldspar and quartz grains embedded in a carbonate-rich matrix. The sandstone beds are more abundant in the lower part of the formation, with individual layers up to 4m thick. Bedding exposed in trenches at the deposit generally strikes NW and dips SW. However, internal folding due to regional tectonics has been observed in core.

ERA	PERIOD	EPOC	Ma	SYMBOL	STRATIGRAPHY	LITHOLOGY	MINERALIZATION
CENOZOIC	Quaternary	RECENT		Qac	Alluvial Deposits (gravel, sand, silt, clay, oxidation)		N/A
	Tertiary		66.4		NO to LITTLE DEPOSITION & EROSION		
MESOZOIC	CRETACEOUS	LATE		Kuc	Caracol Formation - interbedded to laminated calcareous shale, siltstone and lesser sandstone		Veins and Stockwork of Au, Ag, Pb, Zn
				Kui	Indidura Formation - gray, stratified, calcareous shale		Veins and Mantos of Au, Ag, Pb, Zn
		EARLY		Kucc	Cuesta del Cura Formation - resistant, dark gray limestone with persistent thin to medium bedded wavy stratification; common lenses of shale and chert		Minor vein and mantos; primarily skarn replacement
					La Pena Formation - calcareous shale unit		??
			144				

**Figure 4:** The stratigraphic section of Camino Rojo. The pink intrusion in the figure represents the inferred magmatic body responsible for the intrusive dikes at Camino Rojo.

### 2.3.2 Intermediate Composition Dikes

The Caracol, Indidura, and Cuesta del Cura formations were intruded by several discontinuous, intermediate-composition dikes. The dikes proximal to mineralization at Camino Rojo are altered, and original textures and chemistry are obscured. A previous petrographic study (Leitch, 2008b) described the dikes as felsic, high level intrusions that contained variable amounts of relict hornblende, biotite and plagioclase phenocrysts most often in a groundmass of fine K-feldspar. Dikes within the deposit are generally altered to mixtures of K-feldspar and carbonate, with lesser sericite, chlorite and pyrite. Less altered dikes, often with intact biotite grains, are present at greater distance from Camino Rojo mineralization.



The dikes are intermediate in composition, as inferred from phenocryst assemblages. Two distinct dike types are distinguished: (1) fine grained dikes with variable amounts of hornblende and plagioclase phenocrysts, often with a preferred orientation on elongate crystals, and (2) coarse-grained, amphibole-rich type, which contains variable amounts of biotite in a fine, crystalline groundmass. A third dike type is medium grained and appears to be a textural transition between the coarse- and fine-grained dikes. The fine- and medium-grained dike types are altered and cut by mineralization. The coarse-grained dike type is unmineralized and locally weakly altered.

An internal Goldcorp report by B. Scorrar (2014) identified three dike types: (1) fine-grained hornblende porphyry (fgH); (2) medium-grained hornblende porphyry (mgHP); and (3) coarse-grained hornblende plagioclase biotite porphyry (cgHPB). The dikes identified by Scorrar (2014) are consistent with the three intrusion types identified in this study. Scorrar's observations that the coarse-grained dikes are barren and the fine- to medium-grained dikes are mineralized are consistent with what has been observed in this study, as described below.

### Mineralized Dikes

#### **(1) Fine- grained type**

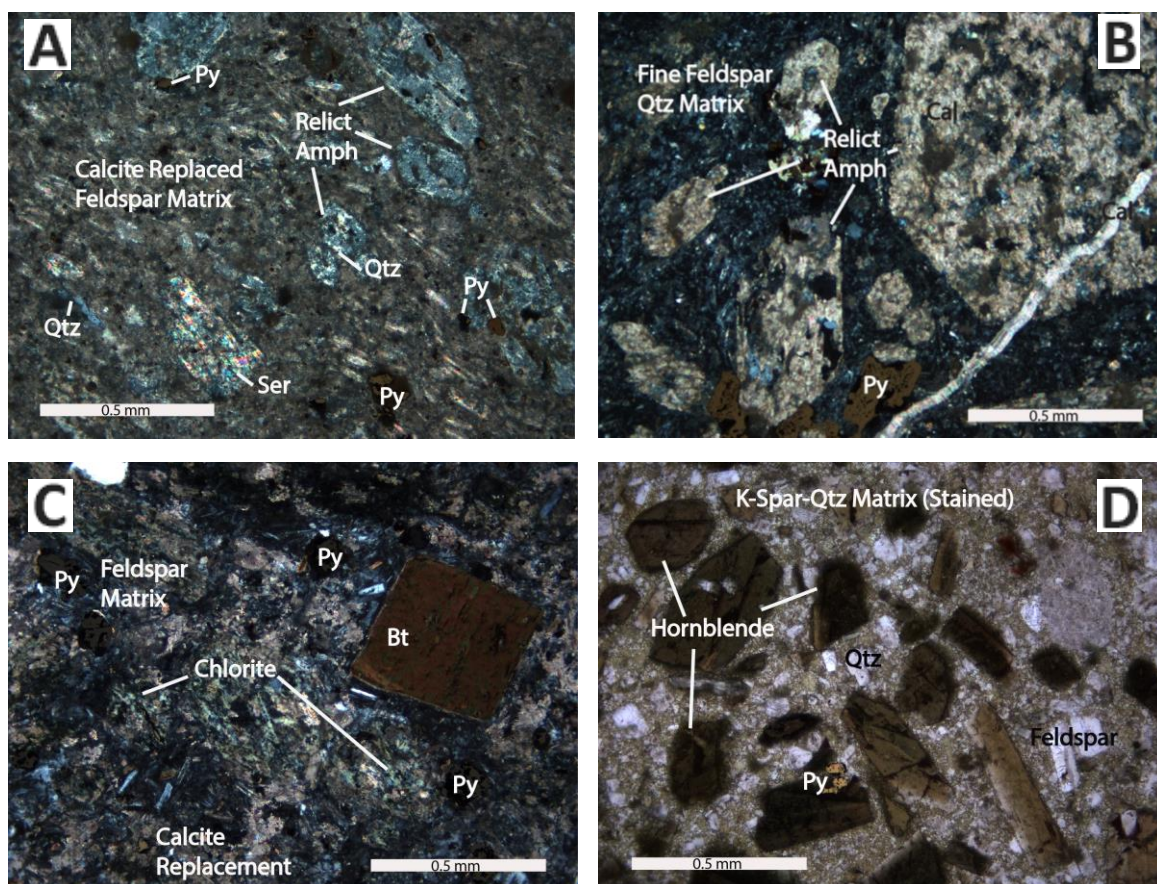
The porphyritic dikes are characterized by fine hornblende and plagioclase phenocrysts (5-20%), ranging from 0.1 to 0.5 mm in length. The matrix is aphanitic and composed of finer, anhedral feldspar and minor quartz (Figure 5A). The elongate feldspar and other minerals are commonly aligned. Due to location within the deposit, this type of dike tends to be strongly altered and mineralized.

**(2) Medium- grained type**

The medium-grained porphyritic dikes contain hornblende and plagioclase phenocrysts ranging in size from 0.15 to 1.5 mm. The matrix is variably aphanitic, and is composed of fine, anhedral plagioclase and minor quartz, with a few subhedral plagioclase crystals (Figure 5B, Figure 5C). This dike type tends to be moderately altered and mineralized.

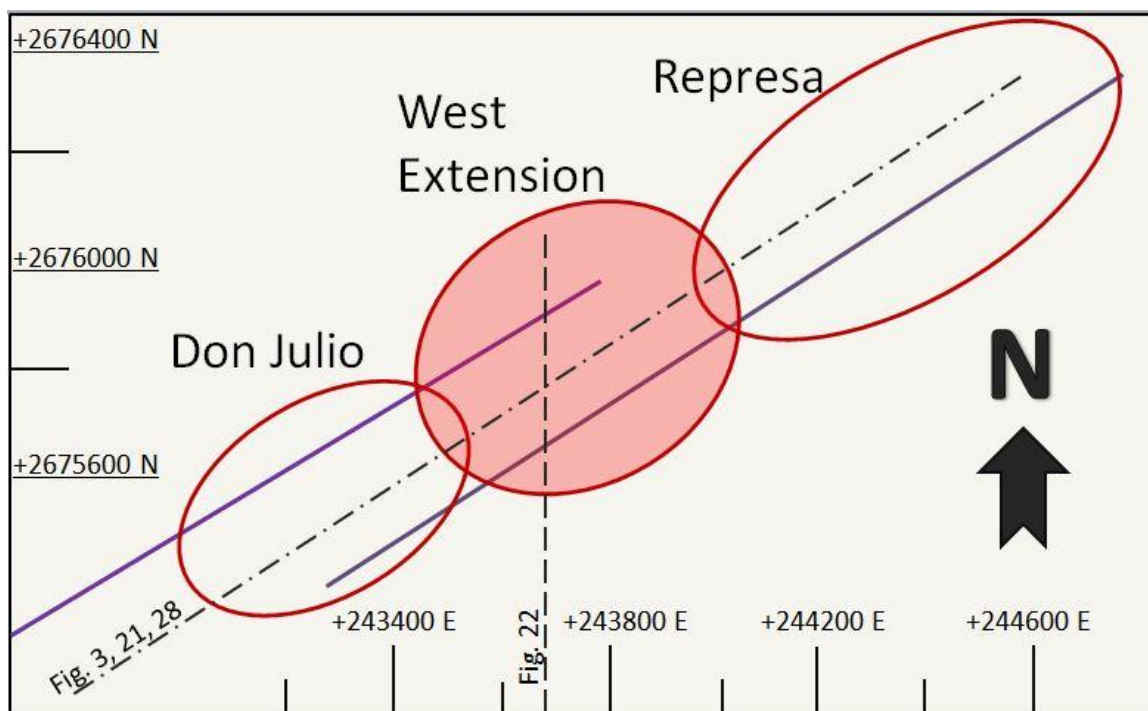
Barren Dike**(3) Coarse- grained (hornblende) type**

The coarse grained porphyritic dikes are distinguished by large hornblende and biotite phenocrysts ranging in size from 0.1mm to 6mm. The groundmass is composed of fine, crystalline, subhedral plagioclase crystals. Hornblende and biotite phenocrysts are more abundant than feldspar phenocrysts (Figure 5D). The greater amount of amphibole and the presence of biotite suggest that the barren dike is distinct compositionally from the fine- or medium-grained dikes.



**Figure 5:** Photomicrograph examples of the three dike types at Camino Rojo. A) fine-grained dike from Hole 348/378m (1CR15), calcite-altered matrix; crossed polars (xPL); B) medium- to coarse-grained dike from Hole 282/696m (2CR04), xPL; C) medium-grained dike from Hole 354/706 m (1CR23), xPL; note euhedral, little-altered biotite; D) coarse-grained dike from Hole 433/294 m (2CR18), plain light (PL); note unaltered hornblende and feldspar phenocrysts; very fine k-feldspar in the groundmass.

Drilling indicates that the dikes occur in two subparallel, planar arrays that dip 80 degrees north and strike NE, as modeled in Leapfrog 3-dimensional software (Figure 6). The arrays are inferred to represent NE-trending, high-angle faults perpendicular to the major N-NW trending San Tiburcio fault system. Mineralization at Camino Rojo is primarily concentrated around the southeastern array of dikes. The dikes at Camino Rojo are inferred to be sourced from a deeper, not yet defined magmatic body.



**Figure 6:** Schematic map of planar dike trends at Camino Rojo shown by solid lines; ellipses represent generalized >1ppm Au trends projected to the surface. Mineralized zones become deeper to the SW. Dash-dot line indicates plane of cross section shown in Figures 3, 21, 28. Dashed line shows plane of cross section show in Figure 22. UTM grid NAD 27.

### 3 MINERALIZATION AT CAMINO ROJO

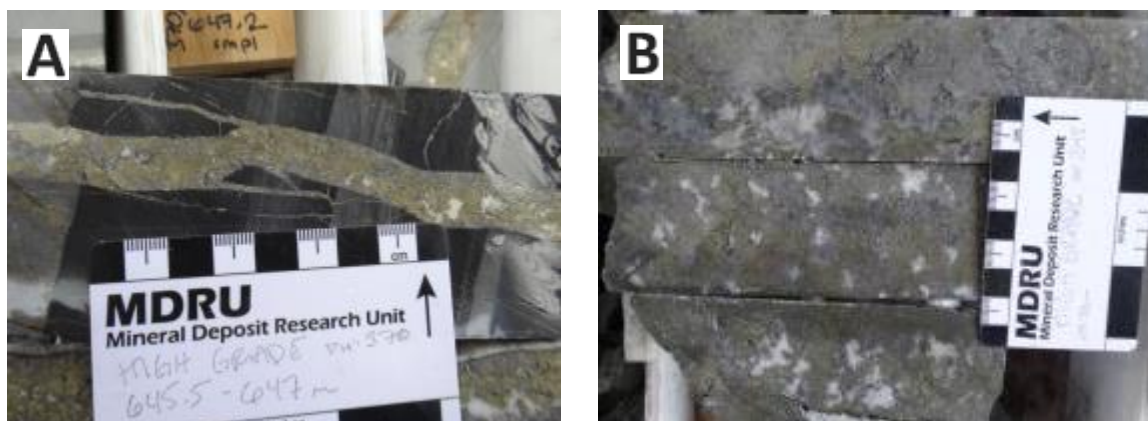
Proven and probable gold and silver reserves and measured and indicated resources at Camino Rojo are located in the Represa and West Extension zones. The Represa zone contains proven and probable reserves that total 1.85 Moz gold at 0.68 g/t and 37.49 Moz silver at 13.8 g/t (Anonymous, 2014). Potential ore in these zones is primarily hosted in vein networks and, to a lesser extent, in manto (replacement) bodies found deeper in the system. The vertical distribution of mineralization extends from the Caracol Formation, at the base of the Quaternary alluvium, to almost one thousand meters in depth. Skarn alteration and lower-grade mineralization exist in the Cuesta del Cura Formation, and additional mineralization may

be present at even greater depths. The deep skarn mineralization was not described in this study and is not discussed in detail in this paper.

Oxidation due to weathering in the Represa zone has converted hypogene sulfides into varying amounts of iron oxides, primarily goethite, as well as limonite, hematite, and less abundant jarosite. Only goethite and hematite have been observed in thin section. Both the vein and disseminated sulfides at Camino Rojo have been completely oxidized in a large portion of the Represa zone. Where oxidation is prevalent, the host rocks have been bleached and are more porous due to leaching of the pyrite and carbonate. Iron oxides decrease with depth, until only hypogene sulfides remain.

### **3.1 Mineralization Style (Vein vs Manto)**

Veins and mantos are the two principal styles of mineralization at Camino Rojo, as shown in Figure 7. Veins and vein networks are primarily developed within the Caracol Formation and formed in fractures related to the linear arrays outlined by the dikes (Figure 6). Disseminated sulfides are concentrated along bedding planes and decrease with distance from sulfide vein margins. In some cases, sulfides have partly to completely replaced small sedimentary beds, and may be termed mini-mantos. Vein mineralization at depth in the West Extension zone gradually and continuously shallows in a NE direction into the Represa zone (Figure 3). In mineralized zones, where veins are present, sulfides make up between 5-25% of the rock. Where there is manto mineralization, the host rock is generally composed of more than 25% sulfides.



**Figure 7:** Visual comparison of (A) vein- vs (B) manto-style mineralization in core. A) Hole 370/646 m; high grade pyrite-arsenopyrite-calcite vein, near-parallel to the core axis; B) Hole 345/500 m; High grade manto with an intergranular/ mottled texture of pyrite-arsenopyrite-calcite in the Caracol Formation.

### 3.1.1 Vein Sulfides and Textures

Veins are the primary ore type, in terms of volume. All sulfide veins at Camino Rojo are similar in texture, structure, and overall mineralogy. Vein stockworks and sheeted veins are common, and individual vein thickness ranges from 0.5cm to 10cm. The majority of sulfide veins are planar, with margins that are straight and well-defined (Figure 8A). Sinuous, undulate, irregular, and even diffuse vein margins also occur (Figure 8B). Veins are primarily fracture-controlled, and are often parallel to the core axis, cutting bedding at nearly right angles (Figure 8A). Some veins split into multiple, smaller veins with the same mineralogy (Figure 8C). No significant changes in vein texture or composition have been recognized laterally or vertically from hole to hole. Collected samples span a lateral distance of 750m.

Although veins tend to become more abundant with depth, overall vein density is sparse and cross-cutting relationships are almost non-existent in core. Veins begin beneath alluvium in the Caracol Formation in the Represa zone, and extend to over 1000m below the surface to the Cuesta del Cura Formation.

Principal sulfides within veins are (in order of relative abundance): pyrite, sphalerite, arsenopyrite, galena, marcasite, and chalcopyrite, with trace amounts of pyrrhotite, electrum, acanthite, and silver sulfosalts. Subhedral to euhedral disseminated sulfides commonly form a halo around veins, and spread outward along bedding planes. Disseminated sulfides associated with veining decrease in size and frequency more than 4cm from vein margins, and are similar in composition to proximal veins. Pyrite is the most common disseminated sulfide and often formed along bedding, even without the immediate presence of large sulfide veins.

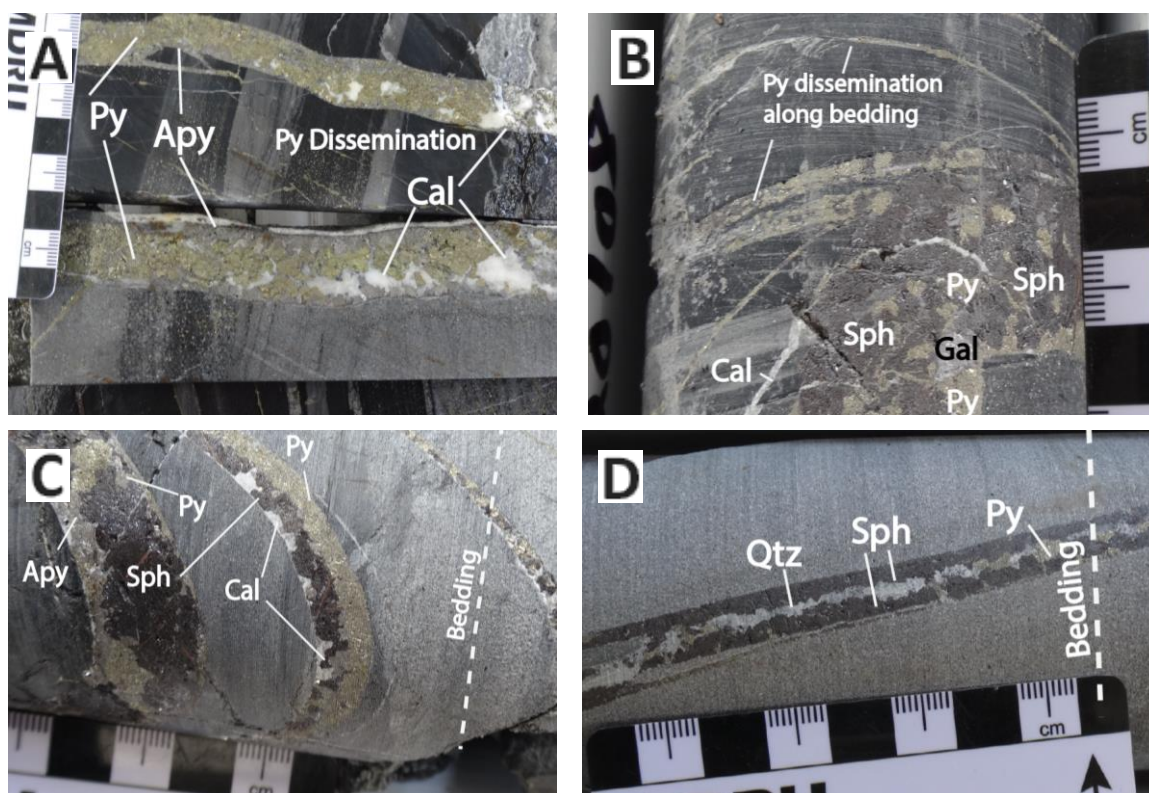
Narrow veins (<1cm) tend to have a simple mineralogy of two to three minerals, including quartz and/ or calcite which are texturally later than the sulfides (Figure 8D, Figure 8E). Thicker veins (1-10cm) are often composed of two or more intergranular sulfides (Figure 8F, Figure 8G). Thin, fine-grained pyrite veins and/ or replacements parallel to bedding are common, and formed by an amalgamation of disseminated pyrite along bedding planes (Figure 8B).

The most common vein sulfide texture at Camino Rojo is a mottled, intergranular mix of pyrite, sphalerite, arsenopyrite, and calcite, with lesser galena, chalcopyrite and quartz. Veins can have crude, asymmetrical zoning with distinct layers of two or more sulfides (Figure 8E, Figure 8F). Figure 8E depicts crudely layered pyrite-sphalerite-calcite, with minor galena and arsenopyrite near the vein center. Cross-cutting relationships are rare, though one hand sample collected has a 1cm sphalerite-quartz vein cutting a 0.5cm massive pyrite vein.

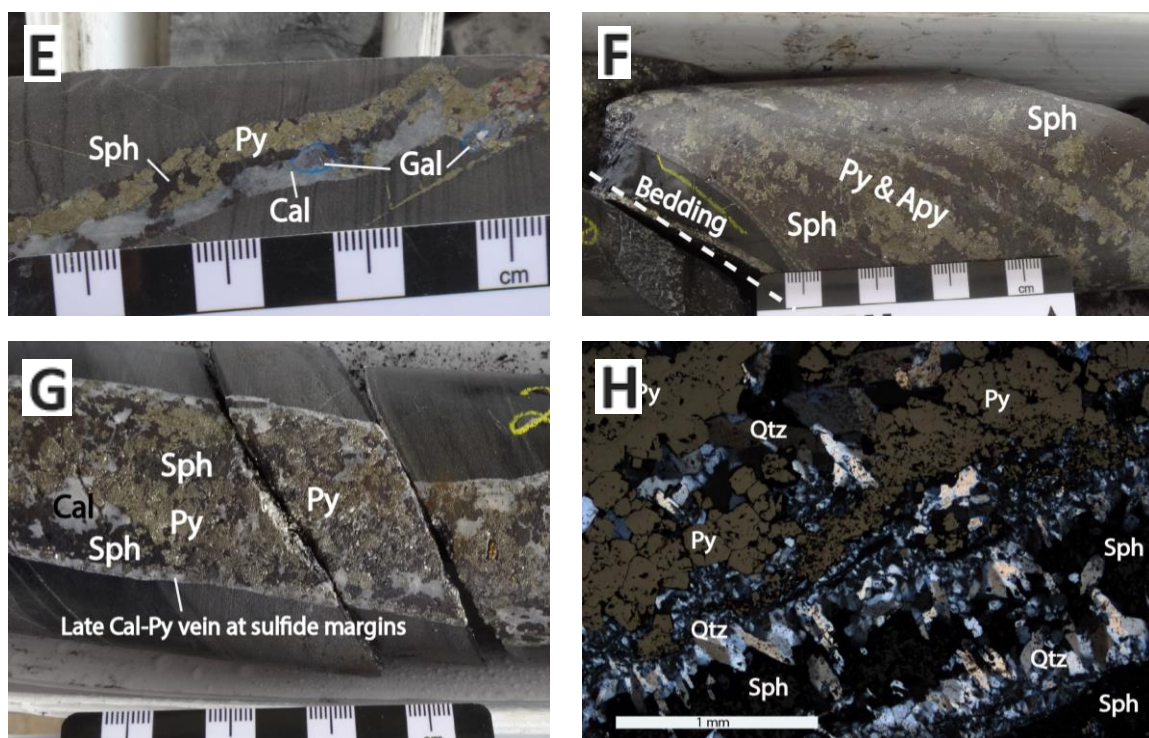
Veins with a distinct bimodal nature, where the margins of the vein are of a different composition than the vein center, are not common. Where present, such veins provide evidence for a change or evolution of hydrothermal fluids. Figure 8D illustrates this relationship;

in this example, euhedral to subhedral sphalerite has formed along the vein edges with later quartz and pyrite filling the center.

Figure 8H is a photomicrograph of a zoned vein with euhedral quartz and later sphalerite and pyrite. In this example, a small vein consisting of euhedral quartz along the vein margin has been surrounded and infilled by later sulfide grains. Hydrothermal quartz, either as in veins or wallrock alteration, is not abundant at Camino Rojo, and even fine veins composed dominantly of quartz are unusual.







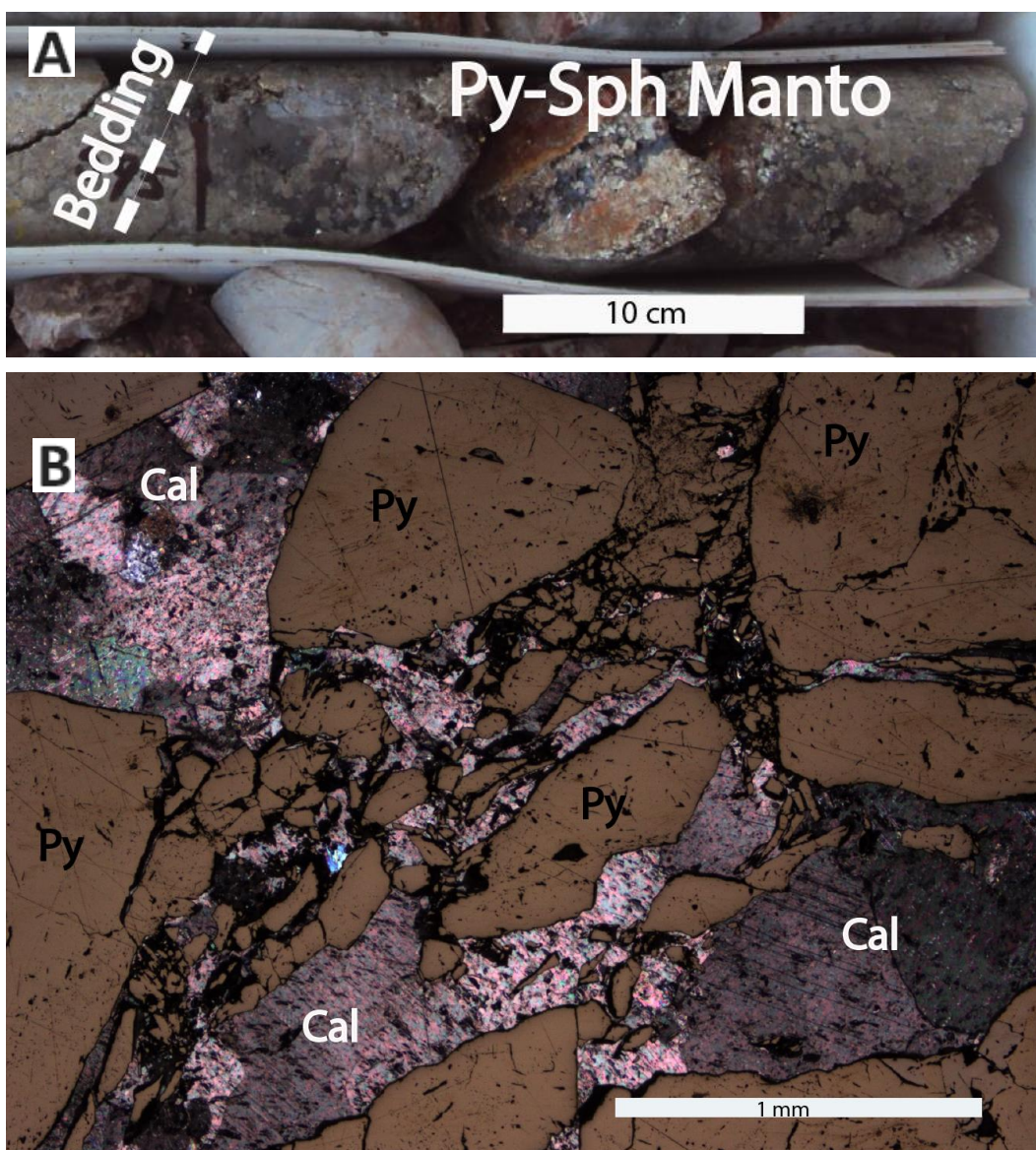
**Figure 8:** Photographs depicting sulfide vein mineralogy, texture and structure at Camino Rojo. A) Hole 370/646 m; the core-parallel vein changes in texture and sulfide composition throughout the sample length; B) Hole 439/424 m; sphalerite-pyrite-minor galena vein with irregular margins and disseminated sulfides along bedding planes; C) Hole 438/588 m; a sulfide vein splays into smaller veins of the same composition; D) Hole 376/613 m; bimodal vein texture with sphalerite along edges and quartz-pyrite in the center; E) Hole 394/690 m; crude zonation in a pyrite-sphalerite-calcite sulfide vein; F) Hole 438/463 m; crude layering of sphalerite and pyrite within 8cm sulfide vein; G) Hole 439/272 m; mottled pyrite-sphalerite-calcite vein with later calcite adjacent to vein boundaries; H) Hole 354/ 681 (1CR22), crossed polars (xPL), 5x: Crude banding of pyrite-quartz-sphalerite, with minor adularia and quartz.

### 3.1.2 Manto (Replacement) Sulfides and Textures

Meter-scale, manto-style mineralization tends to replace the calcareous sandstone beds of the Caracol Formation. The discontinuous, manto-style replacement intervals range in width from less than 1cm to over 3m and do not correlate well from hole to hole. The contact between the massive manto sulfides and the sedimentary host is irregular (Figure 9A), but in general is more lithologically controlled than the sulfide veins at the deposit. In this study, the term mini-mantos is used to describe the small sedimentary beds which have been replaced by sulfides. The width of these mini-mantos is typically less than a few centimeters.

The sulfides making up the mantos are similar in mineralogy to veins at Camino Rojo, though arsenopyrite can be more abundant than sphalerite. Pyrite, arsenopyrite, and sphalerite are coarser grained (1-15mm) in the mantos than in sulfide veins. Intergranular and mottled sulfide textures are common within mantos (Figure 7B). The massive textured sulfides commonly have a distinct, puzzle-piece breccia texture with interstitial calcite and quartz (Figure 9B). Later calcite and quartz are also interstitial to non-brecciated sulfides, can be massive textured or finely intergranular, and calcite is more prevalent than quartz. Puzzle-piece brecciation has not been observed in veins.

A third style of mineralization has been observed in a few of the deepest holes. Garnet-magnetite skarn formed along bedding in the Cuesta del Cura Formation and below. In places, the skarn is mineralized. Very few skarn samples were available at the time of this study and the mineralogy has not been defined here.



**Figure 9:** A) Hole 390/595.4 m (3CR05); Photograph of thin manto-replacement within the Caracol Formation, primarily composed of mottle-textured sphalerite, pyrite, and minor arsenopyrite and galena, core is 5cm in diameter; B) Hole 345/533 m (1CR08); puzzle-piece brecciation of pyrite cemented by massive calcite; combined reflected and crossed-polars transmitted light.

### **3.2 Mineral and Sulfide Petrography and Paragenesis**

Camino Rojo is a polymetallic deposit, and two distinct, paragenetic ore stages (Figure 10) have been identified in polished thin sections. Stage 1 is volumetrically greater, and comprises base metal sulfides and minor electrum mineralization in the form of veins and mantos. Stage 2 includes electrum, acanthite, silver sulfosalts, galena, and minor chalcopyrite. For this study, ore stage 2 at Camino Rojo has been subdivided into two parts, 2a and 2b, which are discussed further below. The cross-cutting and textural relationships between ore stages 1 and 2 were not recognized in core hand samples. However, stage 2 cross-cuts stage 1 in polished thin sections. Cross cutting relationships were not observed between stages 2a and 2b.

The paragenesis was identified through polished section study, and includes both vein and manto minerals as shown in Figure 10. Overall, pyrite, sphalerite, and arsenopyrite are the most common sulfides at Camino Rojo. The majority of electrum and the silver-bearing minerals at Camino Rojo formed during ore stages 2a and 2b, respectively. Microscopic examination of polished sections indicated that roughly 10%-15% of the electrum, by volume, was deposited in stage 1 and 85%-90% in stage 2a. This percentage only applies to electrum visible under reflected light petrography, and does not account for any potential sub-microscopic gold.

Mineral	Pre-Ore	Ore Stage			Post-Ore
Quartz	-?-	---	---	---	
Calcite	--	---	---	---	-----
Py	---	---	---	---	-----
Apy		---	---	---	
Sph		-----			
Cpy		-----	---	---	
Gal		-----	---	---	
Mar		---			---
Po		---	---	---	
Pyg				---	
Ten				---	
Ac			---	---	
El			---	---	
Ted			---	---	
		<b>STAGE: 1</b>	<b>2a</b>	<b>2b</b>	

**Figure 10:** Paragenesis of vein and manto mineralization at Camino Rojo. Mineral abbreviations: apy = arsenopyrite; ac = acanthite; cpy = chalcopyrite; el = electrum; gal = galena; mar = marcasite; pyg = pyrargyrite; py = pyrite; po = pyrrhotite; sph = sphalerite; ten = tennantite/tetrahedrite; ted = tetradymite. Early, stage 1 base metal-arsenic-gold mineralization is highlighted in gray; ore stage 2 is highlighted in red, with 2a calcite-galena-chalcopyrite-electrum-acanthite and 2b calcite-pyrargyrite-tennantite-acanthite and varying quartz-pyrite-arsenopyrite noted. Marcasite is not included in the paragenetic diagram, due to its close relationship with pyrite. Dashed lines indicate a continuous formation and gaps indicate episodic formation; question marks denote a timing uncertainty. \*signifies brecciation in manto samples.

The **Pre-ore** stage (Figure 10) is marked by barren calcite and minor quartz. Diagenetic pyrite is present as framboidal pyrite. Pre-ore disseminated pyrite associated with potassic metasomatism (see Section 4.1) formed as anhedral grains (Figure 11A). The non-diagenetic, pre-ore pyrite can be confused with post-ore pyrite, which is clearly associated with late stage calcite veining and flooding.

### Stage 1 – Base Metal Mineralization

The first ore stage began with extensive pyrite and near-contemporaneous arsenopyrite formation, followed by precipitation of sphalerite (generally dark in color and iron-rich), chalcopyrite, and later galena (Figure 10). Subhedral pyrite, sphalerite, and arsenopyrite make

up the bulk of sulfide veins and mantos, with lesser amount of chalcopyrite and galena (Figure 11B). Calcite formed both contemporaneously with and slightly later than pyrite and arsenopyrite.

Disseminated sulfides in vein halos include pyrite, arsenopyrite, and sphalerite.

Disseminated sulfides tend to become coarser with depth in the system. Occasional sphalerite rims around disseminated pyrite grains are associated with sphalerite-rich sulfide veins.

Sphalerite is the defining stage 1 mineral, as it is not present in stage 2.

Electrum blebs in stage 1 are somewhat round, and often formed adjacent to fine, near euhedral arsenopyrite grains, and less commonly adjacent to pyrite. The electrum grains were completely surrounded by massive-textured sphalerite, and formed in the latter portion of stage 1 (Figure 10).

### **Stage 2 – Electrum and Silver-bearing Mineral Deposition**

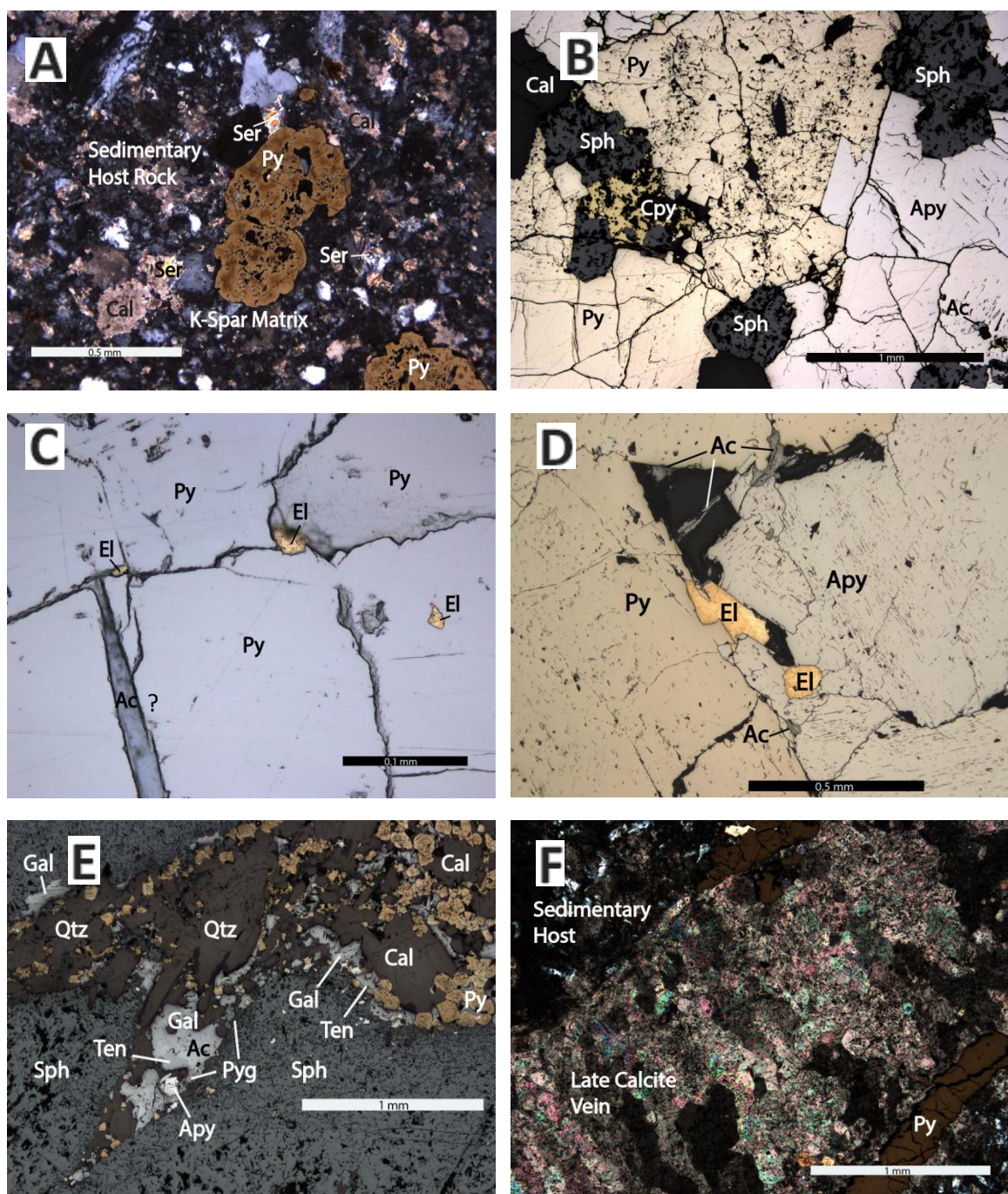
Stage 2 mineralization has been subdivided into sub-stages, 2a and 2b, which both cut stage 1. The majority of electrum observed in Camino Rojo samples was deposited during stage 2a in fractures which cut stage 1 sulfides, as described below.

**Stage 2a** – Stage 2a mineralization fills fractures within stage 1 base metal sulfides, and is clearly later than stage 1 mineralization. Electrum in 2a filled fractures in stage 1 sulfides, and is accompanied by calcite, galena, chalcopyrite, acanthite, and trace tetradymite (Figure 10). Stage 2a acanthite is fine grained and anhedral, and filled fractures within earlier arsenopyrite and pyrite. The acanthite appears to be near-contemporaneous with electrum (Figure 11C, Figure 11D). SEM analyses of electrum grains show an average composition of 25 wt% Ag and 75 wt% Au.

**Stage 2b** – Stage 2b is characterized by calcite, galena, silver sulfosalts and acanthite in veins which cut stage 1 mineralization (Figure 10). Varying amounts of pyrite and arsenopyrite are also present in stage 2b veins; there is no electrum in ore stage 2b. Acanthite and the silver-bearing sulfosalts pyrargyrite and tennantite- tetrahedrite are closely associated with galena (Figure 10). In one sample, acanthite, tennantite, and pyrargyrite formed along the edges of a quartz-pyrite-arsenopyrite vein which cut earlier, stage 1 massive-textured sphalerite (Figure 11E).

The relative timing between 2a and 2b is not known, because cross-cutting and textural relationships between the 2a and 2b ore stages have not been observed. Without the benefit of high magnification and polished surfaces, stage 2 mineralization could not reliably be determined in hand sample, as it is comprised of very fine sulfides filling micro-fractures within the more abundant stage 1 veins and mantos.

**Post-ore** mineralogy is the result of shallow (<400m), calcite-pyrite alteration which overprints the upper parts of the deposit (see Section 4.3). Post-ore pyrite and calcite have formed as massive calcite veins, vein swarms, and as disseminated masses of calcite and pyrite (Figure 11F).



**Figure 11:** Photomicrographs depicting pre-ore, ore, and post-ore stages at Camino Rojo. A) Hole 256/492m; XPL; potassically altered sample composed of fine sericite and calcite within the sedimentary, potassically altered matrix; ore-stage disseminated pyrite is porous and anhedral; B) Hole 369/643m; Reflected Light; Stage 1 mineralization: near contemporaneous pyrite and arsenopyrite, with later sphalerite and chalcopyrite; C) Hole 370/647.2m; Reflected light; Late electrum and acanthite(?) or galena(?) fill fractures in pyrite; D) Hole 436/618.7m; reflected light; electrum and acanthite fill fractures between arsenopyrite and pyrite grains; E) Hole 375/286.4m; Reflected light; 2b quartz-pyrite-calcite-galena-acanthite-tennantite-pyrargyrite vein cuts a stage 1 massive-texture sphalerite vein; F) Hole 349/763m; xPL and reflected light; post-ore pyrite borders late calcite vein, minor calcite flooding in host matrix.



### **3.2.1 Calcite Petrography**

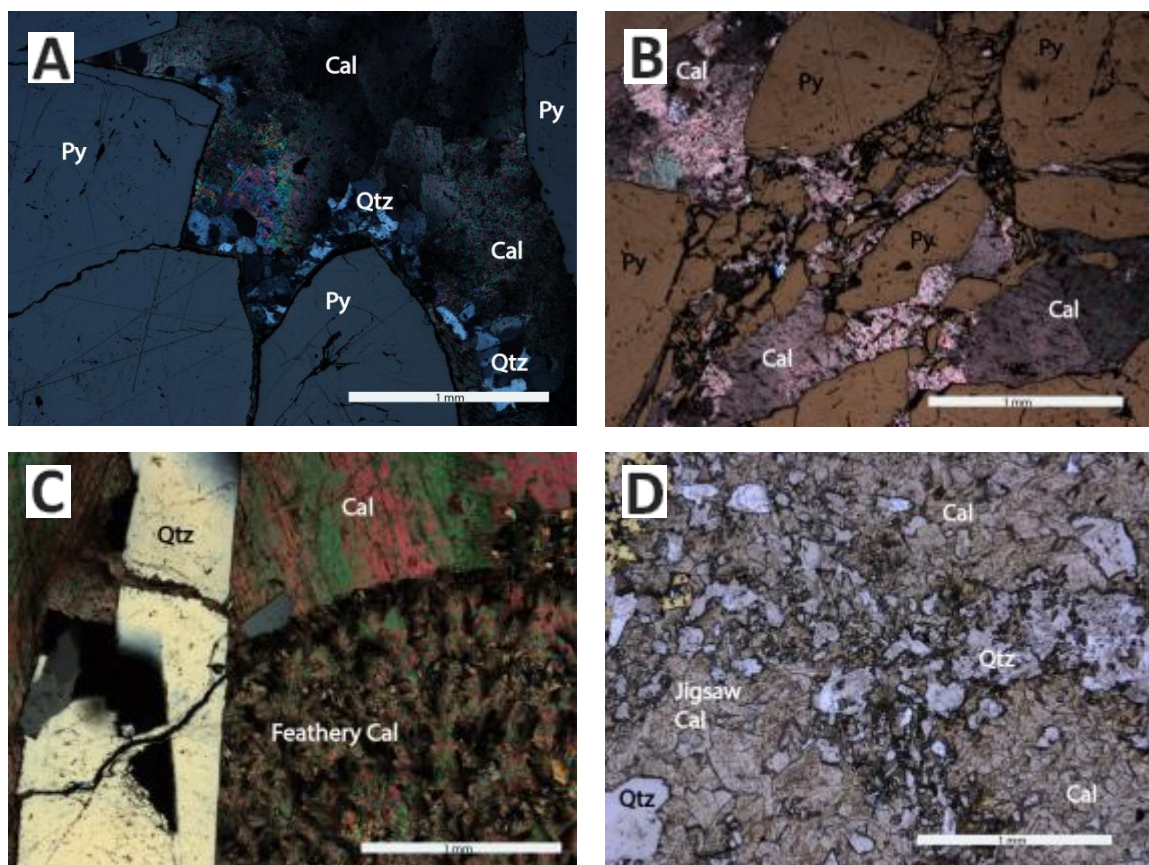
Calcite is one of the most abundant gangue minerals at Camino Rojo. It is an accessory mineral in sulfide veins and mantos, and late stage alteration has resulted in flooding and partial replacement of the host rocks by calcite. Hydrothermal calcite grains at the deposit range in size from 0.001mm, in some recrystallized host matrices, to  $\geq 3$ cm in coarse-grained mantos and dog-tooth calcite veins. Distinguishing between sedimentary and hydrothermal calcite is difficult in wallrocks where no sulfides were deposited. Bladed calcite textures indicative of boiling in low sulfidation epithermal systems (Simmons et al., 2005) have not been observed at Camino Rojo.

**Pre-Ore** - Calcite is a minor component of the pre-mineralization potassic alteration (see Section 4.1), and was deposited as fine disseminated grains through the host rock. It is also a common alteration mineral in the dikes, commonly having replaced hornblende and some portions of altered dike groundmass.

**Stage 1** - Calcite is an accessory mineral in ore stage 1. The calcite, often with undulatory extinction (Figure 12A), filled the center of sulfide veins and formed euhedral crystals at vein margins. Coarse- to fine- grained, crystalline calcite, most often subhedral, is the most common calcite form. Calcite is commonly intergrown in a polygonal texture with stage 1 sulfides. Less common textures include feathery calcite (Figure 12C), where elongated calcite crystals with undulatory extinction have grown in a 'feathered' pattern, and jigsaw calcite (Figure 12D), where near-rhombohedra shaped calcite are interconnected in a 'jigsaw' pattern. The jigsaw and feathery calcite tend to occur with fine, euhedral quartz grains. In the mantos, calcite often cemented brecciated sulfides (Figure 10, Figure 12B).

**Stage 2** – Calcite was deposited during stage 2a in micro-fractures, along with electrum, silver-bearing minerals, galena, chalcocite, and trace tetradymite. Stage 2b silver-bearing veins contain abundant calcite, which formed adjacent to 2b sulfides.

**Post-Ore** –The last paragenetic stage at Camino Rojo consists of late calcite and variable amounts of pyrite (Figure 10). The late calcite formed multiple generations of cross-cutting veinlets and veins. Late calcite and minor pyrite overprinted the host rocks as fine, anhedral, disseminated masses, and occasionally formed unusual feathery and jigsaw textures within the altered host matrix.



**Figure 12:** Photomicrographs of calcite textures at Camino Rojo. A) Hole 370/660m, crossed polars (xPL); massive-textured calcite with undulose extinction fills space adjacent to pyrite; B) Hole 345/533m, xPL; massive-textured calcite cements brecciated pyrite in a manto; C) Hole 376/610.4m; xPL; feathery calcite texture in a calcite-quartz vein related to ore stage alteration; D) Hole 291/615.7m; PL; rare jigsaw-calcite texture: interlocked, tan crystals of calcite

formed adjacent to interstitial, subhedral quartz during the late, post-ore stage.

### **3.2.2 Quartz Petrography**

As previously mentioned, there is a notable lack of quartz associated with mineralization at Camino Rojo. Nevertheless, quartz is present in small quantities. Several quartz textures were observed in thin sections of sulfide veins, mantos, and altered host rocks.

**Pre-Ore** – The only clearly pre-ore quartz grains are detrital and within the sedimentary rocks. Some of the original quartz appears to have been recrystallized as part of the pre-ore potassic metasomatism (see Section 4.1), but otherwise little or no quartz appears to have been added to the system before ore stage events.

**Ore Stage** – The majority of ore-stage quartz is associated with the ore-stage alteration assemblage of calcite-sericite  $\pm$  pyrite  $\pm$  quartz (see Section 4.2); the ore-stage quartz is less abundant than ore-stage calcite. The alteration quartz formed a jigsaw or chaotic texture in the matrix of host rocks proximal to sulfide veins and mantos. Jigsaw-textured quartz appears as fine, anhedral, interlocked quartz grains, ranging from 0.1mm to just over 1mm in grain size (Figure 13A). Coarser jigsaw-textured quartz formed within the mantos, filling spaces or cementing brecciated manto sulfides (Figure 13B). Chaotic-textured quartz formed as very fine grained, anhedral masses within the altered sedimentary host (Figure 13C), with individual grains being less than 0.01mm. Jigsaw quartz grains tend to be more angular than chaotic quartz grains. Both the jigsaw and chaotic textures may in part represent a recrystallization of original, sedimentary quartz, and some may be hydrothermal in origin.

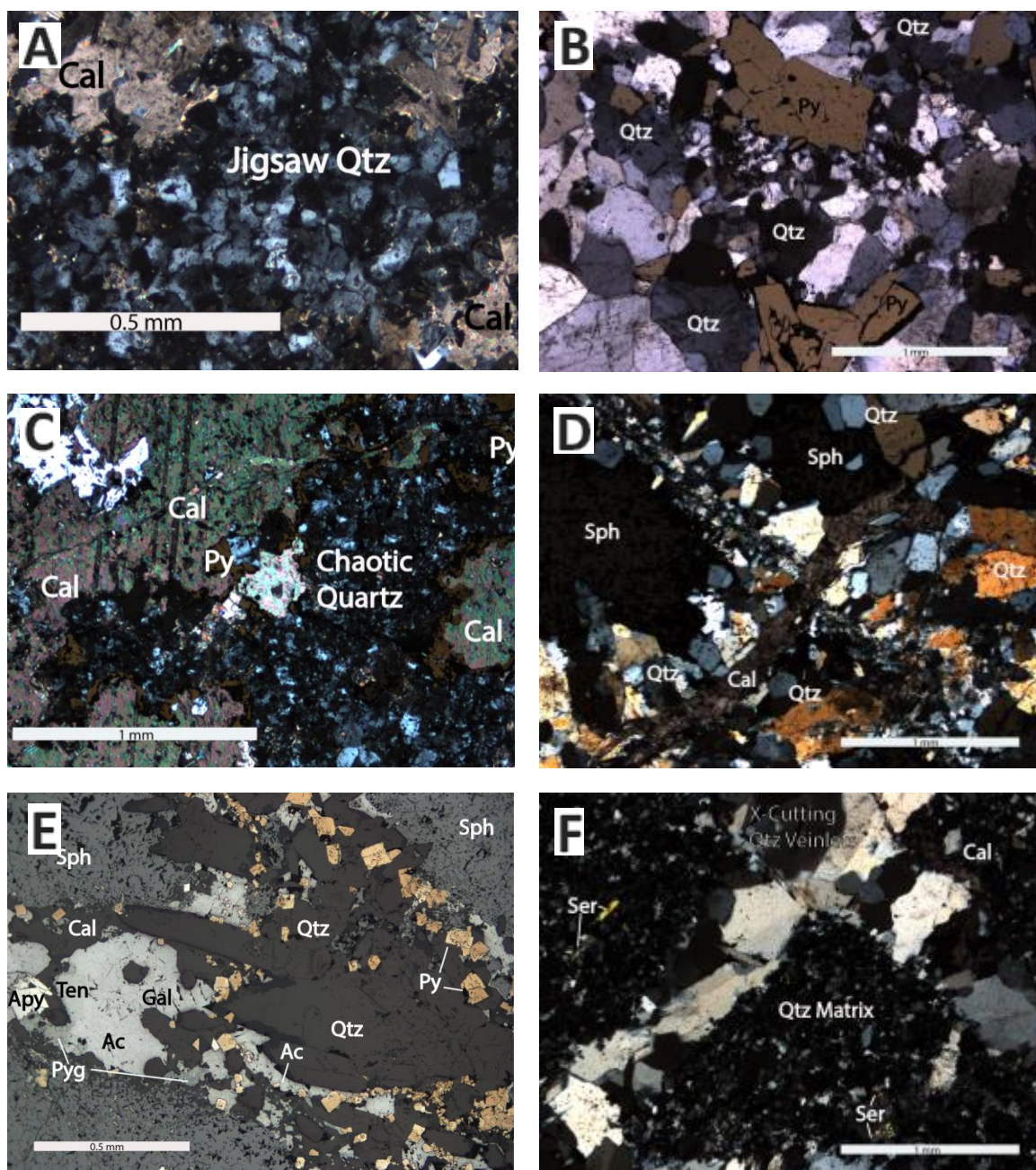
Quartz is also a relatively minor constituent of stage 1 veins and mantos. The quartz tends to be euhedral and often with undulatory extinction. Though not common, some sulfide veins contain euhedral to subhedral prismatic quartz crystals formed along one side of the vein

with growth toward the vein center (Figure 13D). Prismatic quartz surrounded by massive-textured calcite between sulfides is a minor texture within the replacement bodies.

One silver-rich sample contained an ore stage 2b vein partly filled with prismatic quartz, which paralleled and cut through a stage 1 massive-textured sphalerite vein (Figure 13E). Quartz has not been observed in ore stage 2a.

A few occurrences of mutually cross-cutting quartz veinlets were observed in thin section. At least one of the examples includes abundant sphalerite, which is associated with ore stage 1 (Figure 13D). Other cross-cutting quartz veinlets were composed almost entirely of quartz, as shown in Figure 13F, but their paragenetic timing is unknown.

**Post-Ore** – Quartz is absent in the post-ore calcite-pyrite alteration.



**Figure 13:** Photomicrographs of quartz textures at Camino Rojo. A) Hole 390/595.4 m (3CR05); crossed polars (xPL); jigsaw quartz within the sedimentary host matrix with later calcite; B) Hole 345/533.4 m (1CR08); xPL; Coarse, interlocked quartz in mantos cementing brecciated pyrite; C) Hole 349/771.7 m (1CR20); xPL; fine, chaotic-textured quartz within a fracture through massive-textured calcite with minor, fine pyrite at the boundary between quartz and calcite; D) Hole 449/437.7 m (2CR11); xPL; vein of sphalerite and euhedral quartz cut by a calcite veinlet; E) Hole 375/286.4m; Reflected light; quartz-pyrite-silver mineral bearing vein through stage 1 massive-textured sphalerite; F) Hole 370/647.2 m (1CR29); xPL; cross-cutting quartz veinlets within a fine quartz matrix.

### **3.2.3 Pyrite and Marcasite Petrography**

**Pre-ore** Diagenetic pyrite and pyrite associated with pre-ore alteration make up less than 5% of the total pyrite at the deposit. Original, diagenetic pyrite formed as framboids (Figure 14A). Pyrite associated with the early potassic alteration formed as disseminated, subhedral to euhedral grains. In unaltered samples, framboidal pyrite is distinct from the disseminated pyrite associated with alteration and mineralization.

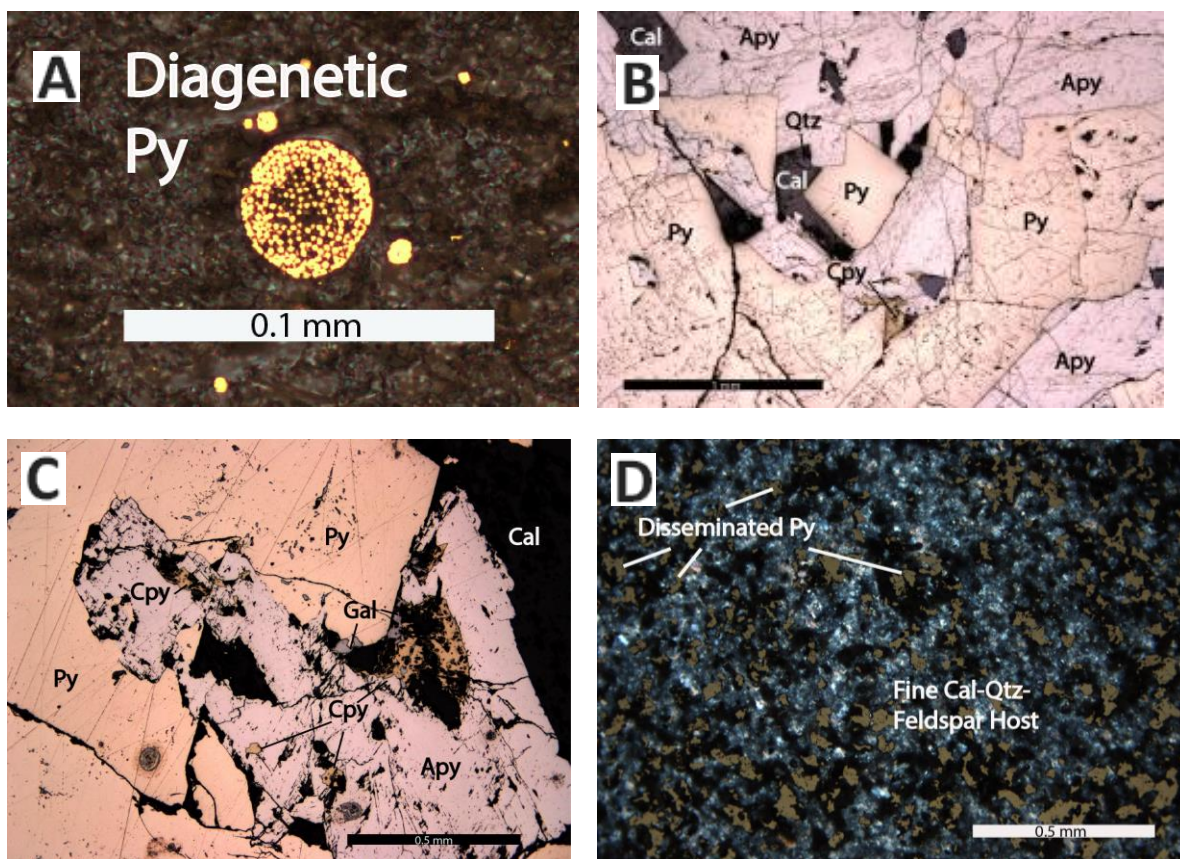
**Ore Stage 1** Pyrite is extensive in veins and mantos, and makes up roughly 50%-70% of the total sulfides associated with the base-metal mineralization. The primary texture is an intergranular relationship with arsenopyrite (Figure 14B). Pyrite and arsenopyrite are largely contemporaneous (Figure 14C). Pyrite grain size ranges from disseminated, 0.001mm grains (Figure 14D) to coarse 2.5cm crystals which formed within veins and mantos. Disseminated pyrite formed halos around sulfide vein margins with coarser, more abundant, and more euhedral grains closer to the sulfide vein margins. In some cases, silicate or other sulfide inclusions resulted in a porous pyrite texture. The disseminated pyrite extended outward from vein halos along thin sandy beds.

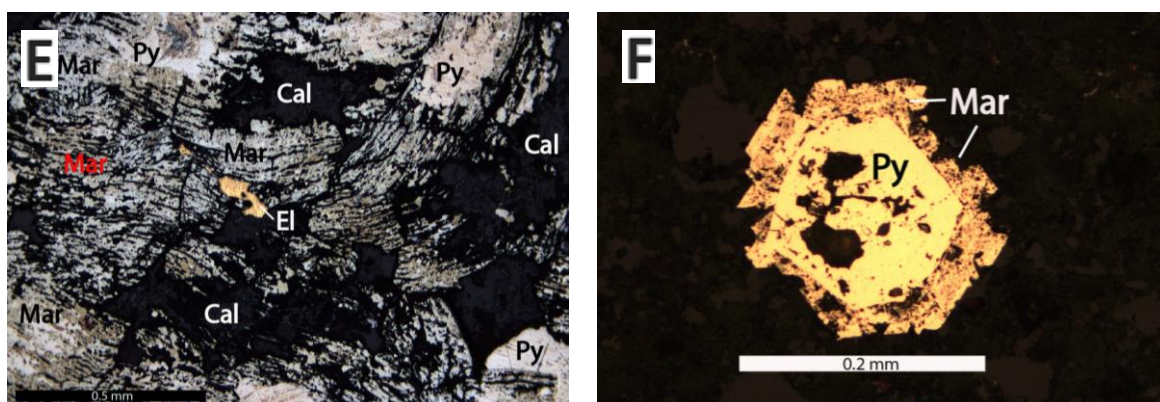
Marcasite, where present, is associated with pyrite, but is relatively uncommon. Primary marcasite is distinct in reflected light examination, and commonly formed as the outer layers of concentric pyrite-marcasite growths (Figure 14E), or as rhombohedral crystals along the edges of earlier pyrite grains (Figure 14F). Marcasite not texturally distinct from pyrite was likely a pseudomorph after pyrite.

**Ore Stage 2** Pyrite is not associated with ore stage 2a, which deposited galena, electrum, and acanthite. One silver sulfosalt vein, part of ore stage 2b mineralization, included

minor euhedral pyrite along the vein edges, and cut earlier, massive-texture sphalerite (Figure 11D).

**Post-ore** Pyrite is part of the late, overprinting calcite alteration (see Section 4.3). Post-ore pyrite is euhedral, and formed within late calcite veins and as disseminated grains. Disseminated, post-ore pyrite can be difficult to distinguish from disseminated pre-ore, and ore-stage pyrite, except where post-ore pyrite is accompanied by late, post-ore calcite veining and flooding through the altered host rock.





**Figure 14:** Photomicrographs of pyrite and marcasite textures at Camino Rojo. A) Hole 370/109m (3CR04), RfL; framboids are made up of small pyrite grains in an unaltered sedimentary sample; B) Hole 370/718 m (3CR07); reflected light (RfL); Intermixed pyrite and near-contemporaneous arsenopyrite form a mottled texture in a vein; later, minor chalcopyrite and calcite; C) Hole 347/645 m (1CR12); RfL; contemporaneous pyrite and arsenopyrite with later, fracture-filling galena-chalcopyrite-calcite; D) Hole 345/616.7m (1CR09), xPL and Reflected light; disseminated pyrite-calcite flooding in sedimentary host; E) Hole 345/747 m (1CR10), RfL; fine marcasite (blue-tint) formed around earlier pyrite growth; late electrum and calcite; F) Hole 318/629.4 m (2CR10); RfL; rhombic marcasite surrounding disseminated pyrite.

### 3.2.4 Sphalerite Petrography

**Ore Stage 1** After pyrite and marcasite, sphalerite is the next most abundant sulfide and makes up between 15%-25% of the stage 1 sulfides. Sphalerite is primarily a component of vein and manto mineralization, though it can be disseminated in halos around sphalerite-rich veins. Massive-textured, anhedral sphalerite formed intergranular to pyrite and arsenopyrite (Figure 15A), and sphalerite grain size ranges from 0.01mm to 3cm. Sphalerite was deposited after pyrite and arsenopyrite (Figure 10), but was earlier than stage 1 galena (Figure 15A). Sphalerite at the deposit contains fine, exsolved grains of chalcopyrite. Silicate and sulfide inclusions result in a porous texture (Figure 15B, Figure 15C). Sphalerite is not part of pre-ore, ore stage 2, or post-ore stages.

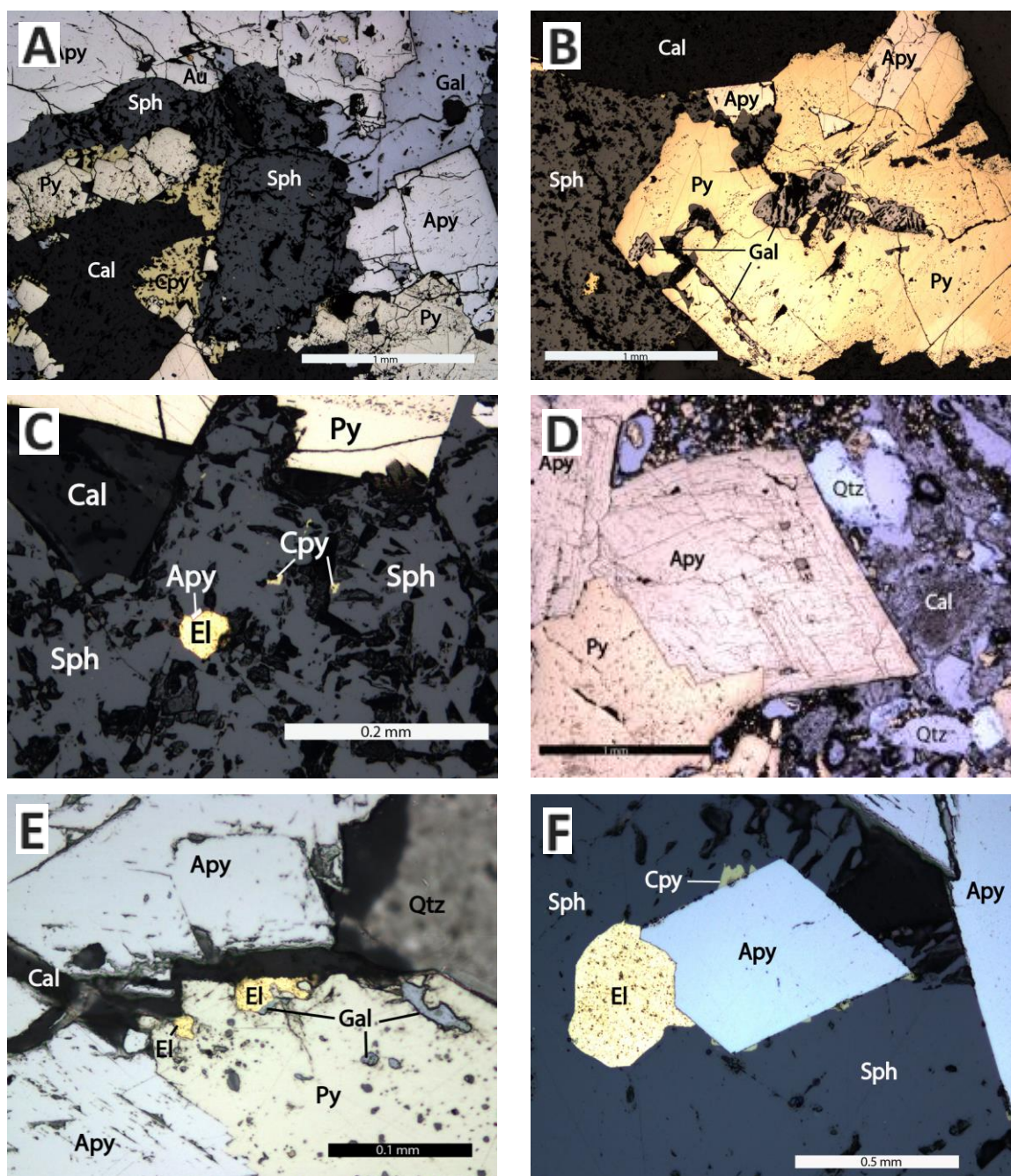


### **3.2.5 Arsenopyrite Petrography**

**Ore Stage 1** Arsenopyrite dominantly formed subhedral masses interstitial to pyrite within veins and mantos (Figure 14B, Figure 14C). Arsenopyrite was disseminated near veins which were relatively arsenopyrite-rich. Grain size of arsenopyrite ranges from 0.005mm to 2cm, and arsenopyrite makes up roughly 5%-15% of ore stage sulfides. Arsenopyrite is similar to pyrite in terms of relationships and timing, though in some samples arsenopyrite was earlier or later than pyrite (Figure 14B, Figure 15D, Figure 15E). Occasionally, euhedral arsenopyrite crystals formed adjacent to stage 1, free electrum grains (Figure 15C, Figure 15F).

**Ore Stage 2b** Minor, stage 2b arsenopyrite was observed only in a late silver-mineral bearing vein that cut earlier, massive-textured sphalerite. The arsenopyrite was euhedral and formed near stage 2b pyrite. Arsenopyrite is not associated with the distinct, stage 2a fracture filling electrum and acanthite. Arsenopyrite is not part of pre-ore or post-ore events.

Growth zonations in both arsenopyrite and sphalerite indicate changes in fluid composition during formation of these sulfides. The zonations were observed in reflected light under a cross polarizing lens, and formed as alternating bands that grew outward from the sulfide grain center.



**Figure 15:** Photomicrographs of arsenopyrite and sphalerite textures at Camino Rojo. A) Hole 369/643 m (1CR26); RfL; intergrown sphalerite-arsenopyrite-galena-pyrite-chalcopyrite and later calcite vein; B) Hole 370/660 m (1CR30), RfL; pyrite-arsenopyrite-sphalerite vein with later galena; arsenopyrite is euhedral and slightly earlier than pyrite; C) Hole 369/643 m (1CR26), RfL; massive sphalerite formed after euhedral pyrite; fine electrum and arsenopyrite are included in sphalerite; D) Hole 436/618.7 m (3CR08); reflected light (RfL); euhedral arsenopyrite crystal within mantos; E) Hole 370/647 m (1CR29), RfL; near-contemporaneous pyrite and arsenopyrite vein with later galena, electrum, and calcite; F) Hole 369/643 m (1CR26); RfL; euhedral arsenopyrite with electrum within sphalerite; small chalcopyrite reaction rim around the arsenopyrite grain.

### **3.2.6 *Chalcopyrite and Galena Petrography***

Though not volumetrically abundant, both chalcopyrite and galena were deposited during ore stage mineralization. Due to their similarity in occurrence, they are described together.

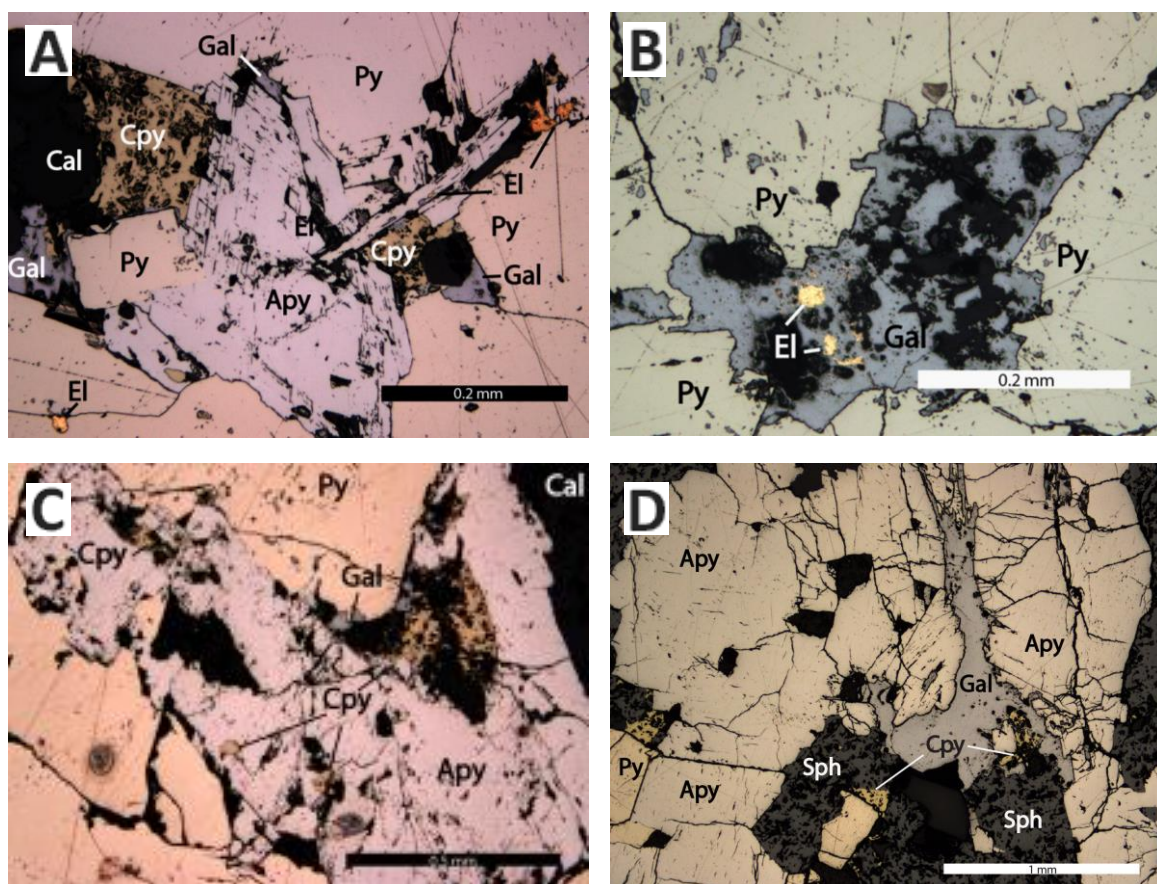
**Ore Stage 1** Chalcopyrite and galena make up approximately 5%-10% of the vein and manto sulfides at Camino Rojo. Both are typically fine grained, though they locally reach almost 1cm in size. These sulfides were rarely observed to be disseminated within the host rocks.

Chalcopyrite is a common exsolution phase within sphalerite (Nagase and Kojima, 1997), and at Camino Rojo the finest chalcopyrite grains occur as exsolved grains within sphalerite. Coarser chalcopyrite formed as anhedral masses later than, and intergranular to, pyrite, sphalerite and arsenopyrite (Figure 10).

Stage 1 galena is similar to stage 1 chalcopyrite in terms of timing (Figure 10). However, galena is typically finer-grained than chalcopyrite (Figure 15E; Figure 16A).

**Ore Stage 2** Chalcopyrite and galena in ore stage 2a fill fractures cutting stage 1 sulfides and are anhedral (Figure 16A, Figure 16B). They range in size from 0.005mm to 0.4mm, though chalcopyrite is typically finer-grained (Figure 16C, Figure 16D). Galena is the most common accessory sulfide to both electrum and the silver bearing minerals (described below).

Stage 2b galena is intimately associated and contemporaneous with the stage 2b silver minerals pyrargyrite, acanthite, and tennantite-tetrahedrite. Chalcopyrite is not part of stage 2b mineralization. Chalcopyrite and galena are not part of pre-ore or post-ore stages.



**Figure 16:** Photomicrographs of galena and chalcopyrite textures within veins and mantos. A) Hole 347/645m; (1CR12), reflected light (RfL); pyrite with later arsenopyrite, pyrite, and chalcopyrite, followed by stage 2a galena and electrum; B) Hole 370/721m (1CR31), RfL; late galena-electrum filled fractures within a pyrite vein; C) Hole 347/645m; (1CR12), RfL; near-contemporaneous pyrite and arsenopyrite with later chalcopyrite, galena, and calcite; D) Hole 369/643m (1CR26) intergranular arsenopyrite, pyrite, and sphalerite is followed by fracture-filling galena-chalcopyrite.

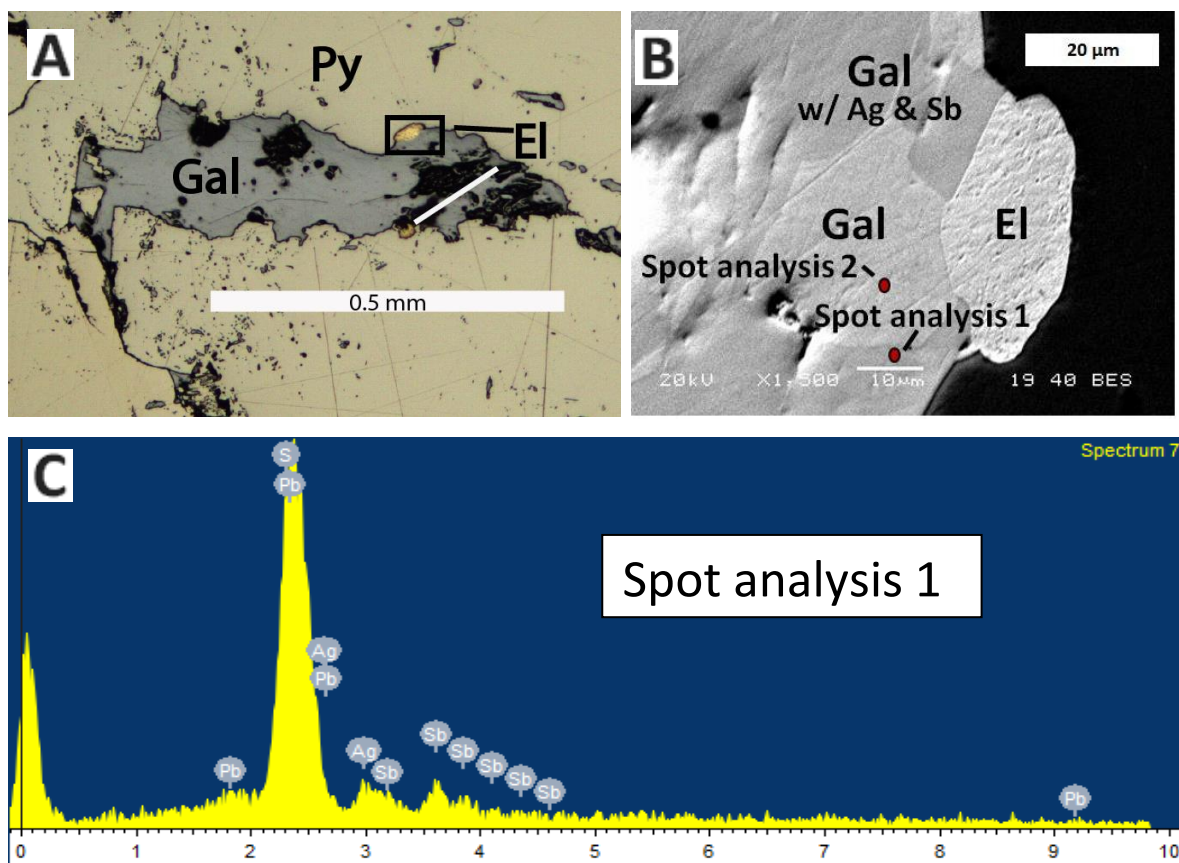
Energy-dispersive X-ray spectroscopy (EDS) with SEM analysis indicated that galena associated with ore stage 2a contained silver and antimony (Figure 17), while ore stage 1 galena did not contain these additional elements. Exact atomic amounts of the silver and antimony present are not known. Un-calibrated, semi-quantitative data collected with the SEM indicated that the atomic percent of silver in stage 2 galena associated with electrum roughly ranged from <2% to 13% Ag.

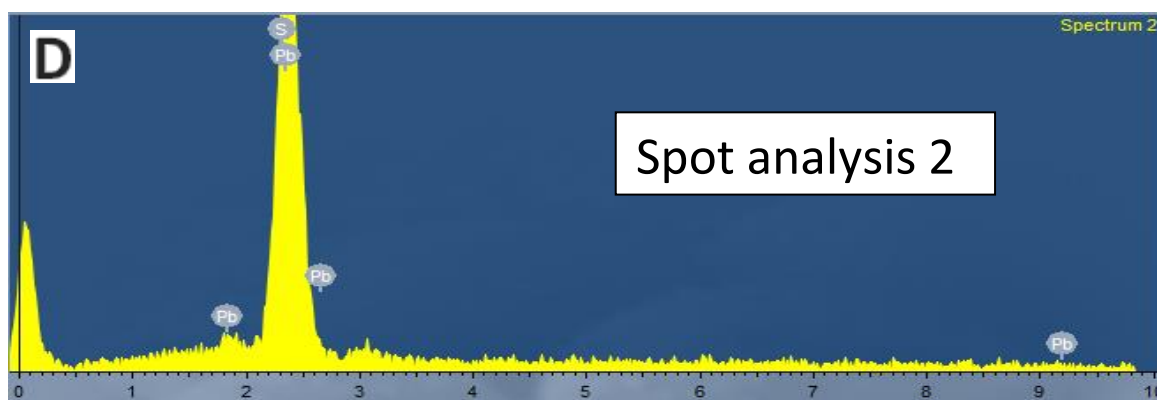
For comparison, in the analysis of silver-bearing galena in the Santa Eulalia district, coupled substitution of silver and antimony for the lead in galena ranged from 0.04 to 5.9 atomic% silver and 0.10 to 7.2 atomic % antimony (Lueth et al., 2000). Argentiferous galena is often a primary silver-bearing phase in ore deposits, including Mexican epithermal systems (Lueth et al., 2000), and galena containing silver and antimony at Camino Rojo follows this pattern.

From review of the assay data for 29 selected drill holes, an average of 400ppm lead can be compared to an average of 5ppm silver. These averaged values were used to calculate the hypothetical mole fraction of silver in galena to determine if it is possible for galena to completely host the silver endowment at the deposit. For this calculation, it was assumed all lead assays were attributed to galena, and the silver was hosted only in galena. The mole fraction of silver in galena necessary to produce the averaged assay values above was calculated to be 0.024 or 2.4 mole%. This hypothetical molar ratio is possible, and the calculation demonstrates that galena may be a significant silver-hosting mineral at the deposit. It is clear the silver endowment is not solely present in galena as the silver minerals acanthite, tennantite/tetrahedrite, and pyrargyrite were deposited at Camino Rojo (see Section 3.2.9).

Though silver was identified within stage 2a galena using a SEM, it is unknown if the silver is present as inclusions or as crystal lattice substitutions, as it is not identifiable as a separate phase with SEM imagery (Figure 17A, Figure 17B - 1500x magnification). Individual grains of silver-bearing minerals were not observed with the SEM resolution of 1 $\mu$ m, and the silver and antimony identified in EDS spectra may instead be substituted into the lattice of the galena (Figure 17C).

The SEM back-scatter electron image (BEI) in Figure 17B shows a compositional difference between lighter- and darker-colored parts of stage 2a galena. EDS spot analysis indicates that the darker-colored galena contains silver and antimony (Figure 17C), though in contrast the smaller, lighter area is only lead sulfide (Figure 17D).



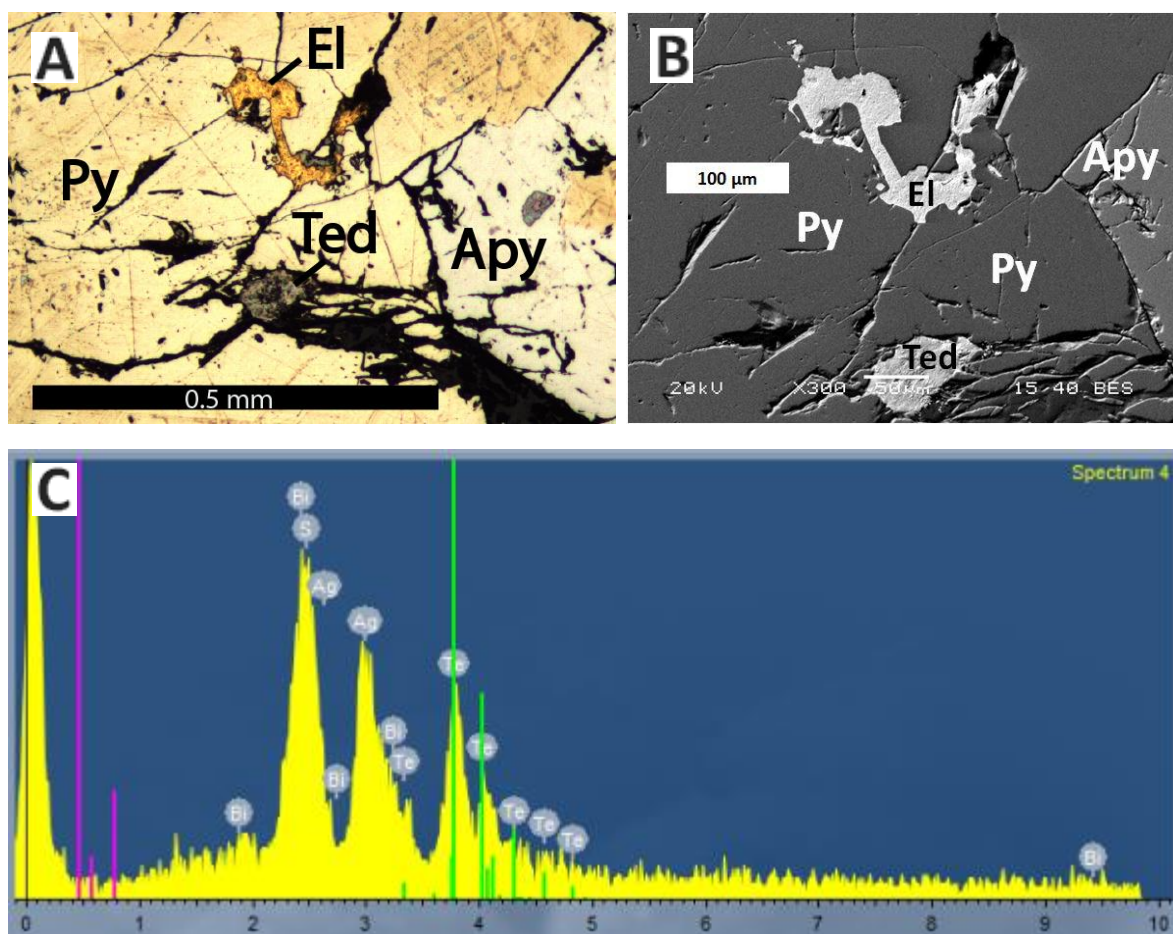


**Figure 17:** Stage 2a galena associated with electrum from hole 370/721m (1CR31). A) Stage 2a galena and electrum in fractures within a pyrite vein; B) SEM BEI image of stage 2a electrum and galena (area is indicated by the black box in 17A); C) spot analysis 1: EDS spectra shows galena with antimony and silver; D) spot analysis 2: comparative EDS spectra of lighter-colored galena lacks silver and antimony.

### 3.2.7 Tetradyomite ( $\text{Bi}_2\text{Te}_2\text{S}$ )

**Stage 2a** Tetradyomite has been observed in stage 2a mineralization near electrum (Figure 18). This bismuth-tellurium sulfide was discovered in only one sample from Hole 345/616.7m with SEM analysis, and has not been observed in other paragenetic stages. SEM EDS spot analysis showed a non-uniform, elemental composition of the tetradyomite grain. The bismuth-tellurium-sulfur grain also included variable amounts of silver, lead, and minor iron.

Bismuth has also been observed as native bismuth in a sample from hole 436/618.7m. This sample contained a pyrite vein with stage 2a electrum, where a 5 $\mu\text{m}$  grain of native bismuth was discovered at the edge of a stage 2a galena grain.



**Figure 18:** Photomicrograph and SEM analysis of stage 2a tetradymite. The sample is from Hole 345/616.7m (1CR09). A) Stage 2a electrum and tetradymite filled fractures within prytite; B) SEM image with similar field of view and scale as A; note the bright tetradymite (ted); C) SEM EDS spectra shows peaks indicating Bi-Te-S-Ag.



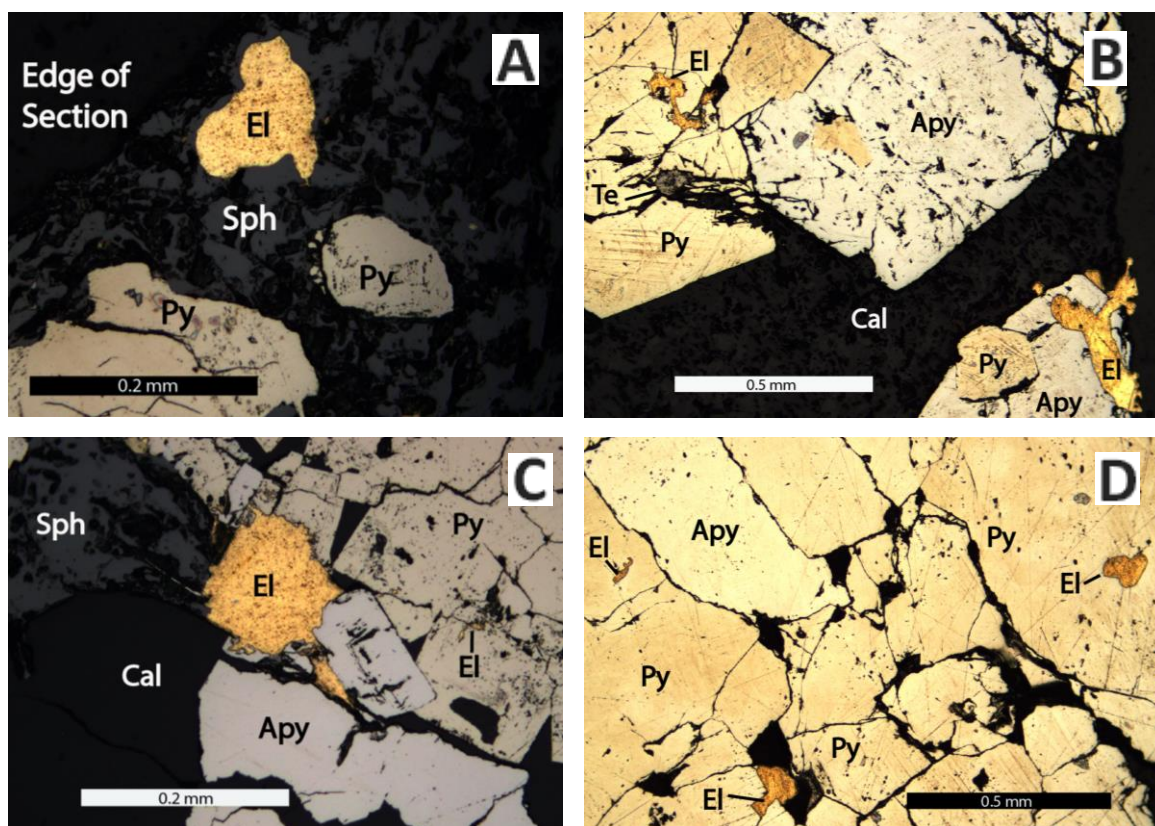
### **3.2.8 Electrum Petrography**

Electrum grains range in size from 0.01mm to as large as 0.5mm, though most grains are between 0.1 and 0.2mm. In the majority of cases, electrum compositions vary from the average of 25Ag/75Au at the center of electrum grains to a thin margin of 45Ag/ 55Au at grain edges, as determined through SEM analysis. No significant electrum compositional zonation was identified based on spatial or temporal variations. Through visual examination of thin sections, roughly 10%-15% of electrum was deposited during ore stage 1 and 85%-90% of electrum formed in ore stage 2a (Figure 10).

**Ore Stage 1** Stage 1 electrum is often equidimensional and associated with stage 1 arsenopyrite and pyrite. It is often encapsulated by sphalerite and adjacent to euhedral arsenopyrite grains (Figure 15C, Figure 19A, Figure 15F). Electrum in stage 1 is located in the outer portions of stage 1 pyrite and sphalerite grains, which suggests it was deposited in the latter portion of ore stage 1 (Figure 10). Stage 1 electrum does not clearly fill fractures through stage 1 massive-textured sulfides, and therefore did not form after ore stage 1.

**Ore Stage 2a** The majority of electrum at the deposit filled micro fractures that cut earlier mantos and veins. Some grains appear to branch into multiple fractures (Figure 19B, Figure 19C). Galena, chalcopyrite, and minor tetradymite were deposited with stage 2a electrum in the same fractures. Stage 1 vein size does not appear to control stage 2a electrum deposition, and late electrum is present in pyrite veins less than 1cm in width.

In some samples, equidimensional electrum grains were found in very fine, discontinuous micro fractures at the edges of stage 1 pyrite or arsenopyrite (Figure 15E, Figure 16A, Figure 19D). It is not clear if these electrum grains are part of stage 1 or stage 2a.



**Figure 19:** Photomicrographs of electrum within sulfide veins and mantos at Camino Rojo. A) Hole 360/ 643m; Reflected Light (Rfl); stage 1, oval-shaped electrum within sphalerite; B) Hole 345/616.7m (1CR09); Rfl; stage 2a electrum filled fractures through arsenopyrite-pyrite vein; C) Hole 360/ 643m; (1CR26) Rfl; stage 2a electrum later than surrounding pyrite-arsenopyrite-sphalerite-calcite; D) Hole 345/616.7m; Rfl; pyrite vein with equidimensional, stage 2a electrum blebs in micro fractures.

### 3.2.9 Petrography of Silver Minerals

The silver sulfide acanthite was deposited during ore stage 2a. Both acanthite and the silver-bearing sulfosalts pyrrargyrite and tennantite-tetrahedrite were deposited during stage 2b (Figure 10). Camino Rojo silver minerals were contemporaneous with galena, and stage 2a galena can contain silver and antimony substitutions, as discussed in section 3.2.6.

**Ore Stage 2a** Acanthite filled fractures through earlier stage 1 pyrite and arsenopyrite.

Stage 2a acanthite tends to be irregular and formed singularly or in the same fractures with stage 2a electrum (Figure 20A, Figure 20B). Additionally, a unique silver-selenium sulfide was identified by SEM EDS spectra, intergrown with stage 2a galena (Hole 370/647.2m - Figure 20C). A small percentage of very fine, stage 2a sulfides have optical characteristics similar to both acanthite and galena, but are too small to be clearly distinguished (Figure 11C).

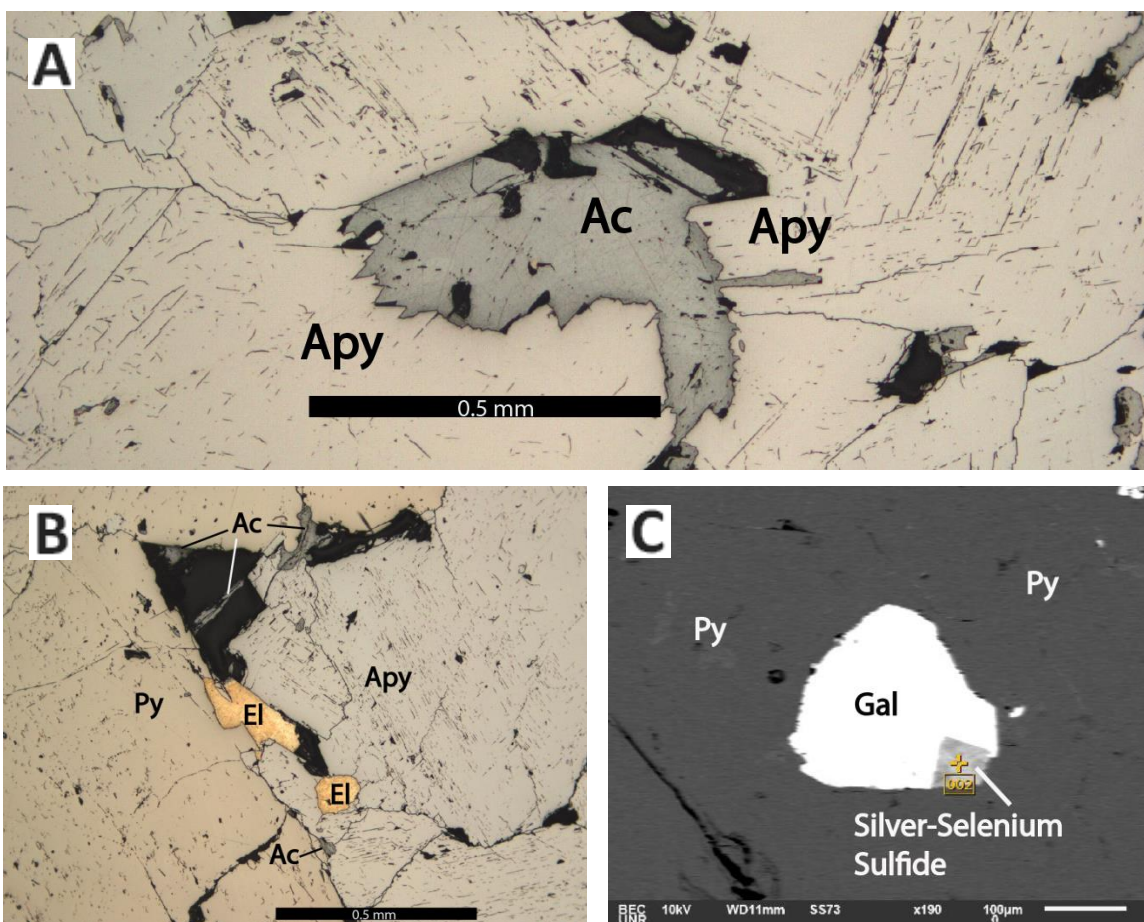
**Ore Stage 2b** Ore stage 2b is represented by a quartz-pyrite-silver sulfosalt vein which cuts an earlier, stage 1 massive-textured sphalerite vein; both veins are perpendicular to bedding (Figure 20D). SEM EDS analysis of this high grade silver vein revealed the silver minerals pyrrargyrite, acanthite, and less abundant, argentiferous tetrahedrite- tennantite containing minor iron (Figure 20E). The stage 2b vein is distinct in texture and mineralogy from the fracture-filling stage 2a galena-electrum-chalcopyrite. This is the only example of ore stage 2b identified in the samples collected for this study, and was found in Hole 375/286m.

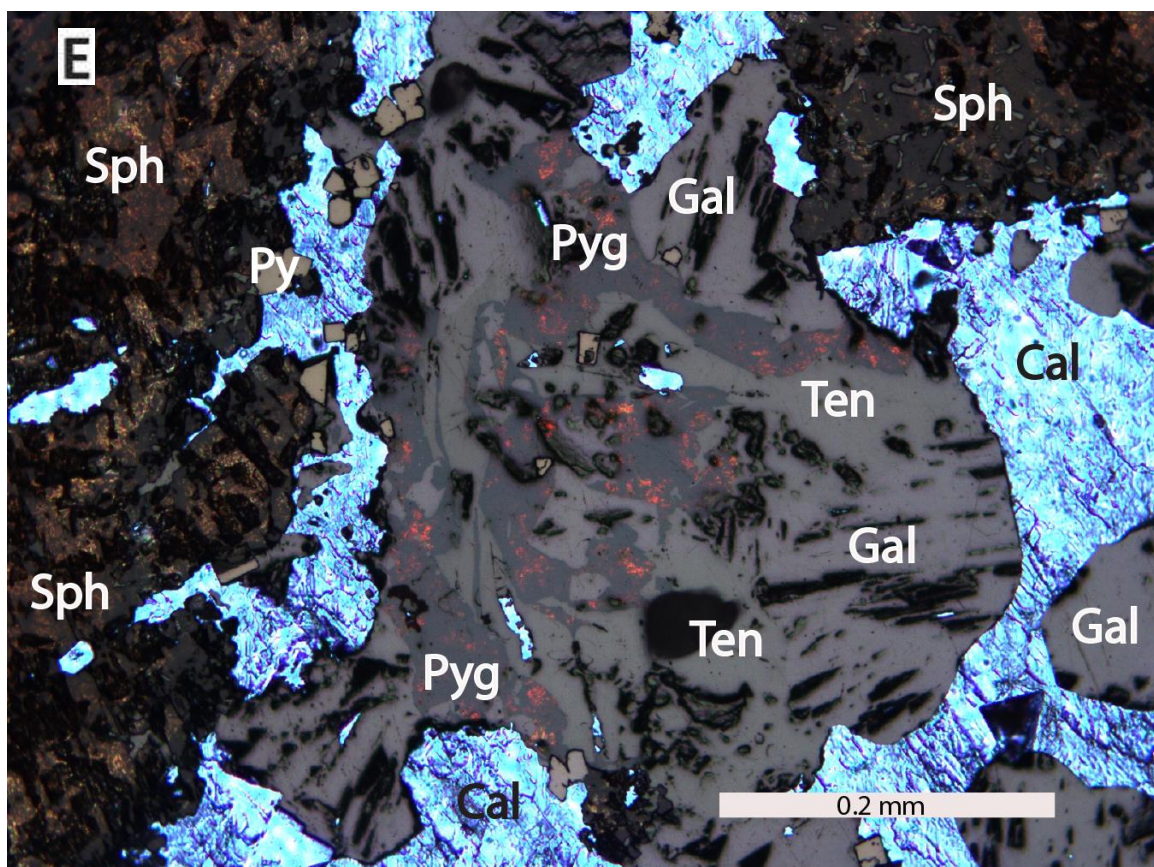
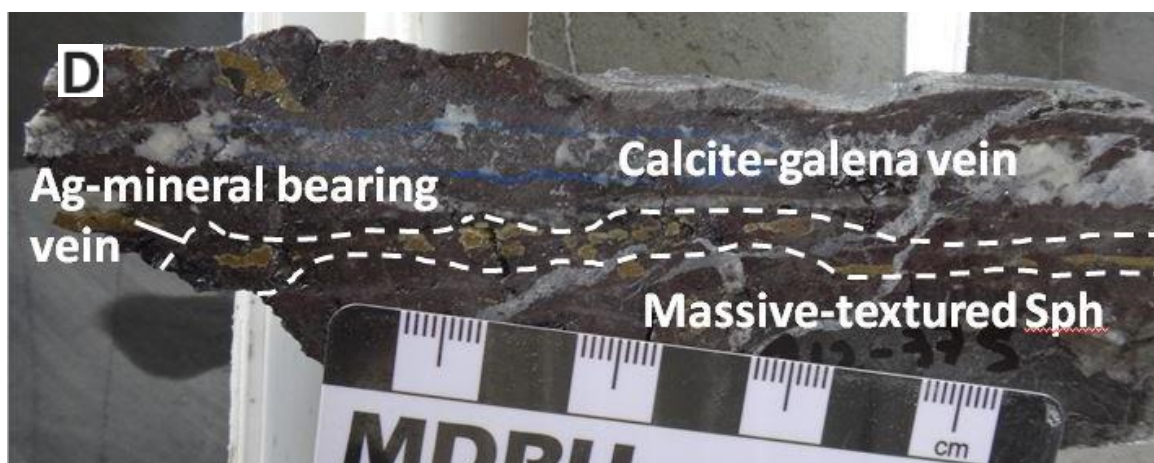
The ore stage 2b sample also contains narrow, discontinuous acanthite veinlets. These veinlets appear to originate at the edges of the larger 2b vein and cut stage 1, massive-textured sphalerite (Figure 20F). The acanthite veinlets are interpreted to be part of stage 2b, and are accompanied by fine-grained inclusions of silver-bearing minerals, possibly acanthite or pyrrargyrite, that occur in sphalerite (Figure 20F).

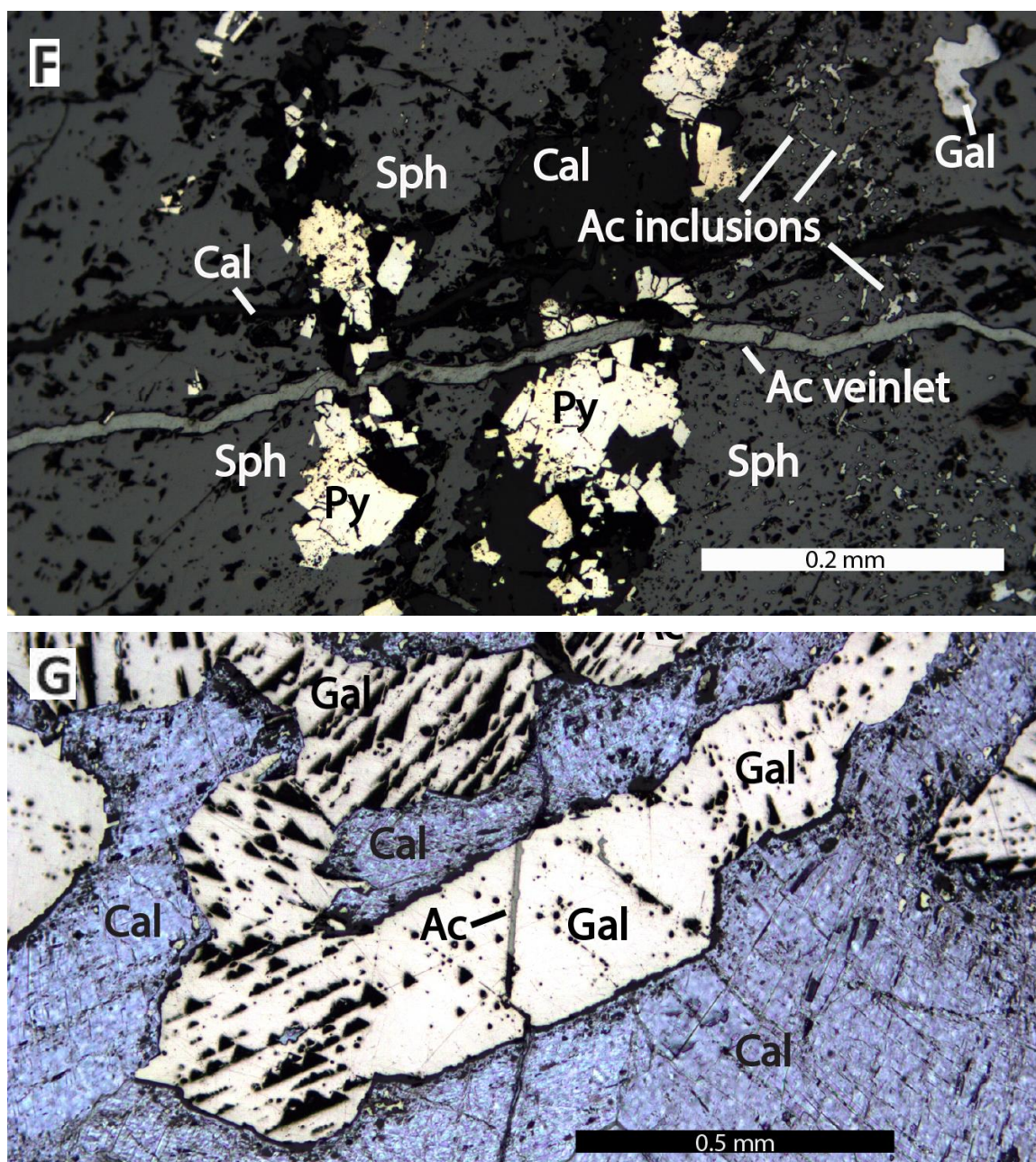
In Figure 20D, the stage 2b silver-rich vein is adjacent to and parallels a prominent calcite-galena-minor acanthite vein, which contains unusual, hexagonal galena crystals and cuts the stage 1 massive-textured sphalerite. The acanthite in this vein forms fine, discontinuous, internal veinlets that in part follow cleavage within the galena and do not continue through the calcite (Figure 20G). The calcite-galena- minor acanthite vein is tentatively assigned to ore stage

2b as it a) cuts stage 1 sphalerite, b) does not fill microfractures with stage 2a chalcopyrite and electrum, and c) is cut by later, post-ore calcite veins.

It is assumed there are additional, silver-rich stage 2b veins at Camino Rojo. The stage 2b sample described in this study may correspond to the silver-rich calcite veins that Goldcorp geologists have identified on the fringes of the West Extension zone and at Don Julio. Samples containing such veins are reported to contain silver contents on the order of 200-1000ppm (personal communication, S. Weiss, 2015).







**Figure 20:** Photographs of silver-rich samples at Camino Rojo. A & B from Hole 375/286m: A) Hole 436/618.7m; reflected light; stage 2a acanthite filled fractures in stage 1 arsenopyrite; B) Hole 436/618.7m; reflected light; stage 2a electrum and minor acanthite in fracture between stage 1 pyrite and arsenopyrite; C) Hole 370/ 647.2m; SEM image of a silver-selenium sulfide on the edge of late, round galena grain within pyrite; D) High grade, stage 2b silver-sulfosalt vein cuts massive-textured sphalerite; a late calcite-galena-acanthite vein also cuts the sphalerite; E) reflected and transmitted light photomicrograph; orange sphalerite around the edges; calcite surrounds a mass of galena, (elongate, triangular pits), pyrrargyrite (red internal reflections), and tennantite/ tetrahedrite (gray-green color); F) an acanthite veinlet cuts massive-textured sphalerite and later pyrite-calcite veins, note the fine silver mineral inclusions within the sphalerite, acanthite in this example; G) transmitted and reflected light; the calcite-hexagonal galena vein also contains minor acanthite which is limited to following the galena orientation.

#### 4 HYDROTHERMAL ALTERATION AT CAMINO ROJO

The alteration patterns surrounding the Camino Rojo deposit are important for understanding the deposit genesis. The timing for the alteration events is inferred from cross-cutting and overprinting relationships observed in thin section and drill core. From pre-ore to post-ore, alteration events at Camino Rojo occurred in the following order and are summarized in Table 4.1:

- (1) Early potassic metasomatism (pre-ore)
- (2) Calcite- sericite  $\pm$ pyrite  $\pm$ quartz alteration (ore-stage)
- (3) Late, overprinting calcite (post-ore)

The alteration stages identified at Camino Rojo are described further in the following sections.

Alteration Stage		Description
<b>Potassic Metasomatism</b> (Pre Ore)		Pervasive alteration of sedimentary host to K-feldspar
	Pyrite-Carbonate K	Weakly disseminated pyrite- carbonate (PC); 0-4% K-feldspar
	Weak K	5%-20% K-feldspar
	Moderate K	21%-40% K-feldspar
	Strong K	41%->75% K=feldspar
	RXL	Garnet-Magnetite metasomatic skarn alteration and recrystallization of the Indidura and Cuesta del Cura Formation
<b>Sericite-Calcite <math>\pm</math>Pyrite <math>\pm</math>Quartz</b> (Ore Stage)		Overprinting alteration associated with ore mineralization; sericite (illite/ muscovite) is the indicator mineral for this alteration stage
<b>Late Calcite</b> (Post Ore)		Calcite and pyrite are disseminated throughout the host, with many generations of cross-cutting calcite $\pm$ pyrite veinlets and coarser calcite veins; the disseminated pyrite is often bedding controlled

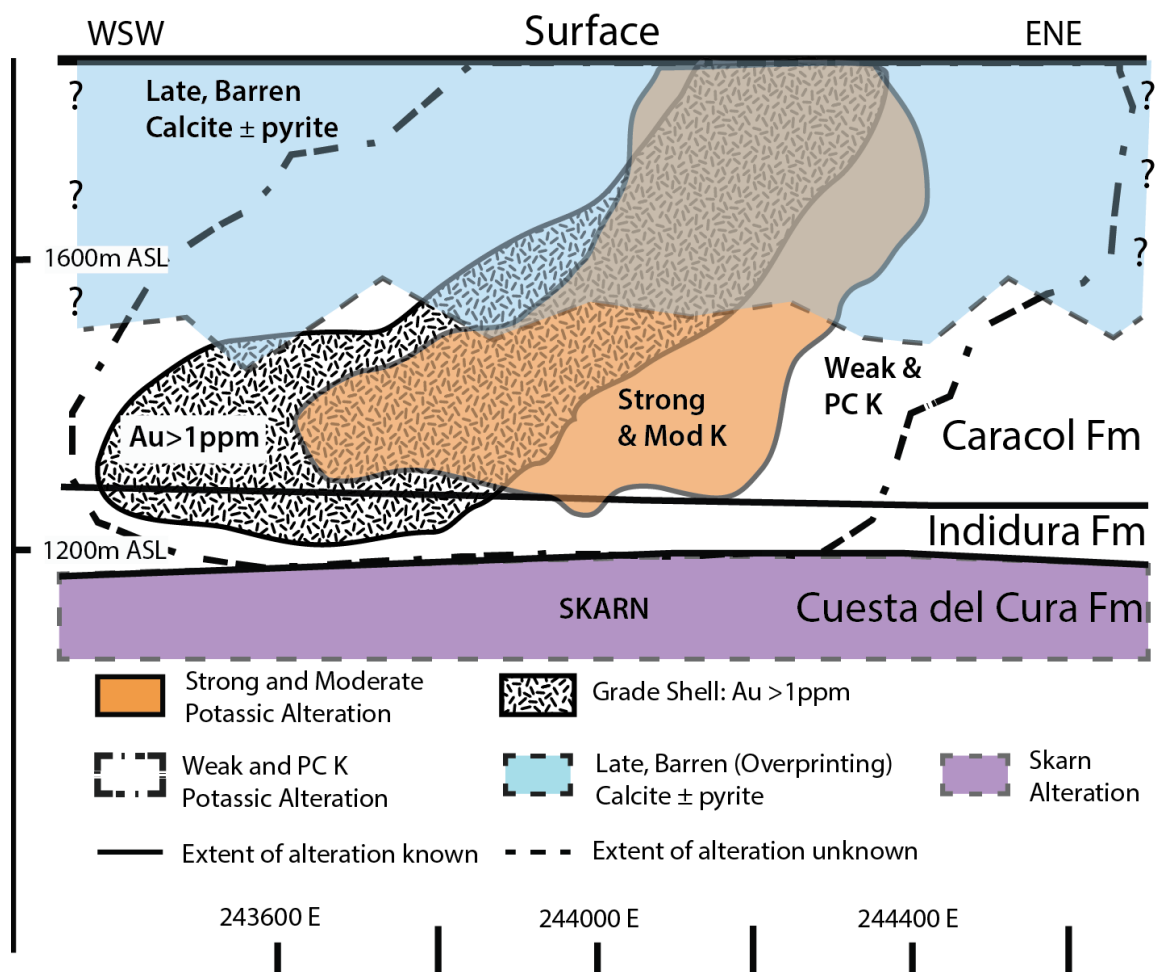
**Table 4.1:** Summary and description of alteration stages at Camino Rojo

Broadly, potassic alteration and gold mineralization are spatially coincident in some drill core. However, strong potassic alteration is slightly offset from the central area of gold mineralization (Figure 22). Additionally, the lack of detailed correlation between gold and the potassium alteration assemblage indicates that the two events are temporally distinct (Figure 21). Also, the ore-stage alteration texturally overprinted the pre-ore potassic alteration.

The ore stage sulfide assemblages are associated with the calcite-sericite alteration. The calcite-sericite assemblage is therefore considered the ore stage alteration. The sericite identified in transmitted light was further defined with reflectance spectroscopy as illite/muscovite and smectite, which are consistent with formation by weakly acidic hydrothermal fluids. The calcite-sericite alteration occurs in all mineralized samples that were examined in thin section, and does not occur in unmineralized specimens. Because the extent of the mineralized thin section specimens is much less than the extent of deposit gold mineralization, a gold >1ppm grade shell (Figure 21; see section 4.2 below) was constructed as a conservative estimate of the minimum spatial extent of the ore-stage alteration.

The late calcite-pyrite alteration cuts and overprints both previous alteration events, and is the last alteration event recognized in drill core and thin section. The calcite-pyrite alteration is identified by a concentration of late calcite ± pyrite vein networks which extend from the present surface to a depth of just over 400m (Figure 21).





**Figure 21:** Generalized schematic long-section with spatial relationships of the three alteration types at Camino Rojo. The Au > 1ppm grade shell was constructed as a proxy to estimate the calcite-sericite alteration geometry. The depth of the late calcite alteration is irregular. Looking north, the schematic cross section is oriented WSW-ENE along the deposit center.

#### 4.1 Potassic Metasomatism

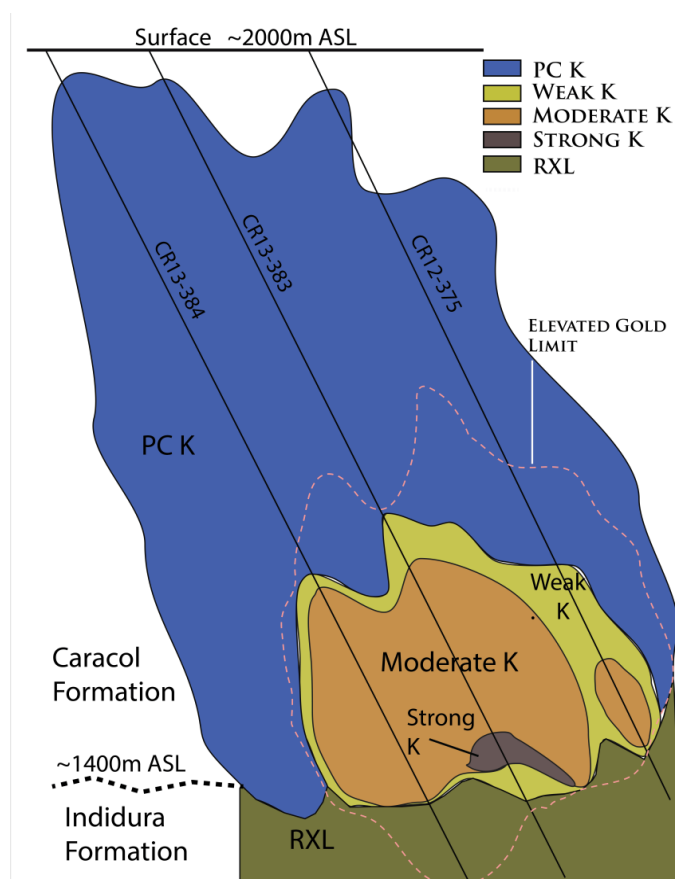
Potassic metasomatism is the most visible and distinct alteration in drill core at Camino Rojo. The potassic alteration is defined by fine-grained K-feldspar flooding of the host rocks. This flooding is accompanied by the loss of organic carbon and bleaching and hardening of the interbedded, carbonaceous shale and sandstone host rocks. In drill core, the potassic alteration extends vertically from the surface at the Represa zone to over 600m depth in the West Extension zone (Figure 21). The intensity of potassic alteration was quantified by visual estimation of the volume % of billet samples stained with sodium cobaltinitrite. In samples with minimal K-feldspar replacement, alteration is evidenced by disseminated, fine and euhedral pyrite and patchy carbonate within the host.

The intensity of potassic alteration in the host rocks changes gradationally in the West Extension zone (Figure 22), with little to no potassic alteration at the surface, to in excess of 75% K-feldspar at depth. For this study, potassic metasomatism at the deposit has been defined as follows: PC K= 0%-4% K-feldspar, with the introduction of pyrite-carbonate (PC); Weak K = 5%-20% K-feldspar; Moderate K = 21%-40% K-feldspar; and Strong K = 41%- >75% K-feldspar.

Four billets stained with sodium-cobaltinitrite are shown in Figure 23A. The amount of yellow staining indicates the location and abundance of K-feldspar, and clearly shows the various degrees of potassic alteration.

Little to no potassic substitution or replacement affected the underlying, carbonate-rich Indidura and Cuesta del Cura formations (generally <5% K-feldspar). Instead, these carbonate-rich host rocks were recrystallized, in some parts to marble, and less extensively to skarn.

The potassic alteration naming scheme defined above differs from the field terms used by Goldcorp's Camino Rojo geologists for core logging during 2012-2013 and earlier. At that time, the terms used to identify increasingly bleached and hardened rock were pyrite-carbonate (PC), weak quartz-sericite-pyrite-carbonate (weak QSPC), moderate quartz-sericite-pyrite-carbonate (moderate QSPC), and quartz-sericite-pyrite (QSP). The more bleached and hardened the rock, the stronger the assumed alteration. Though the Goldcorp terminology did not correctly reflect the potassic alteration which had occurred, Camino Rojo geologists were consistent with these field terms, which generally reflected the intensity of potassic alteration at Camino Rojo.



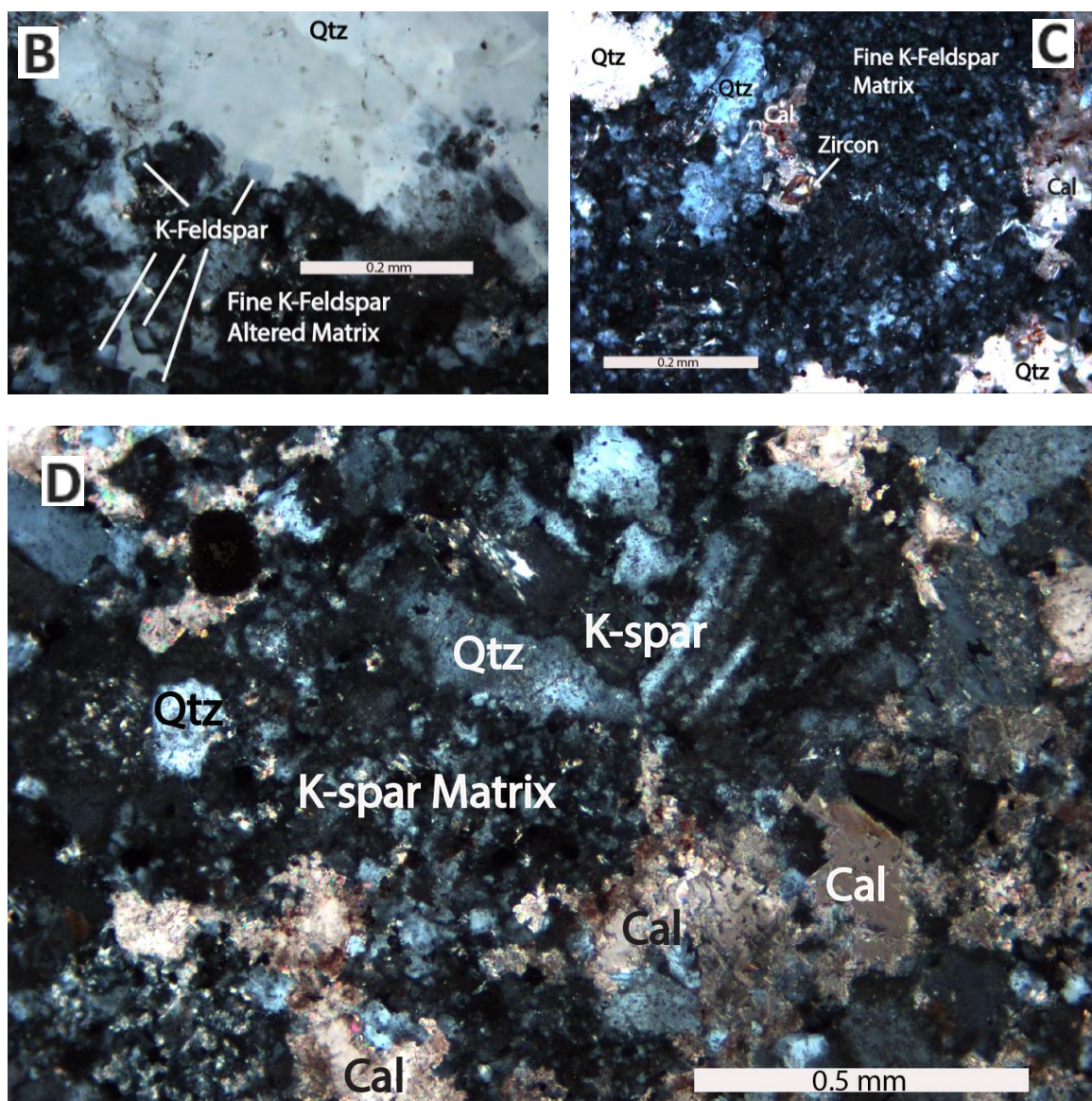
**Figure 22:** North-south cross section along ~243700 E in the West Extension zone, looking west. The Indidura Formation has been recrystallized (RXL). The pink dashed line indicates the elevated gold limit which extends beyond the potassic alteration. Three of several drill holes used to estimate the potassic alteration for this section are shown.

The potassic alteration initially replaced the host rock matrix with K-feldspar, as observed in thin sections. In photomicrographs, the K-feldspar-altered matrix is made up of very fine, intergrown grains that appear as speckled, black and white masses (Figure 23B, Figure 23C, Figure 23D). After the replacement of the sedimentary host matrix, larger detrital grains were replaced with K-feldspar by moderate to strong potassic alteration. In these instances, fine and rhombohedral K-feldspar crystals grew along the edges of original sedimentary quartz (Figure 23B).

Fine, subhedral, disseminated pyrite and carbonate are minor components of the potassic alteration. Calcite associated with potassic alteration occurs in irregular patches through the altered host matrices (Figure 23D). The patchy calcite may be a recrystallization of original carbonate within the sedimentary hosts.

Adularia, a low temperature K-feldspar mineral, is occasionally present as fine, euhedral to subhedral grains in veinlets and along the edges of some sulfide-quartz veins. Little to no secondary quartz is associated with the potassic alteration.





**Figure 23:** Photomicrographs of potassic metasomatism in the sedimentary host rocks at Camino Rojo. (A) Billets stained with sodium cobaltinitrite indicate weak to strong degrees of potassic alteration. The three photomicrographs are from Hole 349/663m (1CR16), crossed polars and Moderate K alteration: (B) matrix replaced by fine K-feldspar and K-feldspar crystal growth on the edges of a quartz grain; (C) The sedimentary matrix was replaced by fine, interlocked, anhedral K-feldspar with minor disseminated calcite; (D) matrix replaced by fine, interlocked, low birefringence K-feldspar with minor, disseminated, patchy calcite; a few original quartz and K-feldspar grains remain.

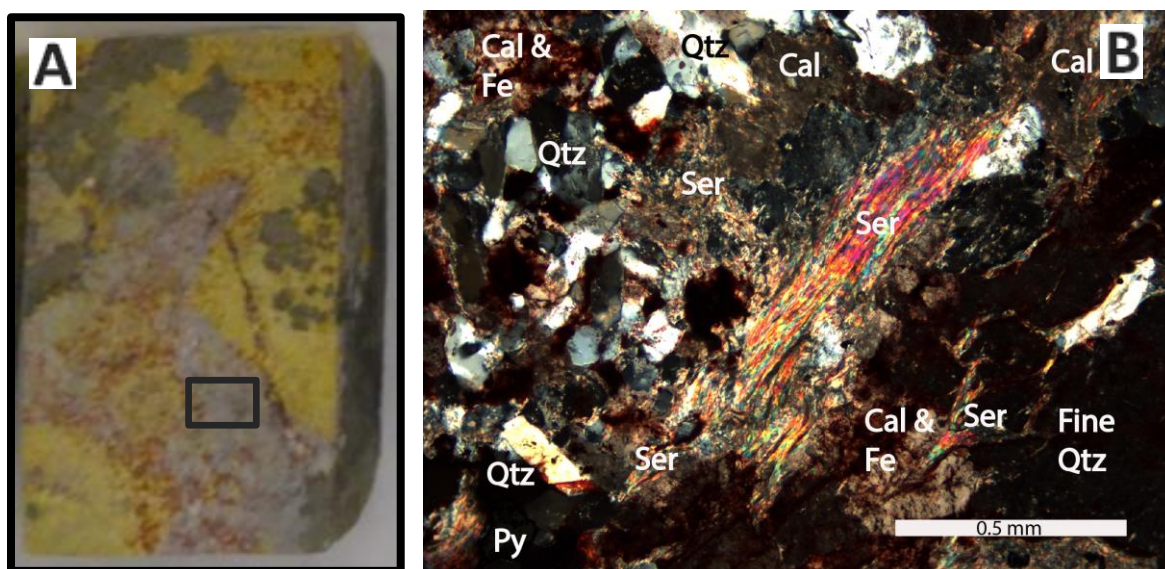
As a result of the widespread potassic alteration, many of the intermediate-composition dikes at Camino Rojo have been pervasively altered to mixtures of potassium feldspar and carbonate, with lesser amounts of chlorite, sericite, and pyrite. The altered dike samples typically contain fine aggregates of quartz in a sericitized plagioclase groundmass, along with aphanitic K-feldspar as an alteration mineral. Commonly, the altered dikes contain outlines of original, rhombohedral-shaped, mafic minerals in the fine, K-feldspar altered groundmass. Larson (2010) reported similar observations at Camino Rojo, and noted that the alteration mineral assemblage within the dikes is consistent with the potassic alteration the sedimentary host rocks at Camino Rojo. No spatial alteration patterns within the dikes were identified in this study.

#### **4.2 Calcite- Sericite- $\pm$ Pyrite $\pm$ Quartz Alteration**

The calcite- sericite  $\pm$ pyrite  $\pm$  quartz alteration is associated with ore-stage sulfide deposition. The diagnostic alteration minerals are sericite and quartz, though calcite is volumetrically more abundant. The ore-stage alteration minerals generally make up less than 5% of the altered samples, and are present in all mineralized thin sections.

The ore stage alteration overprints and cuts the potassic alteration (Figure 21). This relationship indicates that the potassic alteration was earlier than sulfide deposition and its associated calcite-sericite alteration. The relative timing of the potassic alteration and the calcite- sericite alteration is also clear in hole 349 at 669m depth (Figure 24). This breccia sample is composed of rounded, potassically altered clasts cemented by interlocked, subhedral to euhedral quartz grains with lesser amounts of sericite, iron oxides, and later calcite (Figure 24).

The fine-grained ore-stage calcite and sericite were deposited throughout the host rock matrix (Figure 25A). Where the ore-stage sericite was coarser-grained, the elongate micas formed a cross-hatch pattern in the host matrix. This pattern was the result of the calcite-sericite alteration overprinting the potassically altered host rocks, wherein the lattice structure of the earlier K-feldspar controlled the orientation of the growth of sericite crystals (Figure 25B).



**Figure 24:** Breccia sample composed of potassically altered, rounded clasts cemented by the ore-related calcite-sericite- ± pyrite± quartz alteration. The sample is from Hole 349/669m (1CR17). (A) Stained billet of the breccia sample where yellow indicates potassic alteration of the rounded clasts (the billet is 2cm across); (B) crossed polars (xPL): photomicrograph of interlocked, cementing quartz, as well as minor calcite, sericite and oxidized iron.

The amount of ore-stage alteration quartz can vary over small distances (<1m), from no quartz added, to patchy silicification of the host rocks, breccias and some mantos. Some original quartz within the sedimentary hosts appears to have been recrystallized by the hydrothermal fluids associated with mineralization, and a recrystallized quartz texture is common in the sedimentary host rocks (figure 25A). The recrystallized quartz formed a jigsaw texture in the host rock matrix (Figure 25C), similar to the interlocked quartz grains in Figure 24. The most

unequivocal added quartz is present in small amounts in veins and breccia cement.

Hydrothermal quartz as veinlets or breccia cement at Camino Rojo (Figure 25D, quartz veinlet) with or without adularia or calcite present, has been previously noted (Larson, 2010). Overall, hydrothermal quartz is a minor gangue mineral at Camino Rojo.

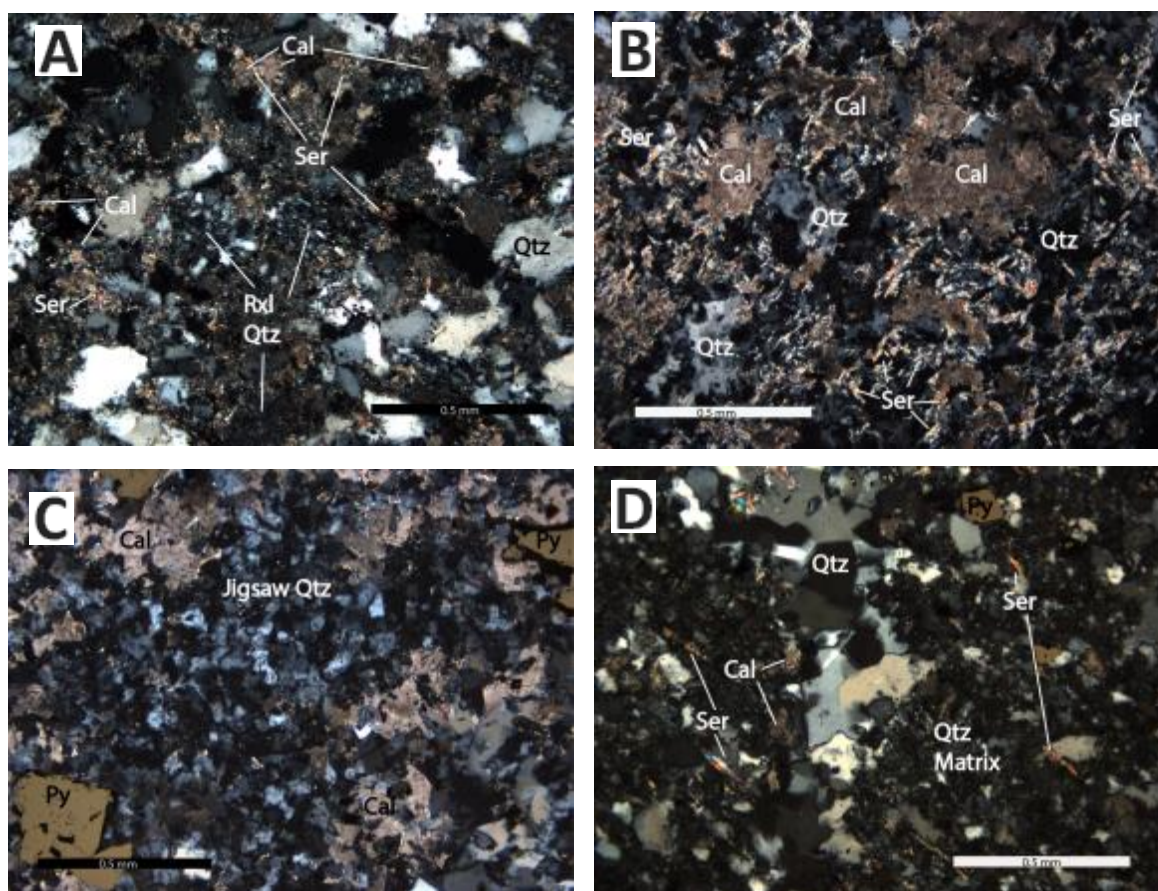
Ore-stage alteration within the dikes consists of a sericite-chlorite-carbonate assemblage with varying amounts of pyrite and minor quartz. This assemblage can be moderately to strongly developed within the dikes, and overprints an earlier potassic alteration of K-feldspar and minor biotite and chlorite. Rutile and apatite remain as minor components within the intrusive groundmass.

The calcite-sericite alteration assemblage extends to the edges of all gold mineralized thin sections, and is absent from unmineralized rocks. Because of this relationship it can be inferred that the calcite-sericite alteration is present throughout the extent of the deposit, even though the sample set is relatively small. To approximate the extent of this assemblage, a gold >1ppm grade shell (Figure 21) was modeled as a proxy for the calcite- sericite± pyrite ± quartz alteration.

The gold >1ppm shell (Figure 21) was modeled from a subset of 22 drill holes selected by Goldcorp from the Camino Rojo assay data base, with the majority of holes concentrated in the West Extension zone. (Note: though assay data were received for 29 drill holes, correlating alteration data were not available at the time for the seven most current drill holes, resulting in only 22 drill holes used within the Leapfrog 3D modeling software.) Assay data for the drill holes were received in the fall of 2014. Gold was determined by fire assay; see section 5 for details. The gold >1ppm assay shell is an approximate and minimum estimate for the ore-alteration extent. Sericite indicative of the ore stage alteration is present in thin section samples with gold



assays as low as 0.3ppm. Lower-grade gold assay shells were poorly constrained and therefore not used.



**Figure 25:** Photomicrographs of the ore-related sericite-calcite  $\pm$  quartz  $\pm$  pyrite alteration within the sedimentary Caracol Formation. (A) Hole 370/618 m (1CR27), crossed polars (xPL); addition of calcite and sericite, and recrystallization of the original, sedimentary quartz; (B) Hole 390/595 m, (3CR05), xPL; crossed-hatched sericite texture, elongated sericite formed with calcite and quartz; (C) Hole 390/595 m(3CR05), xPL; jigsaw quartz texture within matrix of altered sedimentary host rock; (D) Hole 370/647 M (1CR29), xPL; an irregular quartz veinlet cuts through altered host rock with disseminated pyrite-sericite-calcite.

#### **4.2.1 Illite/ Muscovite and smectite as part of ore-related alteration**

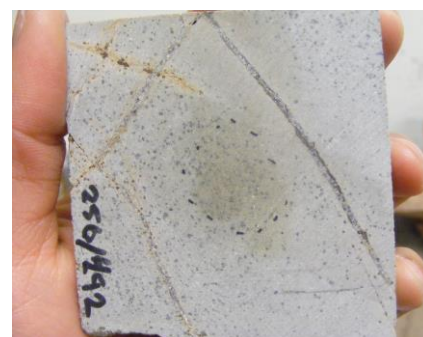
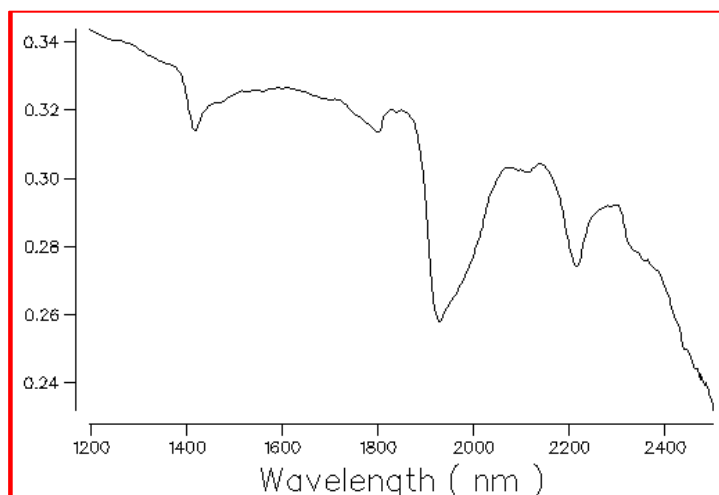
An ASD™ portable reflectance spectrometer was used to investigate the phyllosilicate component of several core samples from Camino Rojo. Illite/muscovite and smectite were the two main phyllosilicates identified using reflected light spectroscopy.

None of the core samples collected from Camino Rojo were ideal candidates for reflectance spectroscopy due to variable amounts of carbon, disseminated pyrite, iron oxides, and calcite. The majority of collected samples were dark in color and non-reflective, and the additional carbonate and sulfide mineralogy in many lighter-colored samples resulted in several near-flat, non-distinguishable peaks and spectra that could not be interpreted. In addition, the mineralogy identified by the reflectance spectrometer does not make up a significant portion of any sample.

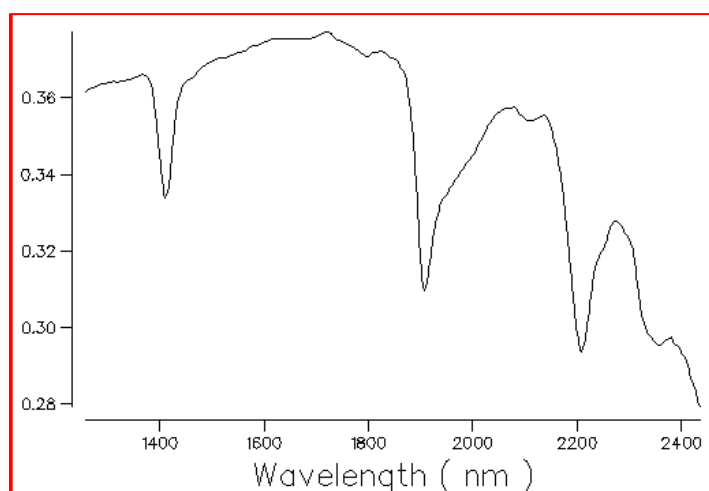
Samples with strong potassic alteration, being lighter in color, gave the most distinguishable spectra for the analyzed rocks. Nearly all analyzed samples contained a mixture of hydrothermal illite/muscovite and smectite (Figure 26), indicating a neutral to near-neutral pH environment. Variable amounts of calcite and rare kaolinite, chlorite, and silica were identified in some samples, in addition to illite/ muscovite and smectite.

The spectra for two analyzed samples are shown in Figure 26. For both samples, interlayered illite and smectite resulted in a deep, downward absorption feature at 1900nm, the indicator for H<sub>2</sub>O. An inflection point indicative of chlorite is observed near the 2250 wavelength. Though both samples in Figure 26 indicate the same phyllosilicate mineralogy, the spectra are shaped differently due to variable amounts of interference from chlorite, sulfides, and calcite. Calcite features were not distinguishable in the resultant spectra though both samples reacted to hydrochloric acid.

Illite is distinguished from muscovite by a water feature at 1900 nm. Small features at 2343 and 2450 would indicate muscovite, though these features are not distinct in Camino Rojo spectra.



**A**



**B**

**Figure 26:** Illite/muscovite clays were determined from reflected light spectroscopy. A) Hole 256/ 492 m, Strong K alteration of Caracol Formation; interlayered illite/ smectite (a broad single downward point at 1420nm, with a small shoulder) is indicated; B) Hole 349/727 m, illite is indicated in this altered dike sample through a single sharp downward spike in data at 1414nm, a large water feature at 1900nm, and a single sharp dip at 2208nm.

### 4.3 Late, Overprinting Calcite ± Pyrite

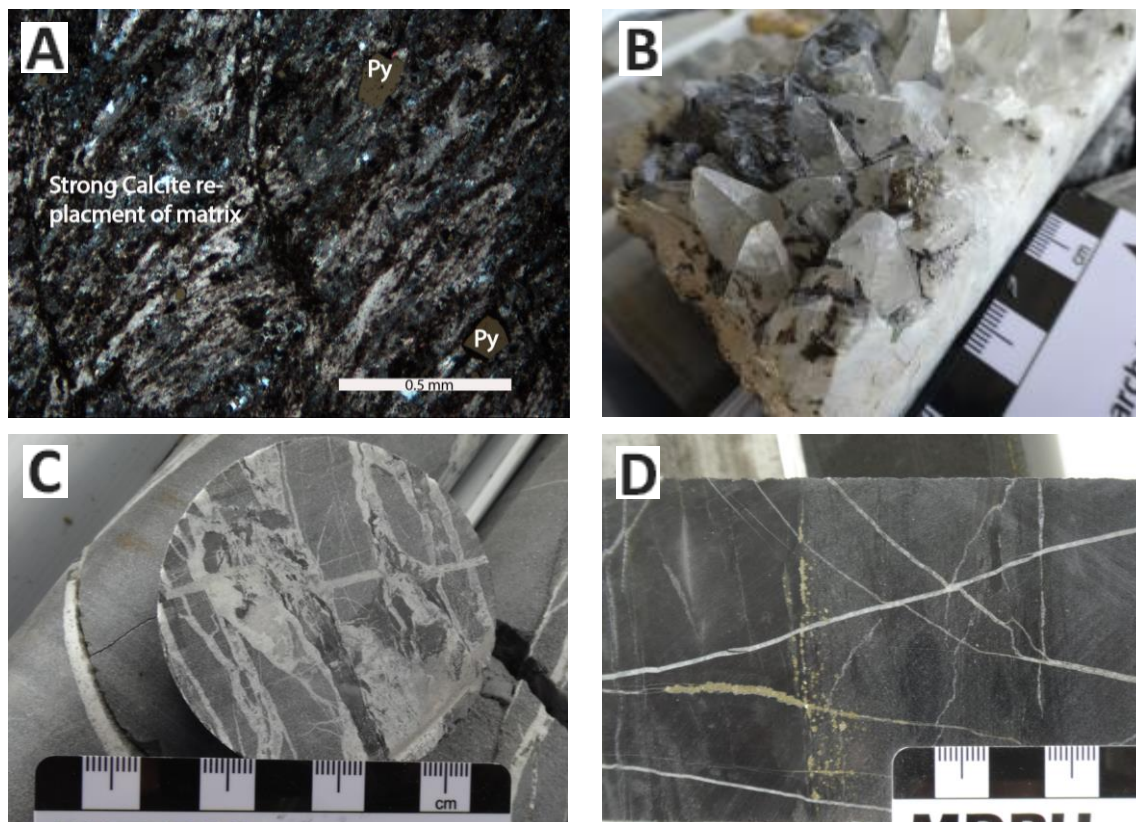
The final alteration stage is barren calcite and pyrite which cut earlier alteration stages and sulfide mineralization. The late alteration produced calcite-pyrite flooding of the host lithologies (Figure 27A), large veins of blocky or dogtooth calcite (Figure 27B), and multiple generations of calcite ± pyrite veinlets (Figure 27C, Figure 27D). The late calcite alteration stage extends variably at depth, to as much as approximately 400m below the surface.

The late calcite alteration contains up to 5% pyrite. Late stage pyrite is euhedral to subhedral, and can be distinguished from earlier pyrite only by clear association with late stage calcite veining or dissemination. The majority of late pyrite was deposited as fine grains (<1mm) along bedding planes, in fractures, and as part of some late calcite veinlets. The largest pyrite grains, up to 1cm in size, were observed only within coarse, dogtooth calcite veins.

Intermittent, patchy, late calcite and pyrite most commonly occur in bands along bedding at Camino Rojo. Flooding of calcite and pyrite outward from late-stage veins is also common. Some pre-existing carbonate within the host rocks may have been recrystallized by the late, calcite-pyrite bearing hydrothermal fluids, similar to the recrystallization of quartz during ore-stage alteration. The density of late calcite veins and veinlets is variable, though stockworks and sheeted calcite veinlets appear to increase with depth in the West Extension zone to just over 400m below the surface, and veining is probably fracture controlled. Black organic carbon, possibly a hydrocarbon residue, is present in some of the late calcite veins (Figure 27C).

Distinguishing between pre-ore (potassic), ore-stage (calcite-sericite) and post-ore (late calcite) disseminated calcite is only possible by clear association with the diagnostic minerals of each alteration stage. Shallow calcite-pyrite dissemination and veining is the result of the late

calcite-pyrite alteration stage, when not associated with pre-ore and ore stage mineralogical suites.



**Figure 27:** Photographs of late-stage calcite-pyrite flooding and veining at Camino Rojo. (A) Photomicrograph, Hole 345/446.7 m (2CR11), xPL: strong calcite flooding (<50%) of sedimentary host rock with minor disseminated pyrite; (B) Hole 448/226.5m; coarse, dogtooth calcite vein with pyrite; (C) Hole 376/517 m; calcite vein swarms; (D) Hole 375/ 311 m; fine, cross-cutting calcite-pyrite veins with pyrite disseminated along bedding (scale in cm).

#### 4.4 Contact Metamorphism, Skarn and Recrystallization at Camino Rojo

In thin section, the altered Caracol Formation rock matrix is composed of fine, prismatic and equigranular, interlocked grains of dominantly potassium feldspar and quartz. This texture is similar to a hornfels texture and could be the result of temperature, instead of, or in addition to, the potassic metasomatism prior to the ore-stage alteration.

The lower Indidura into the Cuesta del Cura and below have been recrystallized to marble. The marble recrystallization (Table 4.1) indicates that Camino Rojo mineralization is peripheral to a major thermal event at depth. In addition, in 2014 Goldcorp geologists at Camino Rojo were keying in on hornfels textures in the Caracol Formation as an important alteration event. The altered and hardened Caracol Formation and the strong recrystallization to marble of parts of the Indidura and Cuesta del Cura formations can be interpreted as the result of contact metamorphism. The dikes within the deposit give evidence for a nearby, perhaps deeper and composite, larger magmatic body. This deeper magmatic body may be responsible for the heat required to produce hornfels and may also be related to the hydrothermal fluids which introduced mineralization and altered host rocks at the deposit.

Hornfels is an effect of the temperature of contact metamorphism, without significant metasomatism. In contrast, skarn is formed by strong metasomatism in a contact metamorphic environment. The potassic alteration at Camino Rojo reflects at least some degree of metasomatism, beyond simple hornfels development, and could be a distal indicator of skarn-forming processes located further at depth or laterally away from the deposit. Garnet-magnetite skarn has been observed at depth in drill core, along beds within the Cuesta del Cura and deeper formations, but has not been studied as part of this thesis.

## 5 ASSAY CORRELATIONS AND SPATIAL TRENDS

Correlation coefficients were calculated by this study for Au, Ag, Pb, As and Cu assay data to identify elemental associations, which could be related to deposit mineralogy. Assays were determined from 1.5m intervals of sawed, half-core from 29 selected drill holes. There were just over 17,000 sample intervals in the dataset. Gold assays were done by ALS Minerals using fire assay with atomic absorption (AA) finish. Samples with >10ppm gold assay were reanalyzed using gravimetric finish. Silver and 34 additional elements were determined by inductively-coupled plasma atomic emission spectroscopy (ICP AES, ALS method code ME ICP61), with four acid digestion.

On a scale from 1 to 0, low correlations indicate a random, non-related pattern. Negative correlations, from -1 to 0 indicate a relationship where one variable increases as the other decreases (Rollinson, 1993). Generally, correlation coefficients  $\leq 0.35$  are considered weak, 0.36 to 0.67 are considered low to moderate, and 0.68 to 1.0 are considered high correlations.

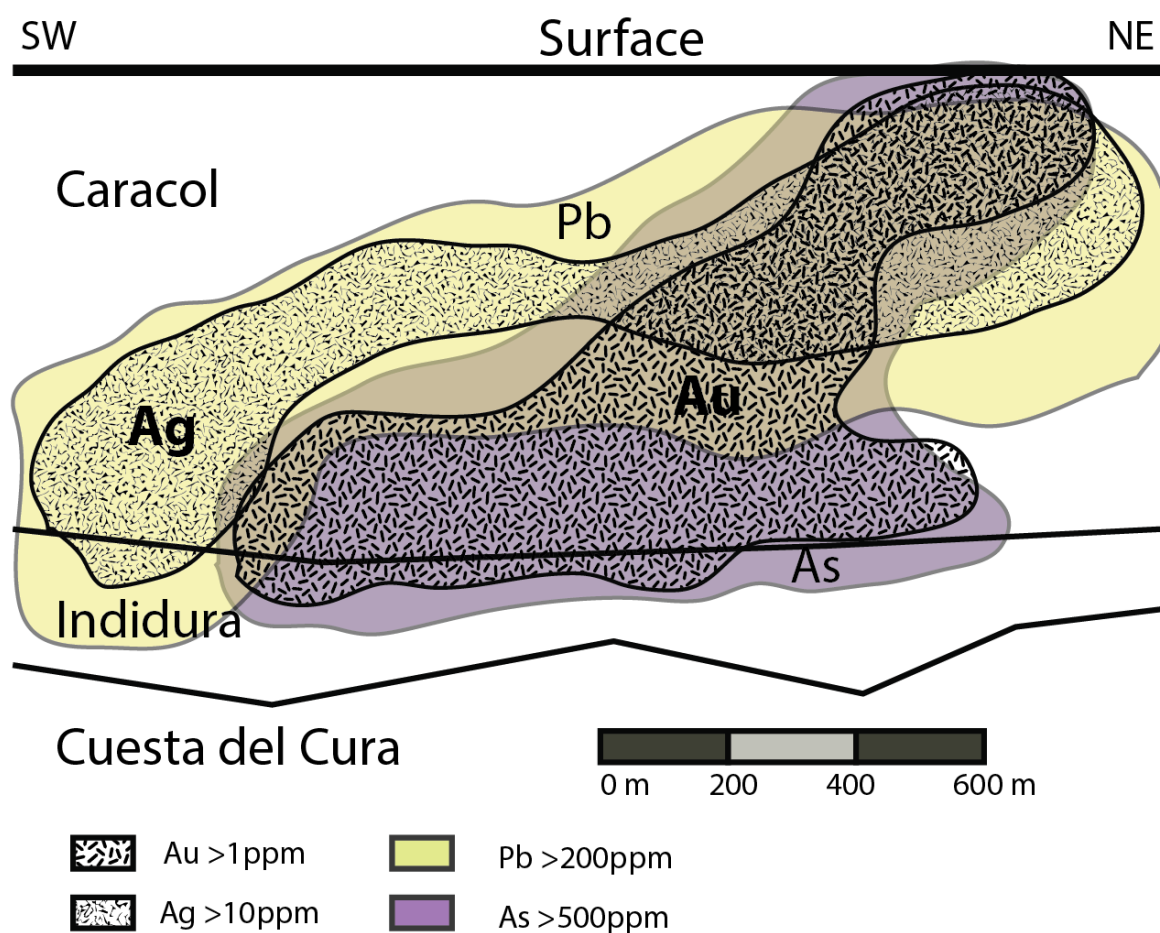
In the Camino Rojo assay data, silver and lead have a moderate to strong, positive correlation coefficient of 0.686 (Table 5.1). Gold- arsenic and arsenic- copper have positive, low correlation coefficients of 0.386 and 0.384, respectively (Table 5.1).

	Au	As	Ag	Pb	Cu
Au	1				
As	0.386	1			
Ag	0.181	0.314	1		
Pb	0.116	0.271	0.686	1	
Cu	0.306	0.384	0.340	0.202	1

**Table 5.1:** Correlation Coefficients of Au, Ag, As, Pb, and Cu Assay data from Camino Rojo drill core.

The assay data were examined for spatial patterns using LeapFrog, a 3D modeling software. In LeapFrog two styles of grade shells can be modeled: soft shells show a generalized, interpolated shape of the assay concentrations; hard shells produce smaller, restricted shapes which intersect drill hole assay intervals. Hard shells were not used in creating figures for this study as they were discontinuous and difficult to spatially recognize.

Soft shells of the Au, Ag, Pb, and As assays were created, as shown in Figure 28, a generalized cross section. This cross section parallels the planar, structural trends which cut the deposit (Figure 6).



**Figure 28:** A schematic cross section through the West Extension zone of Camino Rojo showing soft shells of Au, Ag, As, and Pb assay data. The section is cut along a parallel to the planar dike trends (Figure 6).



### 5.1 Spatial trends of gold, silver, lead, and arsenic at Camino Rojo

Gold (>1ppm) mineralization follows a general trend from the surface, plunging to the southwest at roughly 45 degrees, along the strike of the planar trends outlined by the dike intrusions. The gold >1ppm grade shell spreads out just above the contact between the Caracol and Indidura formations, approximately 600m-700m below the surface (Figure 28). Silver assays (>10ppm) form a pattern which overlaps the upper part of the gold shell, and plunges less steeply to the southwest, steepening at the western margin of the deposit. Silver does not appear to follow the Indidura-Caracol contact (Figure 28). Together, the two precious metals have a very low correlation coefficient of 0.181 (Table 5.1).

The lead >200ppm grade shell is similar to, though wider than, the silver >10ppm grade shell. Lead and silver together have the highest correlation coefficient of 0.686 (Table 5.1). The lead and silver shapes follow a similar trend, both shallowing to the northeast and overlapping the upper part of the gold shape (Figure 28). The high correlation between lead and silver is consistent with the association between galena and the silver-bearing minerals discussed in the mineralogy section of this study.

Elevated arsenic, >500ppm, and elevated gold, >1ppm, both follow the planar trend of the modeled dikes, and are influenced by the contact between the Caracol and Indidura formations. Elevated arsenic and gold grade shells are also spatially coincident, though have a relatively low correlation coefficient of 0.386 (Table 5.1). Stage 1 arsenopyrite and stage 1 electrum are spatially associated in thin section.

The elevated gold and arsenic assay shapes are distinct from the elevated silver and lead shapes. The correlation coefficients between arsenic - silver and arsenic - lead are low, at 0.314 and 0.271 respectively (Table 5.1, Figure 28).

From the grade shells, gold appears more stratigraphically controlled than silver. Silver is strongly correlated with lead. However, gold has a lower statistical correlation with arsenic. The patterns and correlations obtained from assays were consistent with petrographic observations: silver bearing minerals almost always occur with galena, and the electrum was deposited in the same locations as earlier arsenopyrite and other sulfides.

## **6 GEOCHRONOLOGY OF A MINERALIZED (PRE-ORE) DIKE**

Dating of the mineralization at Camino Rojo is made difficult by the lack or absence of coarse-grained adularia, K-feldspar, and other datable phases which can be easily separated. In order to constrain the maximum age of the deposit, zircons from a coarse-grained, mineralized, weakly altered dike were dated.

Both zircon fission track (ZFT) and uranium-lead (U-Pb) age analyses were performed with 22 zircon crystals extracted from the dike at 439m in drill hole CR11-289 (sample no. 1CR05). Assay data for this dike interval (438.5m-440m) included: 4.23ppm gold; 17ppm silver; and 8560ppm arsenic.

Fourteen of the dated zircons gave an average U-Pb age of  $73.72 \text{ Ma} \pm 4.28 \text{ my}$  (million years) (Table 6.10). These fourteen U-Pb ages form a near-linear trend in Figure 29. The eight oldest zircon grains range from 90.26Ma to 1133Ma, which are older than the host Caracol Formation and are inherited from older rocks. Six of these are older than 250Ma and are excluded from Figure 29.

The mean U-Pb age is interpreted to reflect when the pre-mineralization dike was emplaced and cooled below the zircon U-Pb isotopic blocking temperature of  $>1000^\circ\text{C}$

(Blackburn et al., 2011). Sulfide veins clearly cut the dated dike and the U-Pb mean age

indicates that the Camino Rojo mineralization must be no older than about 73 Ma.

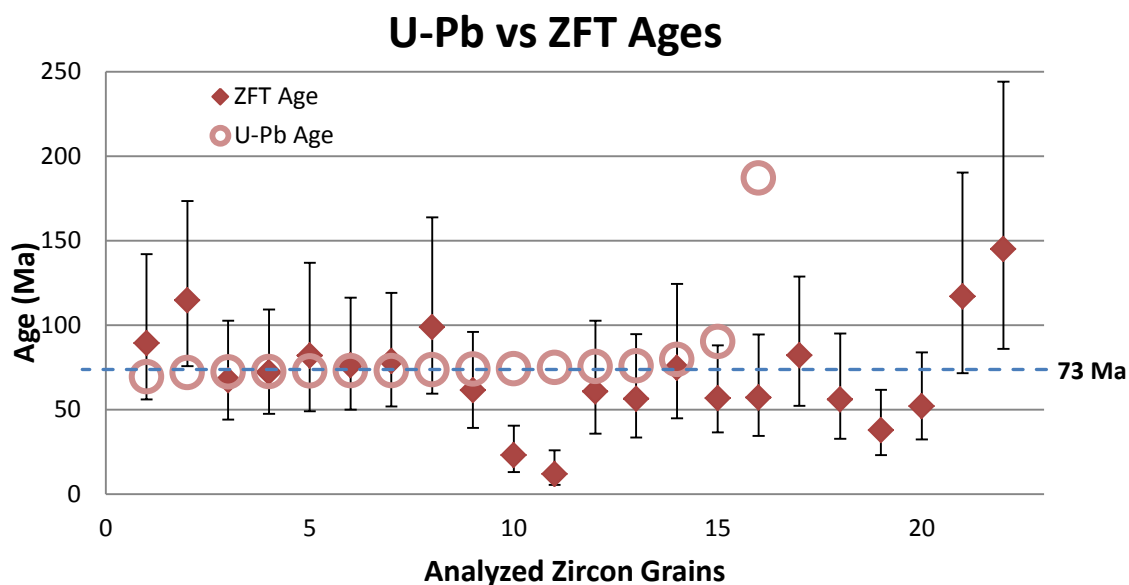
No.	U-Pb Age (Ma)	Error $\pm 2\sigma$	ZFT Age (Ma)	95%-CI	95%+CI
1	69.38	3.62	89.22	33.25	52.78
2	71.84	4.05	114.68	38.97	58.76
3	72.26	3.06	67.32	23.24	35.40
4	72.51	3.84	72.00	24.59	37.23
5	72.74	13.33	81.98	32.99	54.98
6	72.93	3.23	76.21	26.29	40.01
7	73.02	3.79	78.71	26.79	40.49
8	73.59	4.35	98.72	39.37	65.15
9	73.84	2.94	61.38	22.15	34.57
10	74.15	3.32	23.00	9.92	17.44
11	74.82	3.71	11.74	6.40	14.08
12	75.50	4.36	60.68	24.84	41.93
13	75.76	3.69	56.40	22.85	38.31
14	79.71	2.68	74.76	29.90	49.65
15	90.26	8.05	56.69	20.22	31.35
16	187.04	9.15	56.99	22.63	37.41
17	287.97	11.35	82.12	29.84	46.70
18	334.27	23.92	55.89	23.10	39.26
19	560.79	17.78	37.77	14.70	24.02
20	998.59	32.17	52.03	19.77	31.80
21	1107.96	38.20	116.87	45.32	73.60
22	1132.82	34.72	145.05	59.16	99.15

**Table 6.1:** Zircon U-Pb and ZFT analyses of a pre-mineralization dike. The error and confidence interval (CI) are recorded in my (million years). The analyzed zircon grains are listed in ascending U-Pb ages. The highlighted grains have been used to estimate the average U-Pb and ZFT ages. Older U-Pb grains are anomalous and are not included in the mean age. ZFT grains which do not include the average U-Pb age of 73.72Ma when taking into account the 95% confidence interval have been excluded from the calculation of the ZFT mean age.

Fission track ages for the 22 zircons are variable, ranging from 11.7 Ma to 114.7 Ma.

When taking into account the ZFT 95% confidence interval, all but five of the ZFT ages overlap the average U-Pb age of 73.72Ma (Table 6.1, Figure 29).

The 17 highlighted zircon grains in the ZFT section of Table 6.1, that overlap the U-Pb mean age, give an average age of 72.82Ma. The standard deviation of these 17 ZFT ages was used to calculate a 95% confidence interval of  $\pm 17.52$  my.



**Figure 29:** Comparison of zircon ages (Ma): U-Pb vs FT. U-Pb ages do not vary greatly from a late Cretaceous age for dike emplacement. In contrast, ZFT ages range from Cretaceous to Tertiary, with two notable zircons much younger than the majority. The lines express the 95% confidence interval, or uncertainty, for the ZFT data indicated by filled diamonds. Error bars for the U-Pb data are small enough as to be included in the circle indicating the U-Pb data point. The dashed blue line indicates 73 Ma, the rough age determined by both ZFT and U-Pb dating methods.

The three youngest ZFT ages of 11Ma, 23Ma, and 37Ma are outliers (Table 6.1, Figure 29). It is possible the younger ages reflect a later heating event that may have been caused by either hydrothermal fluids and/ or later dike emplacements. The later thermal event may have been short-lived, or did not significantly exceed the effective annealing zircon fission track

temperature of  $\sim 240^{\circ}\text{C} \pm 30^{\circ}\text{C}$  (Bernet and Garver, 2005), because there are only three anomalously young ZFT ages. As the dike is less than 10m in width, and would have cooled rapidly to below the ZFT closing temperature, the three youngest ZFT ages do not reflect the final cooling of the dike. A reasonable conclusion is that a high temperature thermal event did not occur after the dike was emplaced, because all but three of the ZFT ages overlap the 73 Ma average date for the dike.

As a group, both the ZFT and U-Pb ages support the interpretation of a late Cretaceous, roughly 73Ma emplacement age for the pre-ore dike (Figure 29). Most likely, the dike emplacement age is coeval with or occurred shortly before the contact thermal effects and potassic metasomatism present at the deposit. There is no clear evidence for the absolute age of mineralization, as the mineralization may have occurred shortly after dike emplacement, no earlier than 78 Ma, or may be significantly younger. If any of the barren dikes can be shown to cut mineralization, dating of such post-mineralization dikes would better constrain the age of Camino Rojo.

## **7 SUMMARY, CONCLUSIONS, AND DISCUSSION**

### **7.1 Mineralization at Camino Rojo**

Camino Rojo is a polymetallic, structurally and lithologically controlled deposit, with known mineralization over a vertical extent of at least 800m to 1,000m from the surface. The deposit formed almost entirely within the Caracol Formation, though mineralization extends into the Indidura in some locations. There does not appear to be any elevation control on gold grade.

Two principle styles of mineralization have been observed: veins and mantos. The polymetallic veins are generally no larger than 10cm in width, and primarily follow fractures, though some may align with bedding. The manto replacements can be up to 3m wide, and formed within calcareous units of the lower Caracol Formation, close to the Caracol-Indidura boundary.

A third, skarn style of mineralization was observed in a few intervals within the Cuesta del Cura limestone and underlying units. This consisted of patchy replacement of limestone by mixtures of medium-grained magnetite, pyrrhotite, chalcopyrite, sphalerite, pyrite, and garnet (S. Weiss, personal communication, 2013). Intervals of skarn-type mineralization were rarely encountered during 2013 field work, and were not collected for this study.

Veins and mantos appear to transition from one into the other and have a lack of clear cross cutting relationships with each other. Veins and mantos seem to be contemporaneous, though the mantos most likely replaced carbonate rich beds, while the veins may have formed with a preference for potassically altered, likely more brittle rock. Table 7.1 below, summarizes and compares the styles of mineralization at Camino Rojo.

Mineralization Type	Description	Controls	Thickness	Stratigraphic Range	Ore	Associated Alteration
Polymetallic Veins	Multiple veins, vein swarms	Faults, Fractures, weak bedding control	<1cm- 10 cm Avg: 2-4cm	Caracol, upper Indidura	py, sph, apy, gal, el, ag-sulf	Calcite-sericite-qtz-py
Manto-style Replacement	Replacement bodies in lower Caracol	Caracol/ Indidura boundary	1mm to 3m	Near Caracol/ Indidura boundary	py, apy, sph, gal, cpy, el	Calcite-sericite-qtz-py
Skarn	Patchy replacement	Stratigraphic/ bedding	??	Cuesta del Cura & lower	mgt, po, cpy, py, sph	Marble, calc-silicate

**Table 7.1:** Summary of mineralization characteristics in polymetallic veins, manto-replacement, and skarn at Camino Rojo. Minerals are listed in relative order of abundance, with most abundant listed first. Abbreviations: avg – average; m – meter; cm – centimeter; py – pyrite; qtz – quartz; apy – arsenopyrite; gal – galena; el – electrum; cpy – chalcopyrite; mgt – magnetite; po - pyrrhotite; Ag-sulf – silver-bearing sulfides.

Ore stage 1 consists of base metal veins and mantos made up of pyrite, sphalerite, arsenopyrite and galena. Stage 1 also contains traces of electrum, which formed as small, rounded grains interstitial to stage 1 sulfides and/ or calcite.

The majority of gold in the deposit formed during ore stage 2a with galena and chalcopyrite, which filled fractures through ore stage 1 sulfide veins and mantos. The less abundant, rounded electrum grains assigned to stage 1 are not clearly associated with stage 2a fracture-filling mineralogy and textures. It is possible other analytical techniques would reveal that stage 1 electrum is actually more closely related to ore stage 2a.

Traces of tetradymite and bismuth have been detected in ore stage 2a at Camino Rojo. The formation conditions of skarn and intrusion-related deposits allow for an Au-Bi-Te system, and tellurides and selenides of Au, Ag, Bi, and Pb are reported as trace sulfides associated with gold in hydrothermal systems (Ciobanu et al., 2006; Ciobanu et al., 2005). In particular, tellurium has been linked with gold incorporation into pyrite structure. A LA-ICP-MS study done in China by Cook et al. (2009) showed tellurium assisted in the incorporation of invisible, lattice-bound gold into arsenic-free pyrite. They reported the highest gold values in pyrite were up to 1 wt% and were correlated with atomic tellurium. It is speculated that tellurium and/ or bismuth have had an effect on gold mineralogy at Camino Rojo, though it is not currently known if invisible gold exists within pyrite at the deposit, and to what degree it may comprise the estimated amount of gold present.

The silver-bearing minerals of ore stage 2b are suspected to be later than the fracture-filling ore stage 2a electrum because they formed within distinct, macroscopic veins which lack electrum and which cut stage 1 sphalerite. Previously, Goldcorp geologists had identified calcite-silver sulfosalt veins which appeared to account for the high silver/ low gold assay data in

some samples. These calcite-silver sulfosalt veins were banded, included galena, tended to be shallower than gold mineralization, and were not known to be in contact with other sulfide veins (S. Weiss, personal communication, February 2016). The field observation of shallow calcite-silver sulfosalt veins may help explain the elevated silver which has been modeled in this study peripheral to and above the West Extension. The elevated silver assay shell overlaps the elevated gold assay shell in the Represa zone.

There is little evidence for more than one distinct mineralizing fluid at Camino Rojo as sulfide veins and mantos share similar mineralogy and intergranular textures. The differences between stage 1 and stage 2 mineralization could indicate a change and cooling of hydrothermal fluids through time, but is not indicative of distinct and separate fluid events. Additionally, the bimodal composition of some veins and the occasional growth zonation within arsenopyrite and sphalerite grains are evidence for an evolution of the hydrothermal fluid at Camino Rojo. In this respect, Camino Rojo does not have the typical characteristics of central Mexican polymetallic deposits, which are polyphase and multi-episodic (Camprubi and Albinson, 2007).

Fluid inclusion salinities have not been measured for Camino Rojo, though an early brine likely formed the veins and mantos. The pyrite-sphalerite-arsenopyrite-galena-chalcopyrite mineralogy at Camino Rojo indicates some degree of chloride, as base metals are most commonly transported through chloride complexes, and more salt is necessary. As the initial fluid evolved into a less saline, cooler solution through interaction with host rocks and groundwater, ore stage 2 minerals, including electrum and silver-bearing minerals, were deposited. The less saline, second brine could have transported the gold and silver component of stage 2 mineralization by bisulfide complex.



Though rare, cross-cutting quartz veinlets at the deposit (Figure 13F) suggests that the later, cooler, stage 2 mineralizing hydrothermal fluid may have been intermittently quartz saturated. Silica within the hydrothermal fluid at the deposit may have originated from the shaley beds within the Caracol Formation, or from silica left over from dike formation.

## **7.2 Hydrothermal Alteration at Camino Rojo**

The most visually prominent alteration at Camino Rojo is the pre-mineralization potassic metasomatism, with fine-grained K-feldspar replacement and recrystallization of the sedimentary hosts. The ore-related calcite-sericite±pyrite ±quartz alteration overprints the earlier potassic alteration, and is volumetrically minor. Late calcite veins and flooding overprint the deposit, and make up the final alteration stage. Pyrite formed in all three alteration events. Carbonate grains, which may have been part of the original and unaltered sandstone host units, have since been completely replaced by K-feldspar or other alteration mineralogy, or were simply dissolved.

Mineralization and the mineralization-related calcite-sericite alteration overprints or cuts the potassic metasomatism. There is a small, spatial offset of the potassic alteration to the north and east of the Au>1ppm shell at Camino Rojo. This offset between elevated gold assays and the potassic alteration could be the result of earlier, potassium-bearing fluids having blocked fluid conduits and diverting later gold-bearing fluids into offset structures.

The late calcite alteration at Camino Rojo is the result of a carbonate-rich fluid, and did not form more than 400m below the present surface. Simpson et al. (2001) noted that final barren calcite invasion in epithermal systems is often represented by textures such as blocky calcite, crosscutting veins and veinlets, or in vugs with dog-tooth crystal terminations. Such

barren calcite textures are typical of some of the calcite veins observed above mineralization at Camino Rojo.

The deepest holes at the deposit intersected several intervals of marble and garnet-magnetite skarn in the lower part of the Indidura Formation and underlying units. The marble and garnet bearing skarn are broad indicators for a calc-silicate alteration zone in the lower portion of, and beneath, the deposit. The observed hornfels at shallower depths are consistent with deeper skarn and marble. The potassic metasomatism is interpreted to represent a more distal expression of the thermal and hydrothermal system responsible for the skarn, hornfels and marble.

### **7.3 Timing of Camino Rojo Mineralization and Deeper Magmatic Activity**

The dated, mineralized dike was emplaced at roughly 73Ma based on U-Pb zircon ages. This age corresponds to the time of Cretaceous magmatism produced by subduction of the Farallon plate beneath western Mexico. Overall, fission track data provide evidence that mineralization at Camino Rojo took place shortly after dike emplacement or fluid temperatures did not exceed about 240°C for a length of time sufficient to reset the zircon fission track ages in the pre-ore dike. If mineralizing fluid temperatures were above the zircon fission track annealing temperature, the deposit would have formed close to the Cretaceous age of dike emplacement.

The mineralization overprinted the hornfels and the dikes, and therefore may be considerably younger than the dated dike emplacement. Since ZFT data do not reveal a later heating event, younger mineralization would require relatively low fluid temperatures. Though

fluid inclusion studies have not been done, the observed sulfide mineralogy and textures do not require a particular temperature range for deposit formation.

The deposit is centered on and extends into the hornfels and deeper marble and skarn, which were produced by a heating event consistent with a larger intrusion at depth. This inferred larger intrusion has not been delineated by drilling or geophysics, but must be present. The pre-ore potassic metasomatism is interpreted to be related to this intrusion.

Components of the mineralizing fluids, such as a portion of the sulfur, iron, base and precious metals, could have been sourced from this deeper intrusion. Alternatively, mineralizing fluid components could have been derived from a separate, younger intrusion.

The timing and age of mineralization can be partly resolved by constraining fluid temperatures at Camino Rojo. If fluid temperatures were lower, the mineralization could have been close to or significantly younger than 73Ma, and a younger intrusion is possible. Even if the deposit is determined to have formed at a relatively higher temperature, pre-ore ZFTs may not have been completely reset if the event was short-lived and heating and fluid: rock interaction were not sufficient.

Fluid inclusion studies are required to determine the temperature of formation. Studies of quartz are difficult as quartz is rare. Fluid inclusions have been seen in sphalerite samples, however an infrared microscope would be required to analyze the darker sphalerite.

#### **7.4 Overview of Epithermal, Skarn, and Carbonate Replacement Deposit Models**

Epithermal deposits vary between two end member types: low sulfidation (LS) systems dominated by meteoric water, and high sulfidation (HS) systems which are derived from magmatic fluid components. Intermediate sulfidation (IS) systems are similar to LS systems, but

contain greater concentrations of silver and base metals compared to LS deposits (Simmons et al., 2005; Hedenquist et al., 2000). Central Mexico contains many IS and LS epithermal deposits, with HS systems located in the SMO and northern Mexico.

Low sulfidation systems are formed by fluids with a near neutral pH under reducing conditions. The Au-Ag, Ag-Au, or Ag-Pb-Zn ores dominantly form as veins and vein stockworks. Sulfides include varying amounts of pyrite and much lesser quantities of Fe-rich sphalerite, galena, chalcopyrite, arsenopyrite, tellurides, and selenides. Gangue mineralogy includes quartz ± calcite ± adularia ± illite. Quartz is the primary gangue mineral, often deposited in banded crustiform-colloform textured veins. Alteration of host rocks by near-neutral thermal waters primarily forms illite (sericite) and interstratified clays, and depending on host rock composition, chlorite, adularia and epidote may be present. Regional propylitic alteration is common. The reduced fluids can also produce an assemblage of magnetite-pyrite-pyrrhotite and chlorite-pyrite (Simmons et al., 2005). Banded veins, drusy cavities, and breccias are common textures. Platy calcite, partly or entirely replaced by quartz, is another common texture that is produced by boiling. Boiling destabilizes metals carried in solution and leads to deposition of ore metals, calcite and adularia; later cooling precipitates amorphous silica and late calcite in the same location.

The acidic pH and relatively oxidizing conditions of HS systems produce hypogene gangue mineralogy of quartz, pyrite ± alunite ± pyrophyllite ± dickite ± kaolinite. Au ± Ag ± Cu ores are common and typically hosted in vuggy residual quartz (Simmons et al., 2005). The oxygen activity is sufficiently elevated to produce pyrite, alunite and ± hematite ± magnetite. Advanced argillic alteration, the iconic HS alteration, produces intensely leached host rocks at shallow depth. The acid solution leaches the rock outward from the center of fluid flow, and later fluids

may introduce ore mineralogy into the leached zone. Regional propylitic alteration is common outboard of the advanced argillic alteration, and a pyrite-chlorite-calcite-epidote-albite assemblage may be present (Simmons et al., 2005). Ore is deposited as massive-textured veins, manto-replacement, and disseminated sulfides. Massive, vuggy quartz, quartz veins, silicification, and silicified breccias are typical (Hedenquist et al., 2000).

Skarns are formed by replacement of carbonate-bearing host rocks during relatively high temperature contact or regional metamorphism and metasomatism, which can occur in proximity to a pluton, along faults and major shear zones, or in shallow geothermal systems (Meinert et al., 2005). Skarn-related magmatic activity is related to continental subduction (Einaudi et al., 1981).

Both mineralization and alteration in skarns are structurally and stratigraphically controlled. The processes that lead to deposit formation include: (1) isochemical contact metamorphism during pluton emplacement, (2) prograde metasomatic skarn formation as the pluton cools and ore fluids develop, and (3) retrograde alteration of earlier-formed mineral assemblages (Hammarstrom et al., 1995). Ore minerals can form during stages 2 and 3. Early stages of skarn development may be partly or completely eliminated by later stages (Meinert et al., 2005).

Skarn systems have spatial and temporal mineralogical zoning patterns. The width of these zones can be highly variable, with certain zones entirely absent from some systems. The general pattern includes proximal garnet, distal pyroxene, and minerals such as wollastonite, vesuvianite, or massive sulfides/ oxides near the marble front, with or without silicification (Meinert et al., 2005).

Seven major skarn types of metal deposits include Fe, Au, Cu, Zn, W, Mo, and Sn (Meinert, 1993). Most gold skarns are associated with dike and/ or sill complexes with distal, early biotite  $\pm$  K-feldspar hornfels aureoles and are relatively reduced, with an Au-Bi-Te-As  $\pm$  Co geochemical association. Zinc skarns tend to be distal to their associated igneous rocks, and are often also mined for Cu, Pb, and Ag. Zinc skarn districts grade outward from skarn to carbonate replacement ores, veins, and massive sulfide bodies (Meinert et al., 2005).

Carbonate-hosted replacement deposits (CRDs) are polymetallic, intrusion-related deposits, formed at 250°C -500°C, dominated by massive sulfides rich in Pb-Zn-Ag-Cu with lesser amounts of Au, As, Sb, Bi, and Ba (Tittley, 1993, Megaw, 1998). These deposits are commonly associated outboard of base-metal skarns, porphyry copper deposits, or barren porphyry bodies and can be structurally controlled by faults or fractures related to regional deformation (Tittley, 1993). CRDs form elongated bodies known as mantos, which are strata-bound, often continuous lenses within the sedimentary host lithologies. CRDs typically have distinctive deposit- and district-scale zonation of both ore and gangue mineralogy.

## **7.5 Comparison of Camino Rojo to Other Deposit Types**

The Camino Rojo deposit is a Zn-Pb-Ag-Au ore system hosted primarily in veins and mantos. Camino Rojo appears to have some characteristics of polymetallic CRDs and vein systems, with skarn at depth. It is possible that a developed skarn system below Camino Rojo evolved outward with time into CRDs and polymetallic vein systems. The stage 2 hydrothermal alteration and mineralogy identified could be the start of an epithermal system, though Camino Rojo does not have the vertical control, boiling, or abundant hydrothermal quartz associated with epithermal deposits.

Marble and garnet-magnetite skarn have been observed at the deepest levels of drilling, and broadly indicate a calc-silicate alteration. Skarn at Camino Rojo underlies the vein and massive sulfide mantos of ore stages 1 and 2, showing a spatial relationship. As well, the early K-feldspar alteration and hornfels are features present at known Au skarns. Overall, however, the extent, specific mineralogy, and possible zonation of skarn at Camino Rojo are unknown.

Because the veins and mantos at Camino Rojo overlie skarn, it is possible there may be a relation to an even deeper porphyry system. Unfortunately, little research in Mexico has focused on the links between porphyry and distal skarn, CRDs, and epithermal deposit types, despite more than 30 known porphyry deposits in the northwest part of the country (Camprubi and Albinson, 2007).

The sulfide replacement along bedding by pyrite, sphalerite, and galena at Camino Rojo is similar to the style of mineralization of zinc-rich CRDs (Plumlee et al., 1995). The gold-bearing sulfide mantos within the Caracol Formation at Camino Rojo do not show significant mineralogical or elemental zonation through the vertical extent of the deposit. Though the mantos are strata-bound, the massive sulfide lenses do not appear to be laterally continuous from hole to hole. The carbonate-hosted Ag-Pb-Zn (Cu) deposits of northern Mexico range in temperature from 200°C to 500°C (Megaw et al, 1988). If Camino Rojo formed under the relatively higher end of the temperature range, then the ZFT data would indicate Camino Rojo formed around 73Ma.

#### **7.5.1 Camino Rojo Compared to Mexican Epithermal Deposits**

Mexican epithermal deposits are studied for their diversity of geologic settings and for their distinct spatial distribution: Au-Ag vein deposits are located primarily in the west, and Ag-

Pb-Zn vein deposits are found to the east, although there is some overlap (Figure 30, modified from Simmons et al., 2005). According to Simmons and Albinson (1995), these epithermal deposits can be broadly grouped into two types: (1) the western group, largely within the SMO, consists of Au-Ag deposits hosted in Eocene intermediate volcanic and intrusive rocks, where fluid inclusion studies indicate mineralizing fluid salinity of  $\leq 3$  eq. wt. % NaCl and temperatures of  $<300^{\circ}\text{C}$ ; and (2) the Ag-Pb-Zn deposits located in the central, northern half of Mexico (Mesa Central and SMOr), hosted in Paleozoic and Mesozoic sedimentary rocks, with more saline mineralizing fluids ( $\geq 10$  eq. wt. % NaCl) and formation temperatures ranging between  $200$ - $400^{\circ}\text{C}$ .

The massive vuggy quartz, alunite veins and replacements, enargite, and other minerals characteristic of HS systems are absent at Camino Rojo. Instead, Camino Rojo has some similarities to the second group of epithermal deposits identified by Simmons and Albinson (2005). The Camino Rojo veins and mantos are hosted in Mesozoic sedimentary rocks in the Mesa Central. In contrast to the Ag-Pb-Zn ores common to Mexican epithermal deposits, Camino Rojo is more of a Zn-Pb-Ag-Au deposit. Though no fluid inclusions studies have been done at Camino Rojo, mineralizing fluids were likely more saline than the Au-Ag deposits of the Simmons and Albinson (2005) group 1. Higher salinities are evidenced by the abundance of sphalerite and galena. In Mississippi Valley Type deposits, these minerals formed from fluids ranging in salinity from 10 to 30 wt. % NaCl (Leach et al., 2010).

In general, the vertical extent of mineralization at Camino Rojo is greater than the majority of epithermal precious-metal deposits, though some epithermal veins can be mineralized over as much as 1000m (White and Hedenquist, 1990). The typical, finely rhythmic colloform and/or crustiform banding within veins, a ubiquitous characteristic of LS and IS Au-Ag



epithermal deposits, is absent or very rare at Camino Rojo. Instead, the veins contain mainly intergranular to polygonal textures, though crude, weakly rhythmic sulfide banding has been identified, but is not common.

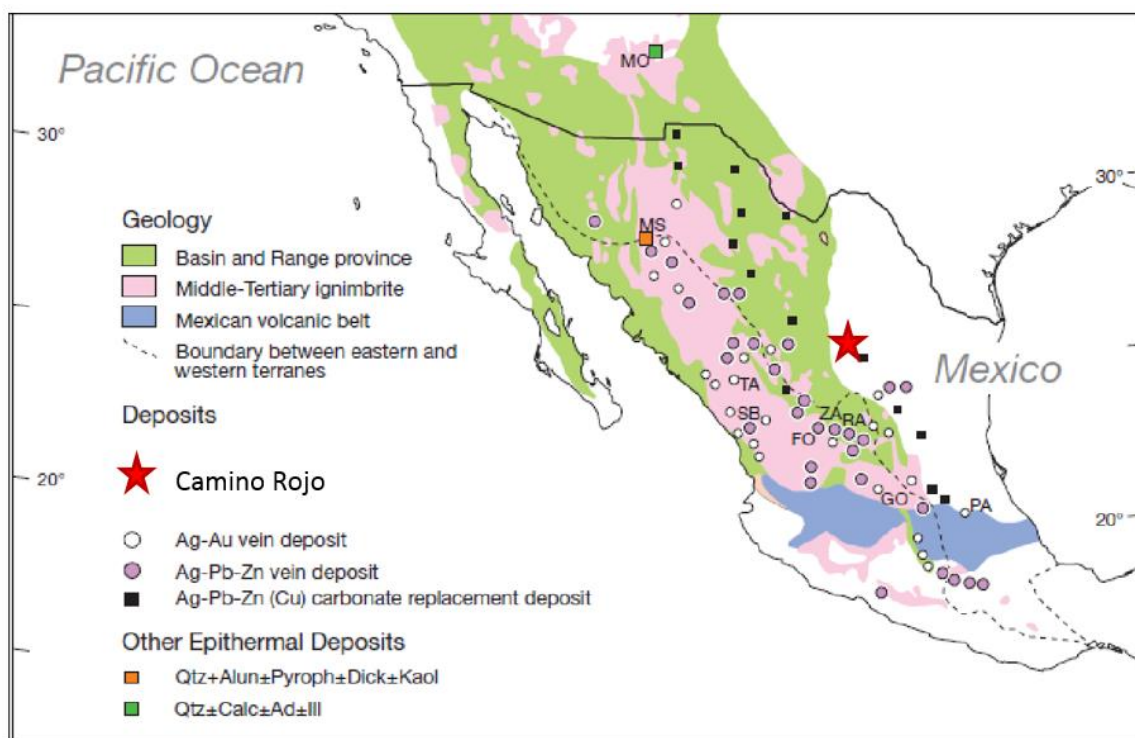
Camprubi and Albinson (2007) discuss the confusion over ascribing Mexican epithermal deposits as strictly IS or LS. This confusion stems from the lack of temporal and spatial distinction between Mexican IS and LS epithermal deposits, which overlap at many scales in the country, from metallogenic provinces, to mining districts, and even within individual deposits. Camprubi and Albinson (2007) concluded the deposits are “born” as IS systems and “die” as LS systems. These authors proposed the hydrothermal fluids evolved from base-metal rich hydrothermal brines toward near-neutral pH, and that the progressive consumption of sulfur allowed IS stable fluids to evolve to a lower sulfidation state.

Epithermal deposits in central Mexico characteristically have extensive precious-metal LS mineralization with IS type roots. These polymetallic IS roots can be either rich or barren in terms of precious metal content. An IS epithermal deposit will often have subordinate LS mineralization above or peripheral to it. In general, the Mexican IS deposits are zinc and lead dominant and relatively copper poor. Greater amounts of copper commonly formed in the skarns at higher temperatures and greater depths (Camprubi and Albinson, 2007). Most IS and LS ore deposits formed at depths between 400 and 1000m below the paleosurface (Albinson et al., 2001).

Boiling is considered one of the most effective mechanisms for the precipitation of metallic minerals in IS and LS epithermal deposits (Simmons, 1991; Albinson et al., 2001). Common boiling textures, such as bladed calcite and its pseudomorphs, have not been observed at Camino Rojo. The lack of boiling textures coupled with vertically extensive

mineralization indicates that boiling is unlikely to have been the principal method for sulfide precipitation, and was not significant or did not take place at Camino Rojo.

The polymetallic veins and mantos of Camino Rojo have mineralogy similar to an IS epithermal system, though textures are not consistent with epithermal deposits. The calcite-sericite ore alteration at Camino Rojo is also comparable to epithermal systems, but there are additional deeper skarn and associated hornfels at the deposit. It is speculated that if there was a distal LS system associated with Camino Rojo, it has since been eroded away.



**Figure 30:** Map of Mexico depicting Ag-Au, Ag-Pb-Zn, or Ag-Pb-Zn (Cu) epithermal vein and carbonate replacement deposits. The basin and range, Middle Tertiary ignimbrites, and the Mexican volcanic belt provinces are also marked. The red star indicates the position of Camino Rojo. (Modified from Simmons et al., 2005)

All epithermal deposits in Mexico are related to the volcanism of the western SMO and the subduction of the Farallon plate (Camprubi and Albinson, 2007). The climax of ignimbrite volcanism in the SMO corresponds to the formation of the majority of epithermal deposits during the Eocene and Oligocene, and dated epithermal deposits in Mexico range from 15 Ma to 60 Ma (Albinson, 1988; Camprubi and Albinson, 2007). Arc magmatism migrated east through Mexico, and was caused by shallowing of the Benioff zone beneath western North America (Sedlock et al., 1993). With this genesis in mind, Camprubi et al. (2003) grouped the epithermal deposits based on their respective ages: 50-40 Ma (Eocene), 36-27 Ma deposits (Oligocene), and 23-18 Ma deposits (early Miocene.)

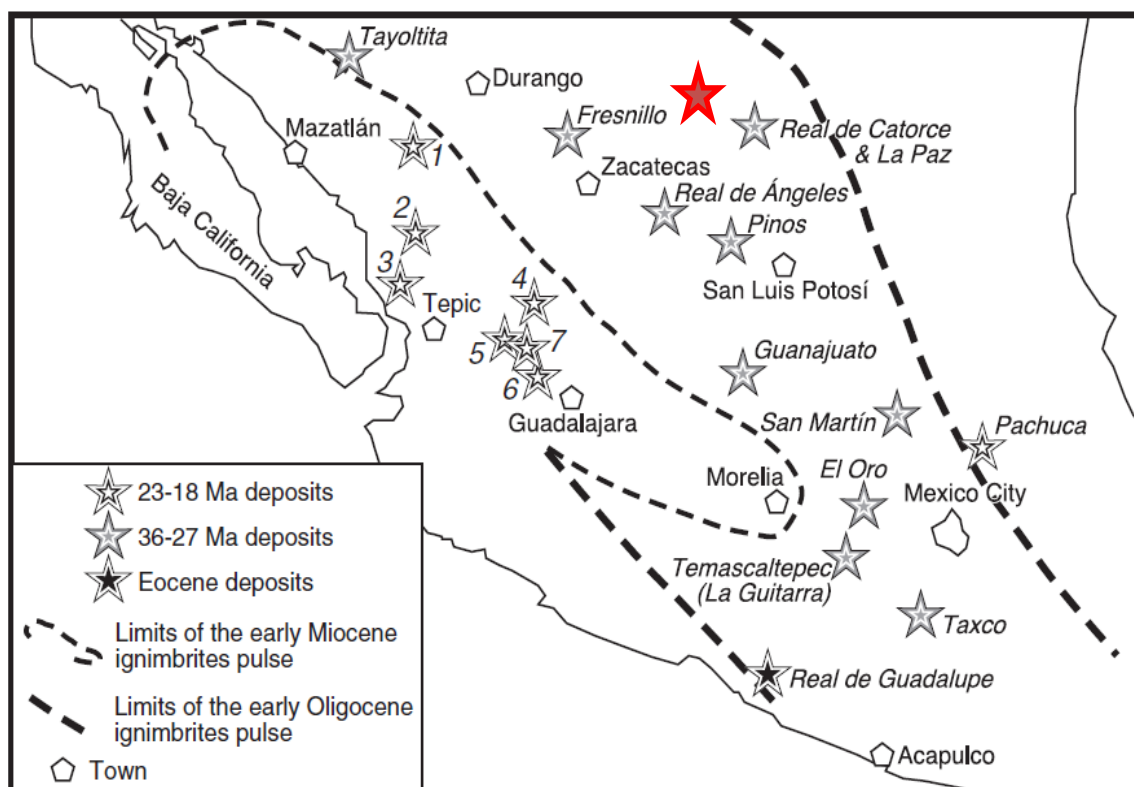
East of the SMO, the bulk of Mexican epithermal deposits formed between 36-27 Ma and occur in a northwest-southeast trend beginning near the US-Mexico border and continuing through the center of the country (Figure 31). The younger, Miocene-aged epithermal deposits are located along the western coast (Figure 31). Camino Rojo is located in the belt of CRDs, and is adjacent to the region of 36-27Ma silver and base metal epithermal deposits.

The largest ore deposit in the region is Peñasquito, located 50km northwest of Camino Rojo, with 9.9 Moz of gold in proven and probable reserves at the end of June 2016. Peñasquito is centered on two funnel-shaped diatreme breccia pipes above a Tertiary felsic intrusive complex emplaced into the Caracol Formation and older Jurassic and Cretaceous sedimentary units. The bulk of mineralization is hosted in the diatremes, with subordinate stockwork veins in the surrounding Caracol Formation. Cu-Au skarn is present in the carbonate host rocks adjacent to the roots of diatreme being mined. Peñasquito mineralization formed from 35.7Ma to 34.9Ma based on Re-Os molybdenite ages, and at about 33Ma based on hydrothermal K-feldspar ages; this post-dated multiple igneous pulses that formed the ore-hosting diatreme

breccias (Rocha-Rocha, 2016). The principle ore minerals are base metal sulfides, complex sulfosalts, oxides, gold, electrum, bismuthinite, and accessory minerals as defined by Rocha-Rocha (2016).

In contrast, Camino Rojo does not contain sulfosalts and no diatreme has been found. Vein and manto styles at CR are similar to veins and mantos peripheral to the breccia pipes at Peñasquito, though the mineralogy is different. Potassic alteration is also found in some drill core through the Caracol Formation at Peñasquito (Rocha-Rocha, 2016).

If Camino Rojo formed at about 73 Ma, as suggested by U-Pb and ZFT data, then this magmatic activity occurred before the magmatism associated with the Mesa Central epithermal systems, and is consistent with Late Cretaceous subduction. However, if Camino Rojo formed at low temperatures, the deposit could be much younger, and may be contemporaneous with the adjacent belt of 36-27Ma epithermal deposits, and perhaps much similar in age to Peñasquito.



**Figure 31:** Ages and locations of dated epithermal deposits in northern and central Mexico. The location of Camino Rojo is identified by a red star. The trend of deposits surrounding Camino Rojo range from 36-27 Ma. (Image modified from Camprubi et al, 2003).

## 7.6 Future Research

This initial research of Camino Rojo focused on the mineralogy and paragenesis of hydrothermal mineralization and alteration. Development of the Camino Rojo deposit to the production state will allow a much more thorough investigation when mining will expose more rocks, especially in the West Extension.

A study of the sulfur isotopes of sphalerite, galena, or chalcopyrite could provide a better understanding of the sources of sulfur at Camino Rojo, and could indicate how significant magmatic fluids were in contributing sulfur and ore-forming metals. Additionally, analysis of

fluid inclusions for the salinity and temperature of the hydrothermal fluids will better determine the deposit fluid conditions, and will provide evidence for the proposed evolution of the saline brines responsible for mineralization. More geochronology and further study of the deeper skarn system would also help constrain the overall hydrothermal environment and provide additional insight for the classification of the deposit, which has characteristics of the classic Mexican LS and IS epithermal deposits, skarn and CRDs.

In the search for a deposit similar to Camino Rojo, extensive alluvial cover in the northern Mesa Central makes exploration difficult. Identification of regional and local faulting and near vertical dike emplacement, coupled with geophysical exploration for sulfides may be the best exploration method. The extensive potassic alteration which has been observed at the deposit is not necessarily indicative of mineralization.

## 8 REFERENCES

Albinson, T., 1988, Geologic reconstruction of paleosurfaces in the Somberete, Colorada, and Fresnillo, Zacatecas state, Mexico: *Economic Geology*, vol. 83, p. 1647-1667.

Albinson, T., Norman, D. I., Cole, D., and Chomiak, B. A., 2001, Controls on formation of low-sulfidation epithermal deposits in Mexico: constraints from fluid inclusion and stable isotope data: *Society of Economic Geologists Special Publication Series*, vol. 8, p. 1-32.

Anonymous, 2015, Annual Report 2015: Goldcorp, 141p.

Anonymous, 2014, Core Strengths Annual Report 2014: Goldcorp, 149p.

Bartolini, C., Vilson, J. L., and Lawton, T. F., (Eds.), 1990, Mesozoic Sedimentary and Tectonic History of North-central Mexico: *Geological Society of America Special Paper* 340, 383 p.

Bernet, M. and Garver, J. I., 2005, Fission-track analysis of detrital zircon: *Reviews in Mineralogy & Geochemistry*, vol. 58, p. 205-238. <hal-00097116>

Blackburn, T., Bowring, S. A., Schoene, B., Mahan, K., and Dudas, F., 2011, U-Pb thermochronology: creating a temporal record of lithosphere thermal evolution: *Contributions to Mineralogy and Petrology*, published online January 26, 2011, 22p.

Blanchflower, J. D., 2009, Technical report on the mineral resources of the Camino Rojo property, Concepcion del Oro district, Zacatecas, Mexico: NI 43-101 report prepared for Canplats resources, on SEDAR, 53p including appendices.

Camprubi, A. and Albinson, T., 2007, Epithermal deposits in Mexico – Update of current knowledge, and an empirical reclassification: *GSA Special Paper 422 Geology of Mexico: Celebrating the Centenary of the Geological Society of Mexico*, p. 377-415.

Camprubi, A., Ferrari, L., Cosca, M. A., Cardellach, E. and Canals, A., 2003, Ages of epithermal deposits in Mexico: Regional significance and links with the evolution of Tertiary volcanism: *Economic Geology*, vol. 98, p. 1029-1037.

Ciobanu, C.L., Cook, N. J. and Pring, A., 2005, Bismuth tellurides as gold scavengers, *in Mineral deposit research: meeting the global challenge proceedings 2005*, *in* Mao, J.W. and Bierlein, F.P. (eds.), *Proceedings of the...Biennial SGA (Society of Geology Applied to Mineral Deposits), Meeting 8*, vol. 2, p. 1383-1386.

Ciobanu, C.L., Cook, N.J., and Damian, G., 2006, Gold scavenged by bismuth melts: An example from Alpine shear-remobilisates in the Highis Massif, Romania: *Mineralogy and Petrology*, vol. 87, p. 351-384.

Clark, K. F. and Fitch, D.C., 2013, Evolution of metallic deposits in time and space in Mexico, 72 p. <<http://www.geo.utep.edu/pub/Clark-Fitch/ClarkandFitchJan2013.pdf>>

Clark, K. F., Foster, C. T., and Damon, P. E., 1982, Cenozoic mineral deposits and subduction-related magmatic arcs in Mexico: Geological Society of America Bulletin, vol. 93, p. 533-544.

Coney, P., 1983, Plate tectonics and the Laramide Orogeny: New Mexico Geological Society, Special Publication no. 6, p. 5-10.

Cook, N.J. and Ciobanu, C.L., 2004, Bismuth tellurides and sulphosalts from the Larga hydrothermal system, Melaiferi Mts, Romania: Paragenesis and genetic significance: Mineral Mag 68, p. 301-321.

Cook, N.J., Ciobanu, C.L., and Mao, J.W., 2009, Textural control on gold distribution in As-free pyrite from the Dongping, Huangtuliang and Hougou gold deposits, North China Craton, (Hebei Province, China): Chemical Geology, vol. 264, p. 101-121.

de Cserna, Z., 1976, Geology of the Fresnillo area, Zacatecas, Mexico: Geological Society of America Bulletin, v. 87, p. 1191-1199.

Díaz-Salgado, C., Amezcua, N, and Sánchez, M., 2006, Formación Caracol...Cretácico (Coniaciano-Maastrichtiano), *in* Léxico Estratigráfico de México, Servicio Geológico Mexicano, 5p.

Dickinson, W.R., and Lawton, T. F., 2001, Carboniferous to Cretaceous assembly and fragmentation of Mexico: Geological Society of America Bulletin, vol. 113, no. 9, p. 1142-1160.

Donelick, R. A., and Donelick, M. B., 2012-2013, Combined Fission Track and U-Pb Dating of Apatite and Zircon by LA-ICP-MS: Apatite to Zircon, Inc., 22p. including appendices.

Einaudi, M. T., Meinert, L. D., and Newberry, R. J., 1981, Skarn Deposits: Economic Geology 75<sup>th</sup> Anniversary Volume, p. 317-391.

Eguiluz de Antuñano, S., Aranda-García, M., and Marrett, R., 2000, Tectónica de la Sierra Madre Oriental, Mexico: Boletín de la Sociedad Geológica Mexicana, vol. 53, p. 1-26.

Ferrari, L., Valencia-Moreno, M., Bryan, S., 2007, Magmatism and tectonics of the Sierra Madre Occidental and its relation with the evolution of the western margin of North America: Geological Society of America Special Paper, vol. 422, p. 1-39.

Goldhammer, R.K., 1999, Mesozoic sequence stratigraphy and paleogeographic evolution of northeastern Mexico, *in* Mesozoic Sedimentary and Tectonic History of North-Central Mexico: Geological Society of America Special Paper no. 340, p. 1-59.



González-Arroyo, A., Martínez-Tovar, M., Ramírez-Gutiérrez, J.G., Chávez-Rangel, F.J., García-Ruiz, J.M., 1998, Carta Geológico-Minera Fresnillo F13-3 esc. 1:250,000, Pachuca, Hidalgo, Mex.: Consejo de Recursos Minerales (Servicio Geológico Mexicano), 1 mapa.

González -Arroyo, A., Arias-Gutiérrez, M.A., Martínez-Tovar, M., Chávez-Rangel, F., Beltrán-Castillo, D., Escalante-Martínez, J., 1999, Carta Geológico-Minera Juan Aldama G13-12 esc. 1:250,000, Pachuca, Hidalgo, Mex.: Consejo de Recursos Minerales (Servicio Geológico Mexicano), 1 mapa.

Hammarstrom, J. M., Kotlyar, B. B., Theodore, T. G., Elliott, J. E., John, D. A., Doebrich, J. L., Nash, J. T., Carlson, R. R., Lee, G. K., Livo, E., and Klein, D. P., 1995, Cu, Au, and Zn-Pb Skarn Deposits (Chapter 12), *in* Edward A. du Bray (ed), Preliminary Compilation of Descriptive Geoenvironmental Mineral Deposit Models; p. 90-111.

Hedenquist, J.W., Arribas R., A., and Gonzalez-Urrien, E., 2000, Exploration for Epithermal Gold Deposits (Chapter 7): SEG Reviews, vol. 13, P. 245-277.

Larson, L. T., October 26, 2010, Unpublished Petrographic Report on 14 Samples from Camino Rojo.

Lawton, T.F., 2012, Age of the Caracol Formation, Sierra de Parras, Coahuila, Mexico: Geological Society of America *Abstracts with Programs*, vol. 44, No. 3, p. 76.

Leach, D.L., Taylor, R.D., Fey, D.L., Diehl, S.F., and Saltus, R.W., 2010, A Deposit Model for Mississippi Valley-Type Lead-Zinc Ores (Chapter A), *in* Mineral Deposit Models for Resource Assessment: U.S. Geological Survey Scientific Investigations Report 2010-5070-A, 52 p.

Leitch, C. H. B., 2008a, Petrographic Report on 8 Samples from Camino Rojo Project (Mexico); Internal Report written May, 2008, 15p.

Leitch, C. H. B., 2008b, Petrographic Report on 5 Samples from Camino Rojo Project (Mexico); Internal Report written July, 2008, 10p.

Lueth, V.W., Megaw, P.K.M., Pingitore, N.E. and Goodell, P.C., 2000, Systematic variation in galena solid-solution compositions at Santa Eulalia, Chihuahua, Mexico: *Economic Geology*, vol. 95, p. 1673-1687.

Megaw, P. K. M., 1998, Carbonate-hosted Pb-Zn-Ag-Cu-Au replacement deposits: An exploration perspective (Chapter 10), *in* D. R. Lentz (ed.), Mineralized intrusion-related skarn systems: Mineralogical Association of Canada, Short course series 26, p. 337-358.

Megaw, P. K. M., Ruiz, J., and Titley, S.R., 1988, High-Temperature, Carbonate-hosted Ag-Pb-Zn (Cu) Deposits of Northern Mexico: *Economic Geology*, vol. 83, p. 1856-1885.

Meinert, L.D., 1993, Skarns and Skarn Deposits: *Geoscience Canada*, vol. 19, no. 4, p. 145-162.

Meinert, L. D., Dipple, G. M., and Nicolescu, S., 2005, World Skarn Deposits: Economic Geology 100<sup>th</sup> Anniversary Volume, p. 299-336.

Mitre-Salazar, L., 1989, La Megafalla Laramídica de San Tiburcio, Estado de Zacatecas: Univ. Nal. Autòn. Mexico, Inst. Geología Revisita, vol. 8, no. 1, p. 47-51.

Mixon, R. B., Murray, G. E., and Diaz-Gonzalez, T. E., 2004, Age and correlation of Huizachal group (Mesozoic), State of Tamaulipas, Mexico: AAPG Bulletin, vol. 43, no. 4, p. 757-771.

Moller, S. A., Islas, J. E., Davila, R. T., 2001, New Discoveries in the La Colorada District, Zacatecas State, Mexico: Society of Economic Geologists, SP8, p. 95-104.

Montañéz-Castro, A., Ramírez-Gutiérrez, J.A., Escalante-Martínez, J.C., Luévano-Pinedo, A., López-López, M., 2000, Carta Geológico-Minera Concepción del Oro G14-10 esc. 1:250,000, Pachuca, Hidalgo, Mex., Consejo de Recursos Minerales (Servicio Geológico Mexicano), 1 mapa.

Moràn-Zenteno, D., 1994, The Geology of the Mexican Republic: AAPG Studies in Geology #39, Wilson, J. L and Snachez-Barreda, L. (translators), 160p.

Moreira-Rivera, F., Martínez-Rodríguez, L., Palacios-García, L., Maldonado-Lee, J.M., Olvera-Campos, A., Mata-Pérez, F., Pérez-Benavides, A., González-Monsiváis, P., 1996, Carta Geológico-Minera Matehuala F14-1 esc. 1:250 000, Pachuca, Hidalgo, Mex., Consejo de Recursos Minerales (Servicio Geológico Mexicano), 1 mapa.

Nagase, T., and Kojima, S., 1997, An SEM examination of the chalcopyrite disease texture and its genetic implications: Mineralogical Magazine, vol. 61, pp. 89-97.

Nieto-Samaniego, A. F., Alaniz-Àlvarez, S. A., and Camprubi, A., 2007, Mesa Central of Mexico: Stratigraphy, structure, and Cenozoic tectonic evolution, *in* Geology of Mexico: Celebrating the Centenary of the Geological Society of Mexico: GSA Special Paper 422, p. 41-70.

Norman, D. I. and Musgrave, J. A., 1994, N<sub>2</sub>-Ar-He compositions in fluid inclusions: Indicators of fluid source: *Geochemica et Cosmochimica Acta*, vol. 58, p. 1119-1131. <doi: 10.1016/0016-7037(94)90576-2>

Plumlee, G.S., Montour, M., Taylor, C.D., Wallace, A.R., and Klein, D.P., 1995, Polymetallic Vein and Replacement Deposits (Chapter 14), USGS Open-File Report 95-0831: Preliminary Compilation of Descriptive Geoenvironmental Mineral Deposit Models, du Bray, E.A. (ed.), p. 121-129.

Rhoda, R. and Burton, T., 2010, *Geo-Mexico: the geography and dynamics of modern Mexico*; Sombrero Books, Canada, 288p.

Rocha-Rocha, M., 2016, Metallogenesis of the Peñasquito polymetallic deposit: A contribution to the understanding of the magmatic ore system; Ph.D. thesis, University of Nevada, Reno, 310p.

Rogers, C. L., de Cserna, Z., Tavera, E., and Ulloa, S., 1956, General geology and phosphate deposits of Concepción del Oro district, Zacatecas Mexico: USGS Geological Survey Bulletin 1037-A, 102p.

Rollinson, H. R., 1993, Using Geochemical Data: evaluation, presentation, interpretation; Longman Scientific & Technical, New York, 352p.

Rubin, J.N., and Kyle, J.R., 1988, Mineralogy and geochemistry of the San Martin skarn deposits, Zacatecas, Mexico: Economic Geology and the Bulletin of the Society of Economic Geologists, vol. 83, p. 1982-1801.

Salvador, A., 1987, Late Triassic-Jurassic paleogeography and origin of Gulf of Mexico basin: American Association of Petroleum Geologists Bulletin, vol. 71, no. 4, p. 419-451.

Scorrrar, B., 2014, Preliminary Descriptions of the Intrusive Rocks at Camino Rojo, Internal Report, 9p.

Sedlock, R.L., Ortega-Gutierrez, F., and Speed, R., 1993, Tectonostratigraphic terranes and tectonic evolution of Mexico: Geological Society of America Special Paper 278, 153 p.

Sillitoe, R.H., 1999, Styles of high sulfidation gold, silver and copper mineralization in porphyry and epithermal environments, *in* PACRIM'99, Proc. 7<sup>th</sup> IEEE Pacific Rim Conference on Communications, Computers and Signal Processing, Canada, p. 29-44.

Simmons, S. F., 1991, Hydrologic implications of alteration and fluid inclusion studies in the Fresnillo District, Mexico: Evidence from a brine reservoir and a descending water table during the formation of hydrothermal Ag-Pb-Zn orebodies: Economic Geology and the Bulletin of the Society of Economic Geologists, vol. 86, p. 1579-1601.

Simmons, S.F., and Albinson, T., 1995, Mexican Ag-Au and Ag-Pb-Zn epithermal deposits; hydrothermal products of a magmatic (?) heritage: Publication Series – Australasian Institute of Mining and Metallurgy, 9/95, Proceedings of the 1995 PACRIM congress, *in* Mauk, J.L. and St. George, J.D., (ed.), Exploring the rim, 1995, p. 539-544.

Simmons, S.F., White, N. C., and John, D. A., 2005, Geological Characteristics of Epithermal Precious and Base Metal Deposits: Economic Geology 100<sup>th</sup> Anniversary Volume, p. 485-582.

Simpson, M.P., Simmons, S.F., and Mauk, J.L., 2001, Hydrothermal alteration and hydrologic evolution of the Golden Cross epithermal Au-Ag deposits, New Zealand: Economic Geology and the Bulletin of the Society of Economic Geologists, vol. 96, p. 773-796.

Titley, S. R., 1993, Characteristics of high-temperature, carbonate-hosted massive sulfide ores in the United States, Mexico, and Peru, *in* R. V. Kirkham, W. D. Sinclair, R. I. Thorpe and J. M. Duke (eds.), *Mineral Deposit Modeling: Geological Association of Canada Special Paper*, vol. 40, p. 585-614.

Weiss, S. I., Delgado, J. G., Vázquez, M. V., and Cazares, H. M., 2011, The Camino Rojo Au-Ag-Pb-Zn deposit: vein network, disseminated and replacement styles of mineralization under post-mineral cover, northern Zacatecas, Mexico, *in* *Case Histories of Discovery: NewGenGold Conference Proceedings*, p. 55-64.

Weiss, S. I., July 19, 2012, Camino Rojo Project: PreFeasibility Study, 25p.

White, N. C., and Hedenquist, J. W., 1990, Epithermal environments and styles of mineralization: variations and their causes, and guidelines for exploration: *Journal of Geochemical Exploration*, vol. 36, p. 445-474.

## 9 APPENDIX A: SELECTED THIN SECTION PETROGRAPHY AND PHOTOMICROGRAPHS.

This appendix describes selected Camino Rojo thin sections in order to better detail the host rocks and sulfide mineralization characteristics, with an emphasis on electrum occurrence.

### CARACOL FORMATION: Sample #: 3CR03      Hole 370/ 100m

**Rock Type:** Fine-grained mudstone/ siltstone of the Caracol Formation.

**Sample Description:** The Caracol sample is composed of siltstone/ shale and mudstone. Pyrite is disseminated as both diagenetic framboids and as euhedral grains, and makes up <1% of the rock. The euhedral pyrite grains indicate the sample may be very weakly altered.



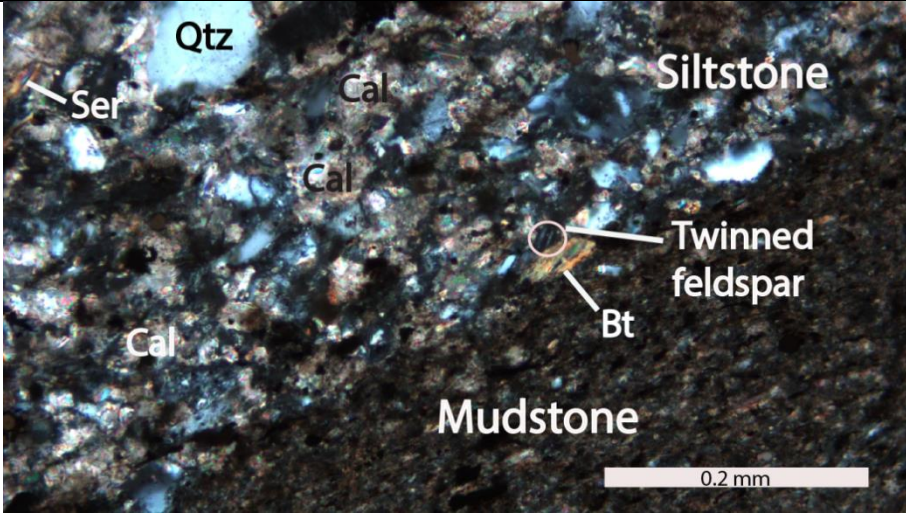
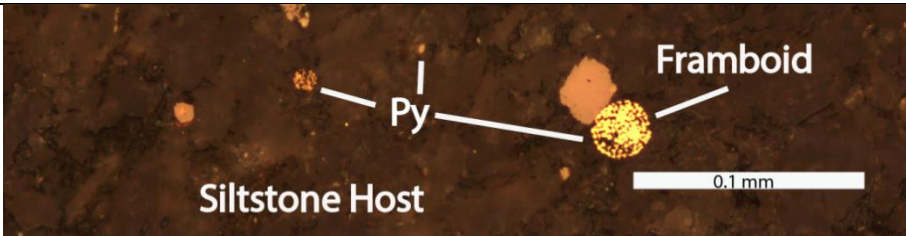
#### **Overall Mineralogy:**

MINERAL	MODE	SIZE (mm)	NOTES
Quartz	30%	.01-.1	Fine, rounded grains hosted in a calcite matrix
Calcite	45%	.01-.1	Fine calcite along bedding makes up the sample matrix
Feldspar	15%?	.01-.3	Fine grains similar to quartz in appearance
Organic Carbon	5%	.01	Very fine organic carbon darkens the unit and is mixed with calcite
Chlorite	2%	.01	Minor mineral that overprints some larger feldspar crystals
Sericite	≤1%	.01-.15	Fine, elongate grains with good cleavage, bright birefringence, and some pleochroism; tends to be associated with calcite; seems to be a small concentration of ser between the siltstone and mudstone units
Pyrite	≤1%	.001-.1	Most of the diagenetic pyrite are framboids (composed of small, rounded to euhedral pyrite grains); occasional fine, euhedral pyrite grains appears to irregularly follow bedding planes.
Biotite?	≤1%	.01	At least one grain found in the siltstone is elongate with brown pleochroism and minor yellow and blue birefringence

#### **Alteration:**

Very weak alteration present as minor sericite, chlorite, and euhedral pyrite in the rock matrix.

No veining.

		<p>The Caracol Formation sample is dark, and nearly unaltered.</p>
		<p>On the boundary between the siltstone/ shale and mudstone, are clear grains of biotite, feldspar, quartz, and calcite.</p>
		<p>Diagenetic pyrite as framboids.</p>

**INDIDURA FORMATION: Sample #: 1CR14 Hole 347/ 827.3m**

**Rock Type:** Recrystallized, massive siltstone/ shale bed in the Indidura Formation.

**Sample Description:** This sample is primarily made up of recrystallized calcite which formed elongate grains along bedding. K-feldspar, quartz and organic carbon make up the rest of the host rock. A 0.6cm pyrite-sphalerite-calcite vein and later calcite veinlets cut across bedding. A quartz- K-feldspar halo with minor oxidation surrounds the sulfide vein. The sample has weak potassic alteration (5-10% K-feldspar).

**Overall Mineralogy:**

MINERAL	MODE	SIZE (mm)	NOTES
Calcite	85%	.01-.4	Recrystallized, elongate calcite has formed along the host rock bedding; calcite veinlets cut the host and also cut a small sulfide vein
K Feldspar	5-10%	.01-.1	The K-feldspar is found within the calcite layers, and is concentrated in a small halo around a pyrite-sphalerite vein
Quartz	3%	.01-.2	Small quartz aggregates are present throughout the host, though seem to be concentrated near the sulfide vein
Pyrite	3%	.01-.6	Anhedral pyrite (and some marcasite) makes up the majority of the sulfide vein with minor pyrite disseminated along the vein boundaries
Carbon	2%	.001	Carbon throughout section is opaque, and tends to concentrate along calcite grain boundaries and mark bedding planes
Sphalerite	1%	.01-.7	Anhedral sphalerite formed adjacent to pyrite in the sulfide vein
Oxides (?)	1%	.01	Trace orange and red, oval shaped minerals near the sulfide veinlet overprint the feldspar alteration; may be goethite.


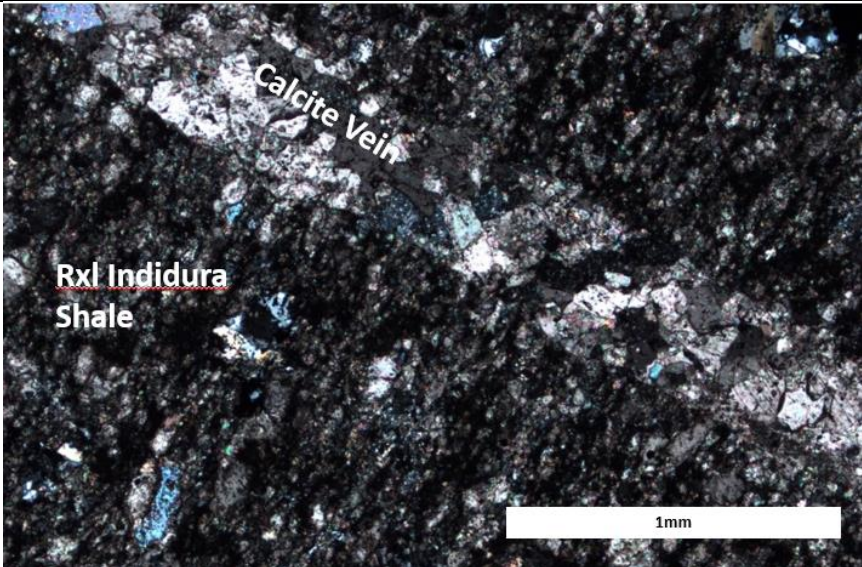
**Alteration:**

POTASSIC ALTERATION (5%-10%) - WEAK

The majority of the sample has been recrystallized, and elongate calcite grains make up the bedding of the Indidura Formation.

**Veins:**

A fine, 0.6cm-wide, pyrite-sphalerite-calcite vein cuts across bedding, and has a small quartz- K-feldspar alteration halo. The sulfide vein is additionally cut by fine calcite veinlets.

	<p>The normally dark-gray Indidura Formation has been altered into a lighter color. Sodium cobaltinitrite staining shows weak to moderate potassic alteration. Pyrite was deposited as veins and as disseminated grains.</p>
 <p>Calcite Vein</p> <p>Rxl Indidura Shale</p> <p>1mm</p>	<p>A calcite veinlet cuts through the recrystallized Indidura Formation shale, which is primarily composed of calcite, with some K-feldspar and quartz grains.</p>



## PETROGRAPHY OF VEIN AND MANTO SAMPLES

The majority of Camino Rojo sulfides were deposited during ore stage 1. Electrum formed during both ore stage 1 and ore stage 2a, and high grade gold samples can contain both stage 1 and stage 2a electrum. Stage 1 electrum formed as blebs commonly within pyrite or other sulfides, and adjacent to subhedral to euhedral arsenopyrite grains. Stage 2a electrum fills later fractures, and is associated with galena and variable amounts of chalcopyrite and tetradymite. The calcite-sericite  $\pm$ pyrite  $\pm$ quartz alteration associated with ore stage mineralization is present when the host rock is included in the thin section, and is indicated in samples below.

**Sample #: 1CR27**

**Hole 370/618.4m**

**Rock Type:** Weakly altered sandstone of the Caracol Formation is cut by a pyrite vein.

**Sample Description:** The Caracol sandstone is made of angular, irregular quartz and feldspar grains. The pyrite vein which cuts the sample includes a later phase of galena-chalcopyrite-electrum. The irregular vein boundary contains subhedral quartz crystals growing into the vein sulfides, and arsenopyrite is concentrated along one vein edge.

The ore stage alteration calcite-sericite  $\pm$ pyrite  $\pm$ quartz is clear. The sericite generally formed finer crystals in a cross-hatch pattern. Disseminated, euhedral pyrite parallel to the vein is common, and appears to follow bedding. Calcite has also been disseminated through the host rock.

Selected Assays	
Au (ppm)	61.8
Ag (ppm)	215
As (ppm)	20000

**Overall Mineralogy:**

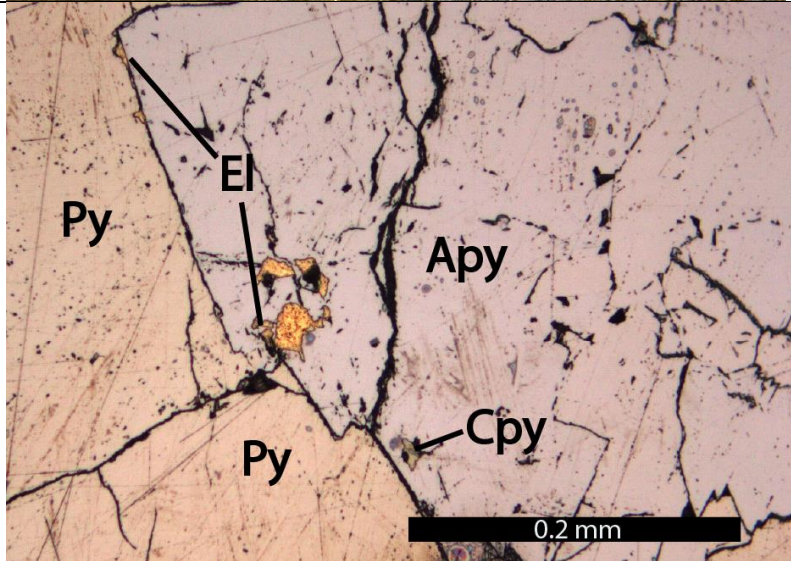
MINERAL	MODE	SIZE (mm)	NOTES
Quartz	40%	.01-.4	Irregular grains within host; excellent undulatory extinction common; euhedral quartz grains along edge of vein
Feldspar	5-15%	.01-.1	The arkosic sandstone also contains irregular feldspar grains
Calcite	12%	.001-.6	Fine and disseminated throughout the host rock;
Pyrite	10-18%	.01-1.2	small disseminated, subhedral to anhedral grains in sandstone; pyrite also makes up most the of the sulfide vein which cuts the sample
Arsenopyrite	5%	.01-.6	Found along edges of the pyrite vein; subhedral with a cracked appearance
Galena	2%	.01-.5	Minor galena fills fractures in the pyrite vein
Chalcopyrite	1%	.001-.1	Fine chalcopyrite grains occur within the pyrite vein
Sericite	1%	.001-.08	Ore-stage alteration mineral within the sandstone host
Sphalerite	≤1%	.01-.3	Anhedral grains within the pyrite vein; often near galena
Electrum	≤1%	.001-.06	Fine, irregular grains are included in py and apy; fracture-filling electrum associated with galena is also present

**Alteration:**

The ore stage alteration calcite-sericite ±pyrite ±quartz is present in the sandstone host. Sericite formed fine, elongate grains in a cross-hatch pattern. Disseminated pyrite follows bedding orientation. In some areas, the host matrix quartz is fine and interlocked, and may have been recrystallized.

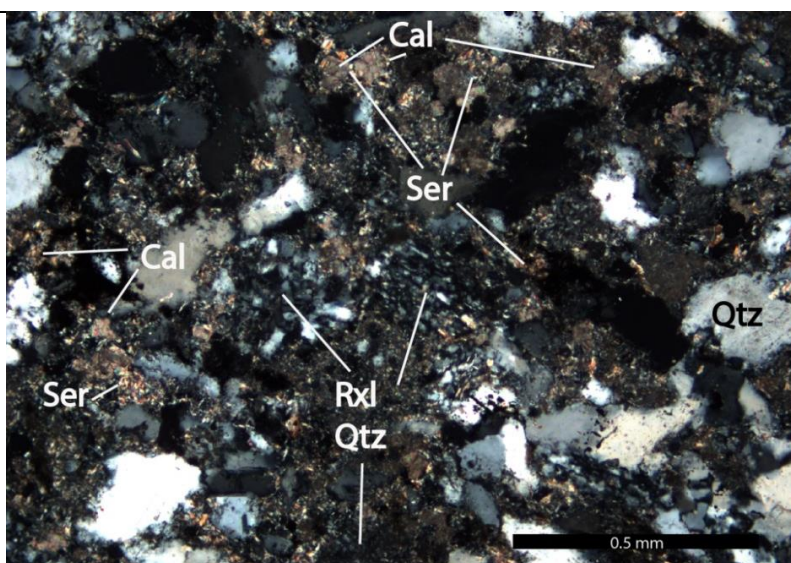
**Veins:**

A pyrite vein contains arsenopyrite along one vein edge. Minor euhedral to subhedral quartz formed along the vein boundary, and is generally in contact with euhedral, infilling Apy. A late phase of chalcopyrite-galena-electrum fills fractures in the earlier sulfides.

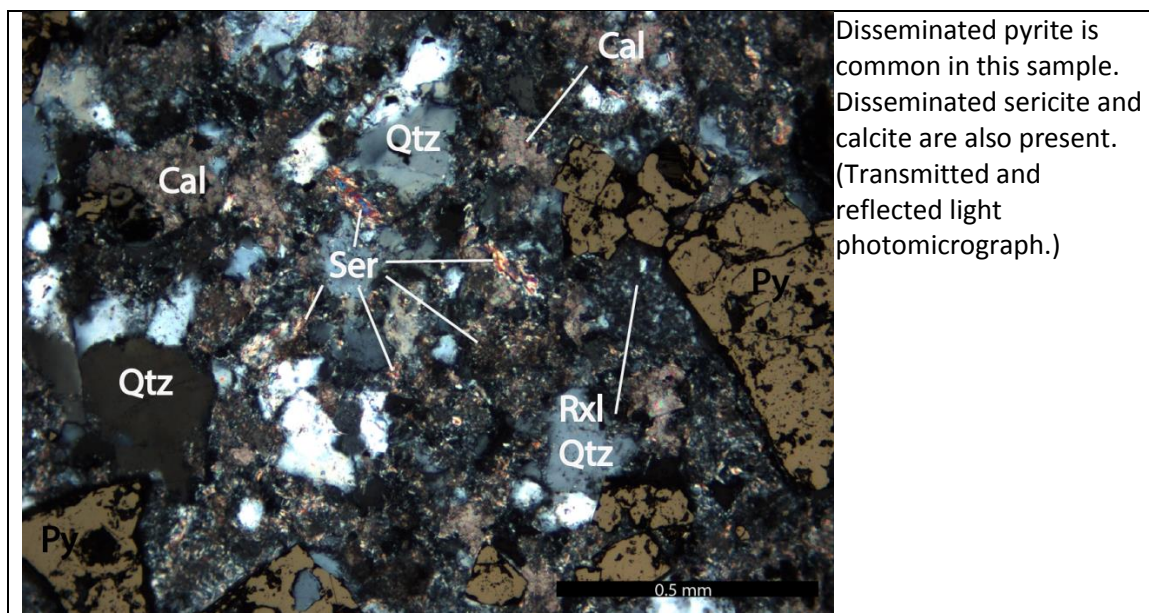


A pyrite vein cuts along bedding orientation through the Caracol Formation.

Electrum was deposited along the arsenopyrite grain boundary, and within fractures through arsenopyrite.



Fine interlocked quartz grains may indicate quartz recrystallization. The disseminated calcite and sericite is typical of the ore stage alteration.



**Sample #:** 1CR09

**Hole** 345/616.7m

**Rock Type:** Weak to moderate potassic alteration of the Caracol Formation.

**Sample Description:** A micro-fault offsets the planar bedding and a small pyrite vein (>2cm) containing electrum occurs along the bottom edge of the billet. Disseminated pyrite is bedding controlled. The electrum was deposited as rounded blebs within pyrite, and as later, larger grains within fractures through the earlier pyrite. Tetradyomite ( $\text{Bi}_2\text{Te}_2\text{S}$ ) was discovered in this sample through SEM analysis, and is associated with the late stage electrum.

Selected Assays	
Au (ppm)	6.3
Ag (ppm)	1.5
As (ppm)	210

**Overall Mineralogy:**

MINERAL	MODE	SIZE (mm)	NOTES
Quartz	20-30%	.001-.2	Fine, anhedral grains making up siltstone/ fine sandstone host; average grain size is roughly 0.05cm
Pyrite	15-25%	.001-.6	Anhedral; occurs both within vein and disseminated in matrix along lith boundary and in microfault zone; oxidized grain edges can appear strongly anisotropic blue-orange; pyrite makes up majority of disseminated sulfides
K- Feldspar	5-15%	.01-.1	Alteration mineral; flooding throughout matrix of sample, especially within sandier units
Calcite	15-25%	.001-.05	Calcite is associated with K-spar alteration textures, and is concentrated in the finer, siltstone beds; also concentrated close to sulfide vein and disseminated sulfides
Adularia	≤1%	.01-.25	Very fine, subhedral growth along edge of sulfide vein
Galena	≤1%	.01-.4	Minor occurrence in sulfide vein; elongate, anhedral inclusions in py, and later phase associated with gold-filling fractures
Electrum	≤1%	.01-.4	Rounded blebs within py/ marcasite/ arsenopyrite
Tetradymite	≤1%	.01	Light gray sulfide, very soft; occurring in fractures with gold; reminiscent of galena...

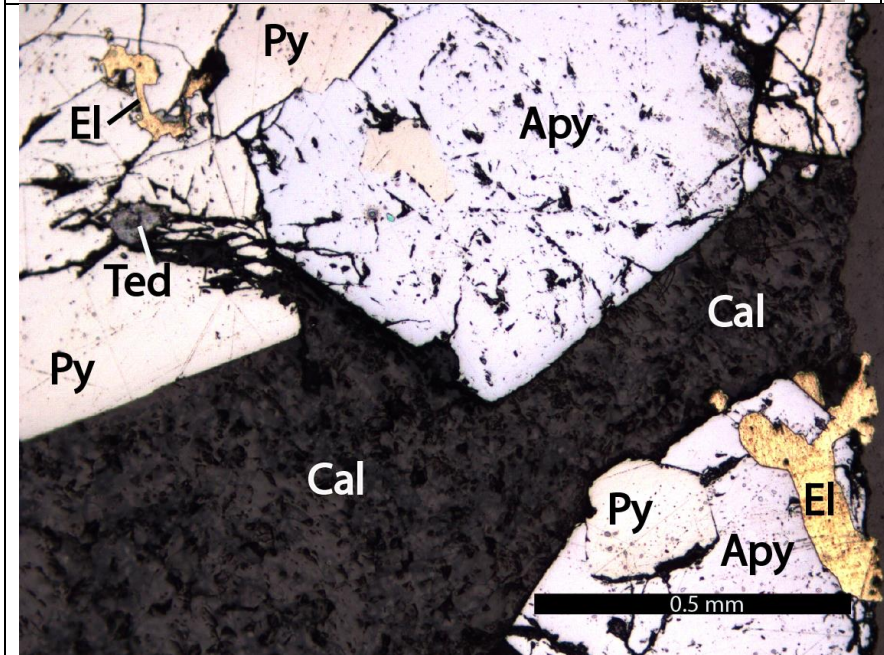
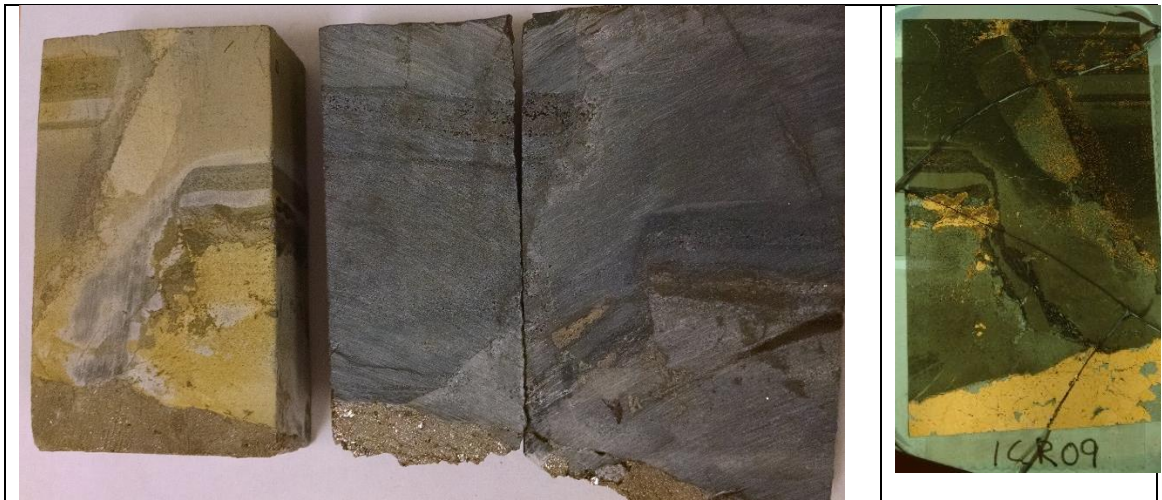
**Alteration:**

POTASSIC ALTERATION (10-20%) - WEAK/ MODERATE

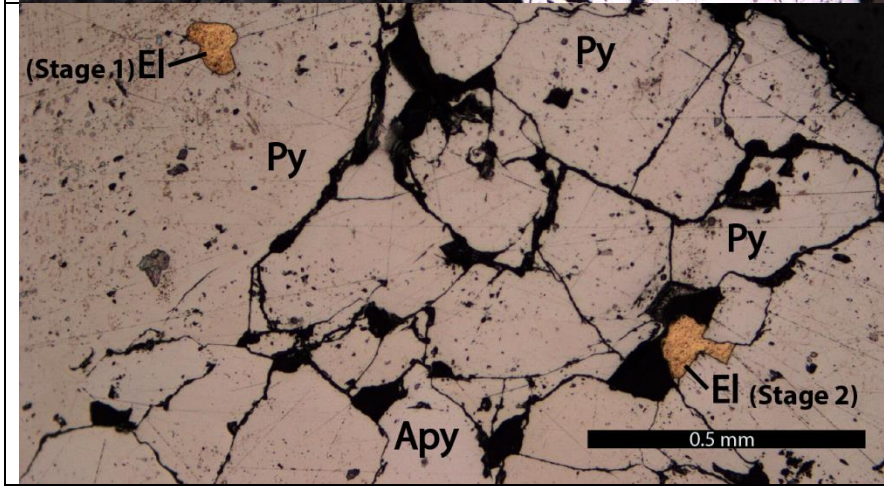
Disseminated pyrite is common in the host rock along bedding boundaries. A few grains of arsenopyrite were also disseminated. A fine jigsaw quartz texture within the sedimentary host may indicate recrystallization. The ore-stage alteration sericite is not as abundant as in other high gold grade samples. The disseminated calcite is associated with disseminated pyrite.

**Veins:**

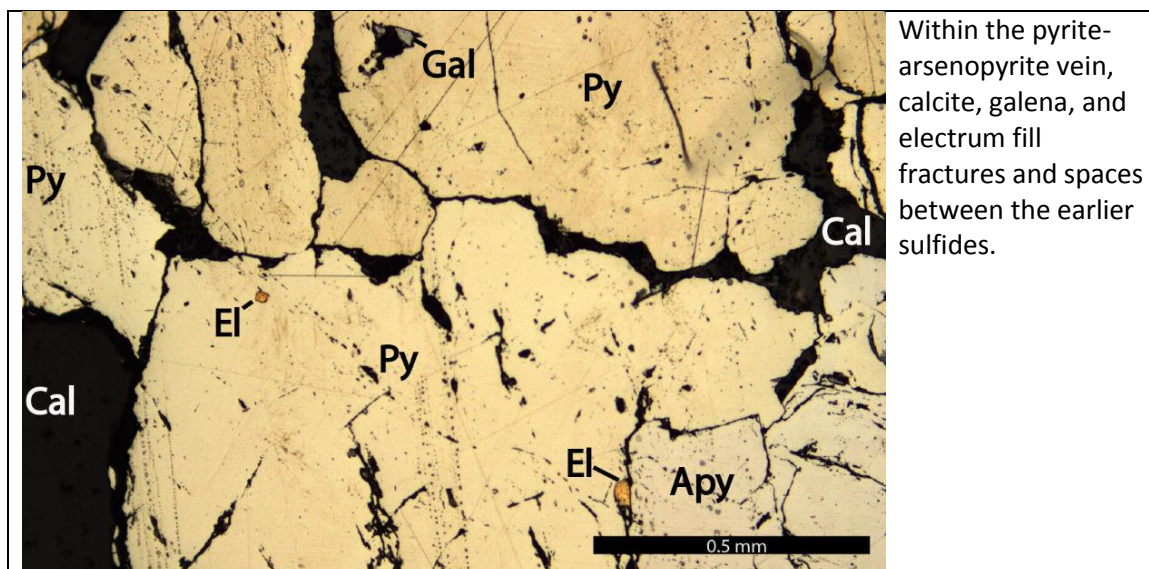
The fine pyrite vein is ≤2cm in width and cuts bedding. Lesser amounts of arsenopyrite are also present. A late, galena-electrum-tetradymite stage filled fractures within the vein.



The pyrite-arsenopyrite-calcite vein. A late stage of electrum (El) and tetradyomite (Ted) filled fractures through the earlier sulfides.



The pyrite-arsenopyrite vein has both stage 1 and stage 2a electrum.



**Sample #:** 1CR26

**Hole** 369/643m

**Rock Type:** Moderately altered Caracol Formation with a 4cm wide py-apy-sph vein.

**Sample Description:** This intergranular sulfide vein contains good examples of Stage 1 electrum. The vein is composed of pyrite, arsenopyrite, sphalerite, chalcopryite, and galena, with calcite between sulfide grain boundaries. Subhedral to euhedral quartz crystals are found on the edge of the vein closest to the host rock. A small, 3mm wide lithic fragment is included in the vein.

Selected Assays	
Au (ppm)	64.5
Ag (ppm)	141
As (ppm)	20000

**Overall Mineralogy:**

MINERAL	MODE	SIZE (mm)	NOTES
Arsenopyrite	30-35%	.1-2.2	Early, anhedral to euhedral grains associated with el deposition; twinning/ zoning in XPL in some grains
Pyrite	15-20%	.01-4.1	subhedral-euhedral pyrite grains intergranular to arsenopyrite in vein
Calcite	10-15%	.01-2.8	Late phase fills space around sulfides; undulatory extinction;

Sphalerite	5-10%	.2-1.5	Subhedral to anhedral grains slightly later than py and apy; minor chalcopyrite inclusions
Chalcopyrite	5%	.05-1.6	Anhedral grains included within sph; also filling spaces with later calct
Quartz	2-5%	.1-1.5	Euhedral grains growing outward from sulfide vein boundary with host rock; apparent qtz vein cuts sph;
Galena	1-4%	.01-.8	Anhedral galena is later than the other sulfides; can fill fractures in py
Marcasite	1-3%	.01-.1	Fine, grouped grains along the edges of some pyrite grains; minor blue anisotrophy; psuedomorph after py?
Electrum	≤1%	.01-.3	Rounded gold blebs included in apy/ sph; in one example, darker-orange electrum formed in cracks adjacent to a round electrum grain, and may represent more pure, remobilized electrum

**Alteration:**

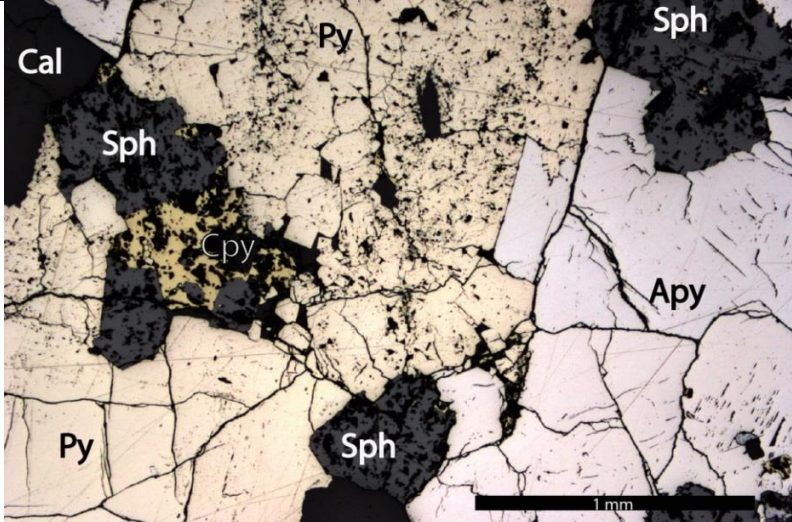
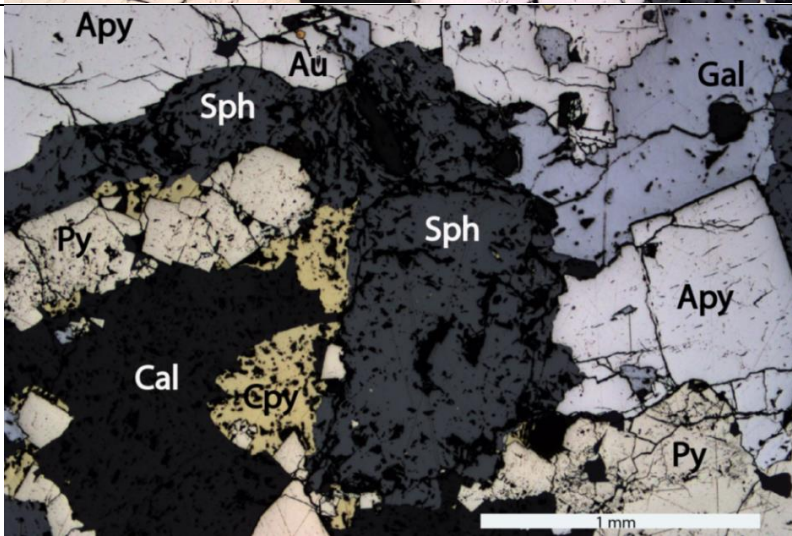
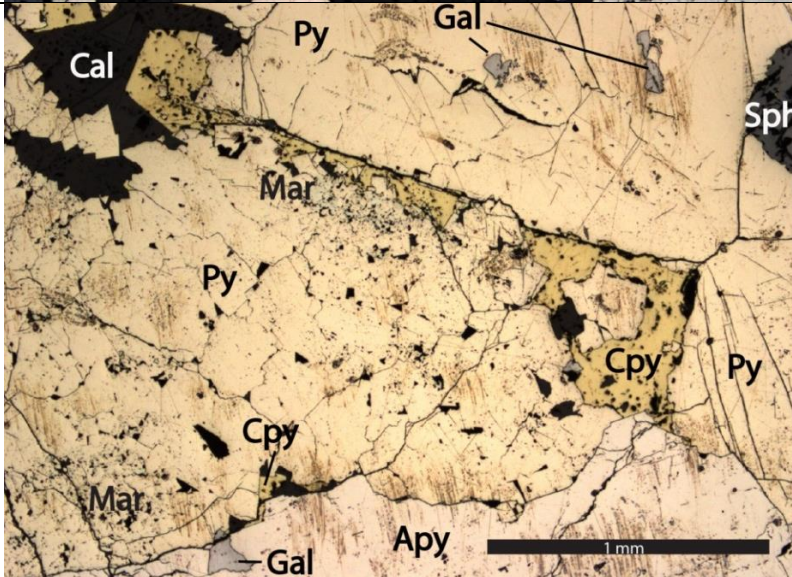
Rounded calcite blebs overprint a finely bedded siltstone

**Veins:**

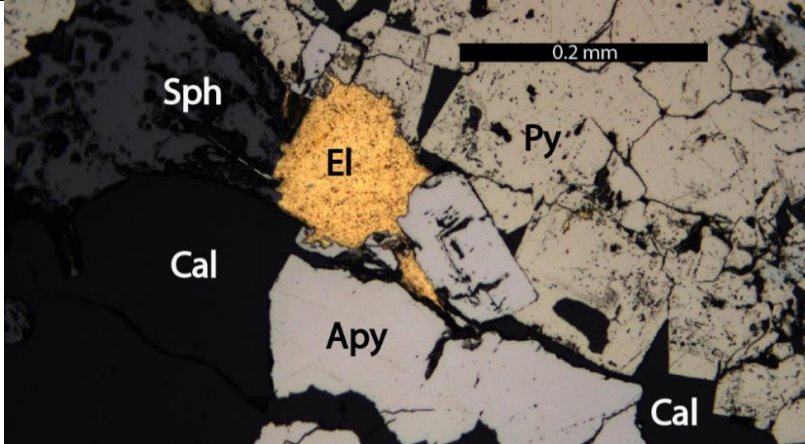
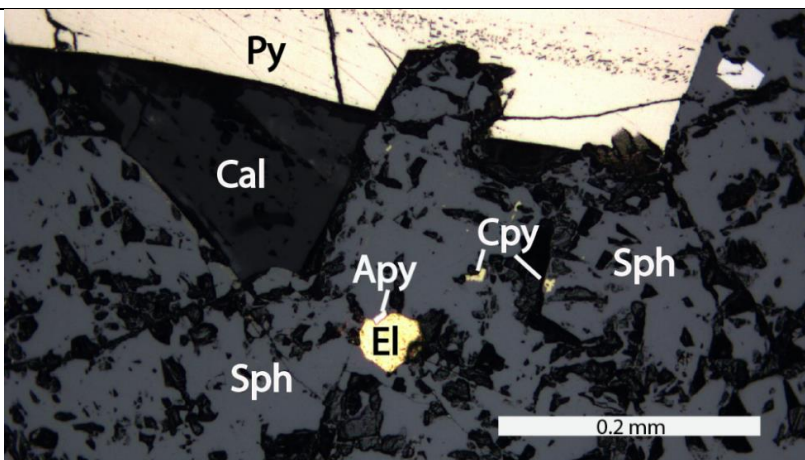
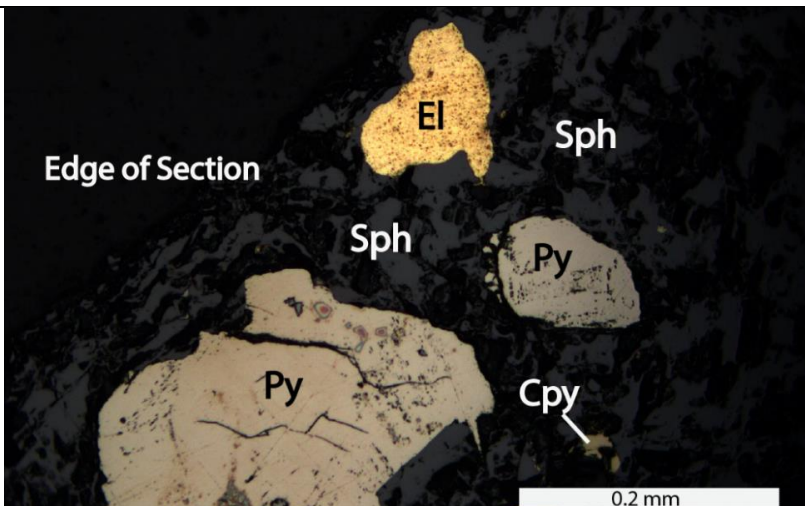
A large, intergranular pyrite-arsenopyrite-sphalerite-calcite vein with lesser amounts of chalcopyrite-marcasite-galena-electrum.

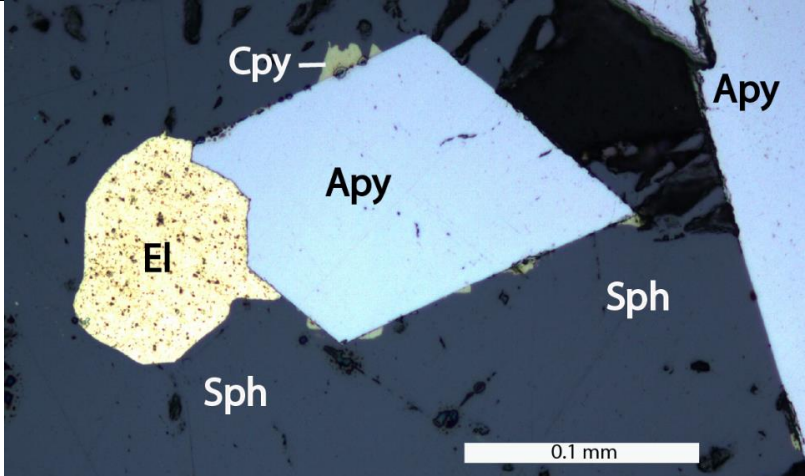
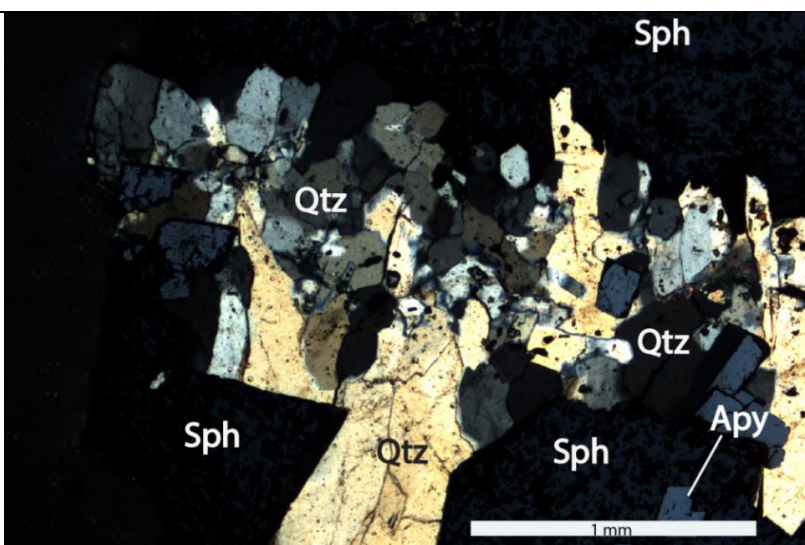
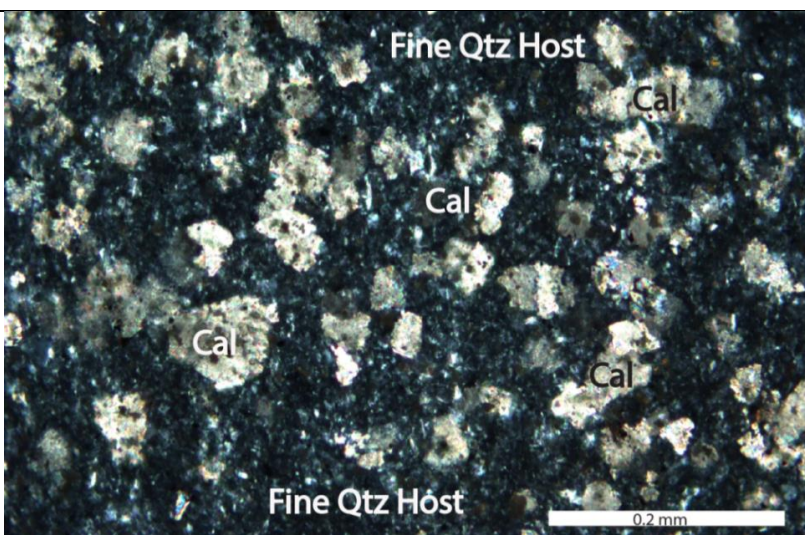




 <p>This micrograph shows a complex mineral assemblage. Dark, irregularly shaped grains of pyrite (Py) and arsenopyrite (Apy) are visible, separated by lighter-colored, more crystalline grains of sphalerite (Sph). Chalcopyrite (Cpy) and calcite (Cal) are also present, filling some of the spaces between the primary mineral grains. A 1 mm scale bar is located at the bottom right of the image.</p>	<p>Intergranular pyrite and arsenopyrite with later sphalerite, chalcopyrite, and calcite.</p>
 <p>This micrograph displays a similar mineral assemblage to the first image. It features pyrite (Py), arsenopyrite (Apy), and sphalerite (Sph). Later-stage minerals include galena (Gal), calcite (Cal), and chalcopyrite (Cpy). A small, bright yellow grain of electrum (Au) is clearly visible near the edge of an arsenopyrite grain. A 1 mm scale bar is located at the bottom right of the image.</p>	<p>Intergranular pyrite, arsenopyrite, sphalerite, with later galena, calcite and chalcopyrite. A small electrum grain (labeled Au) is located near the edge of an arsenopyrite grain.</p>
 <p>This micrograph illustrates the formation of secondary minerals. It shows pyrite (Py) grains with fractures filled by later chalcopyrite (Cpy) and galena (Gal). Chalcopyrite also formed along the boundaries of pyrite grains. Minor marcasite (Mar) is visible at the edges of pyrite grains. Calcite (Cal) and arsenopyrite (Apy) are also present. A 1 mm scale bar is located at the bottom right of the image.</p>	<p>Later chalcopyrite and galena fill fractures. The chalcopyrite additionally formed along a pyrite grain boundary. Minor marcasite formed at the edges of a pyrite grain.</p>

	<p>Intergranular arsenopyrite and pyrite, with later sphalerite, galena, and chalcopyrite.</p>
	<p>Rounded electrum bleb within arsenopyrite. Later galena, sphalerite, and calcite.</p>
	<p>Rounded, stage 1 electrum within arsenopyrite. The electrum appears to have been partially remobilized and also fills small fractures through the arsenopyrite.</p>

 <p>A large yellow electrum (El) grain is visible, surrounded by pyrite (Py), arsenopyrite (Apy), and sphalerite (Sph) grains. Calcite (Cal) is present in the interstices. A scale bar of 0.2 mm is shown at the top right.</p>	<p>A large electrum grain deposited between pyrite, arsenopyrite, and sphalerite grains, with later calcite.</p>
 <p>A round yellow electrum (El) grain is embedded within a sphalerite (Sph) grain. A small, euhedral arsenopyrite (Apy) crystal is located adjacent to the electrum. Pyrite (Py) and calcite (Cal) are also present. A scale bar of 0.2 mm is shown at the bottom right.</p>	<p>A round electrum grain within sphalerite; a small, euhedral arsenopyrite crystal formed adjacent to the electrum.</p>
 <p>Round-shaped pyrite (Py), electrum (El), and chalcocopyrite (Cpy) are visible within sphalerite (Sph). The edge of the section is labeled. A scale bar of 0.2 mm is shown at the bottom right.</p>	<p>Round-shaped pyrite, electrum, and chalcocopyrite within sphalerite.</p>

 <p>A round electrum grain (El) is adjacent to a euhedral arsenopyrite crystal (Apy) within sphalerite (Sph). Chalcopyrite (Cpy) is formed along the arsenopyrite grain edges. Scale bar: 0.1 mm.</p>	<p>A round electrum grain adjacent to a euhedral arsenopyrite crystal within sphalerite; chalcopyrite formed along the arsenopyrite grain edges and may be associated with the electrum deposition.</p>
 <p>An irregular quartz vein (Qtz) cuts through sphalerite (Sph) at the edge of the sulfide vein. Arsenopyrite (Apy) is also visible. Scale bar: 1 mm.</p>	<p>An irregular quartz vein cuts through sphalerite at the edge of the sulfide vein.</p>
 <p>The host rock has extensive secondary calcite (Cal) overprinting a fine-quartz matrix (Fine Qtz Host). Scale bar: 0.2 mm.</p>	<p>The host rock has extensive secondary calcite overprinting a fine-quartz matrix.</p>

**Sample #: 1CR29****Hole 370/647.2m**

**Rock Type:** Altered and bleached Caracol Formation with sulfide veining parallel to core axis.

**Sample Description:** The host rock has been moderately potassically altered. A quartz-sphalerite-pyrite vein is cut by a larger vein of pyrite-arsenopyrite-chalcopyrite-quartz-calcite-with minor galena-electrum. The ore stage calcite-sericite alteration overprints the earlier potassic alteration. Anhedral to euhedral pyrite is disseminated along bedding. Jigsaw quartz is present in the matrix. Late, fine calcite veinlets cut everything.

Selected Assays	
Au (ppm)	31.3
Ag (ppm)	107
As (ppm)	20000

**Overall Mineralogy:**

MINERAL	MODE	SIZE (mm)	NOTES
Quartz	35%	.005-.2	Finer, euhedral to subhedral quartz along edges of vein; anomalous blues and browns in vein; also part of earlier qtz-sph-py vlt
K-Feldspar	25%	.01-.2	K-feldspar grains range from being round to angular and elongate and primarily are fine grained replacing the host matrix
Calcite	15%	.01-.4	Minor calcite disseminated throughout; late calcite vlt cut massive sulfides and matrix; larger, sea-shell texture within vein infill spaces; late-stage associated with sericite, in some cases forming veins
Chalcopyrite	10%	.1-3	Common phase as inclusions in sph and primary sulfide in massive sulf vein; minor dis. cpy overprints calcite veins;
Pyrite	8%	.1-.4	Disseminated through sample; also part of massive sulfide vein; minor component of earlier qtz-cc-sph-py vlt
Arsenopyrite	4%	.1-.3	White, pale mineral, blue anisotropy; lamellar twinning; part of coarser massive sulfide vein
Sericite	2%	.01-.3	Fine alteration mineral replacing feldspar grains in matrix; larger sericite crystals occasionally within sandstone;
Sphalerite	≤1%	.02-.1	Fine inclusions within massive py vein; also part of fine qtz-cc-py-sph vlt
Electrum	≤1%	.005-.02	Late, free gold formed in fracture between py and apy occurring with galena (next to vein intersection)

**Alteration:**

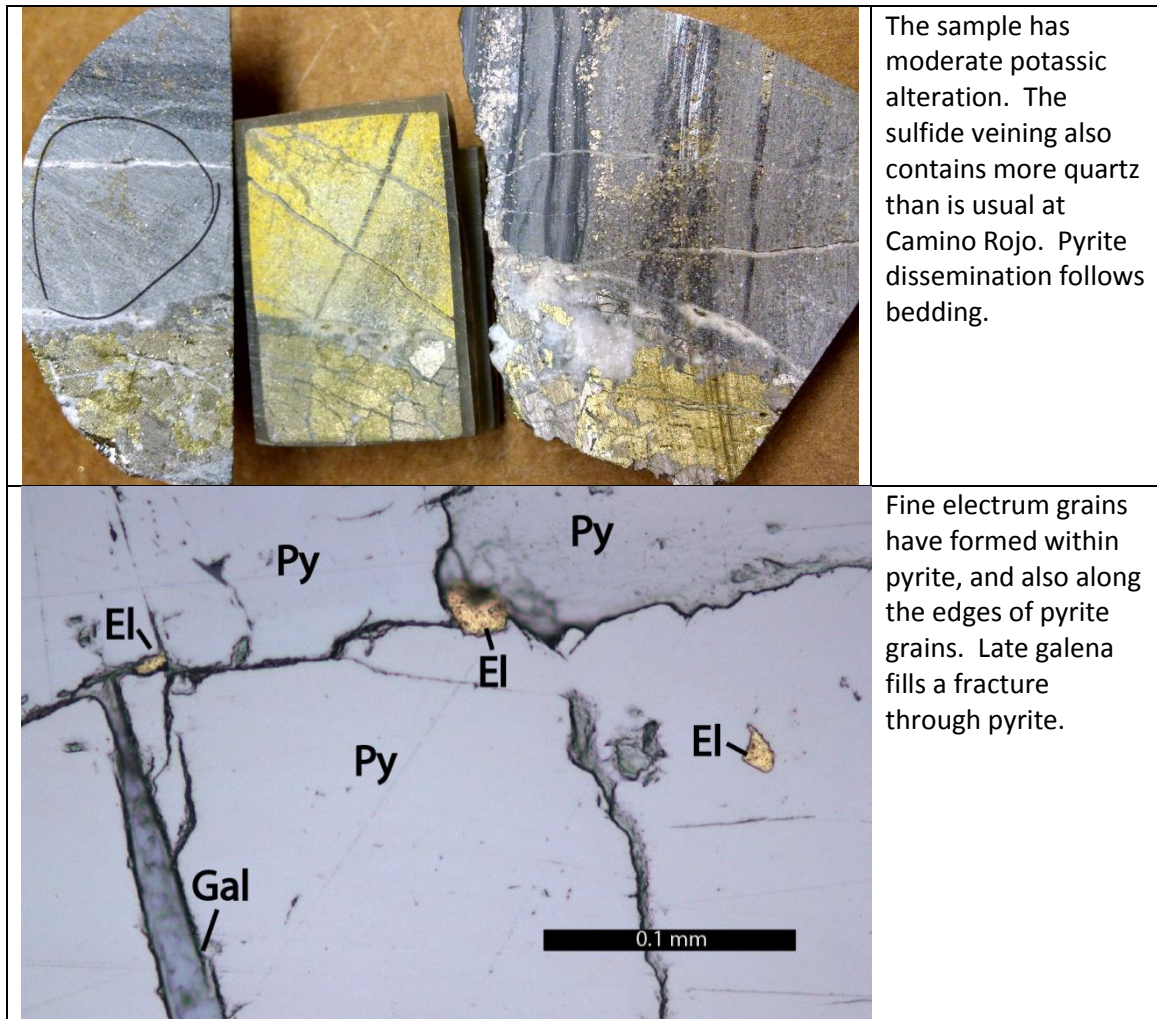
POTASSIC ALTERATION (20%-30%) – MODERATE TO WEAK ALTERATION

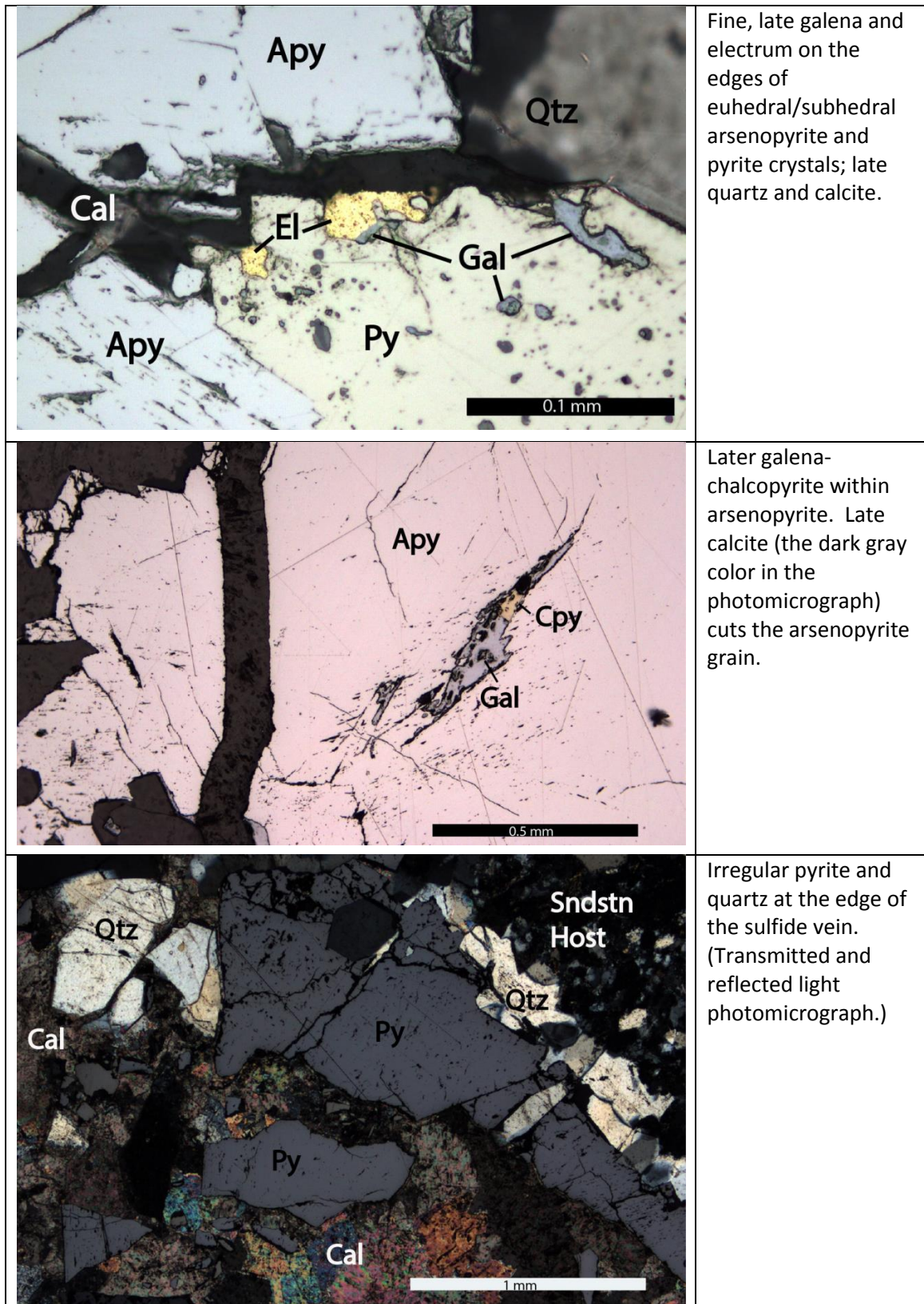
Later calcite-sericitic alteration overprints the potassic alteration. Disseminated pyrite is common. The angular, arkosic sandstone grains appear to be surrounded by a fine, jigsaw-quartz matrix.

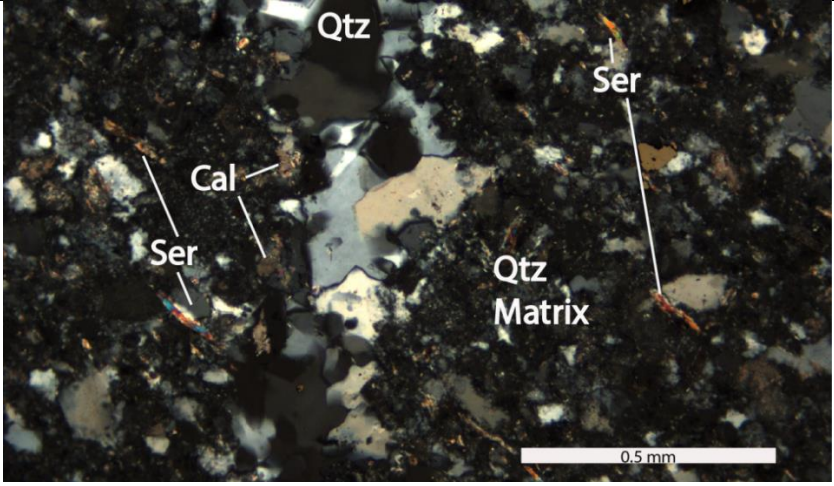
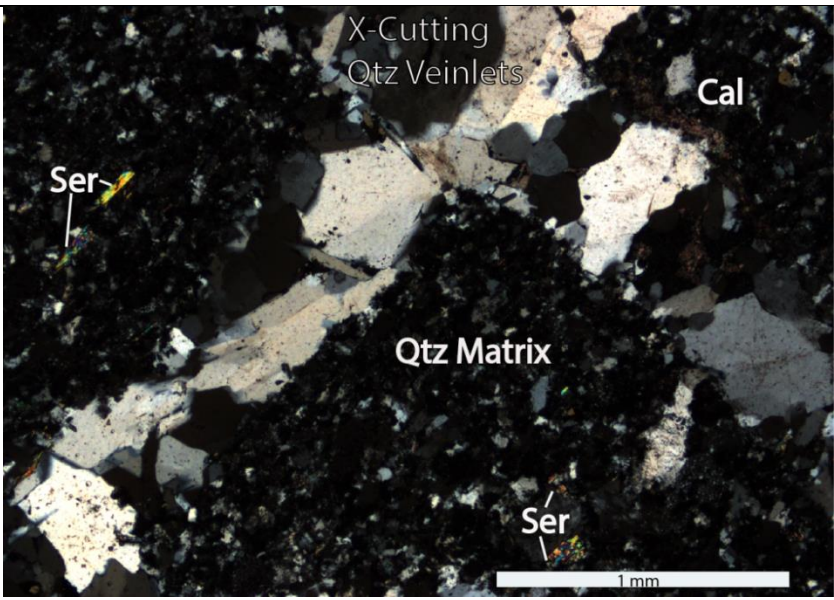
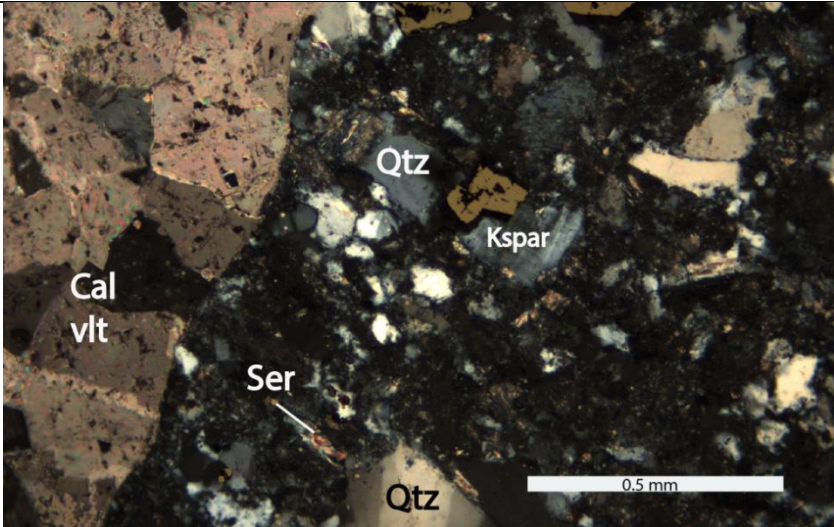
**Veins:**

Sphalerite-Pyrite-Quartz-Calcite veinlet is cut and offset by later calcite veinlets

Cross-cutting, fine quartz veinlets also present ( $\geq 1\text{mm}$ )





 <p>Qtz Ser Cal Qtz Matrix 0.5 mm</p>	<p>The sandstone host with calcite-sericite alteration. A later, irregular quartz lense cuts the host.</p>
 <p>X-Cutting Qtz Veinlets Cal Ser Qtz Matrix 1 mm</p>	<p>Cross-cutting quartz veinlets within the sandstone host.</p>
 <p>Cal vlt Ser Qtz Kspar Qtz 0.5 mm</p>	<p>Potassic alteration of the sandstone host, with overprinting calcite-sericite alteration. Subhedral, bronze-colored disseminated pyrite grains are also present. (Transmitted and reflected light photomicrograph.)</p>



**Sample #: 1CR31****Hole 370/721m**

**Rock Type:** Weakly altered siltstone hosts a massive sulfide vein.

**Sample Description:** A pyrite-sphalerite-calcite vein is hosted in shale. Calcite within the vein is jigsaw textured, with extinction undulating from crystal to crystal. Fine, elongate sedimentary lithics (mudstone?) are found in the vein, and have subhedral to euhedral quartz along their edges.

**Overall Mineralogy:**

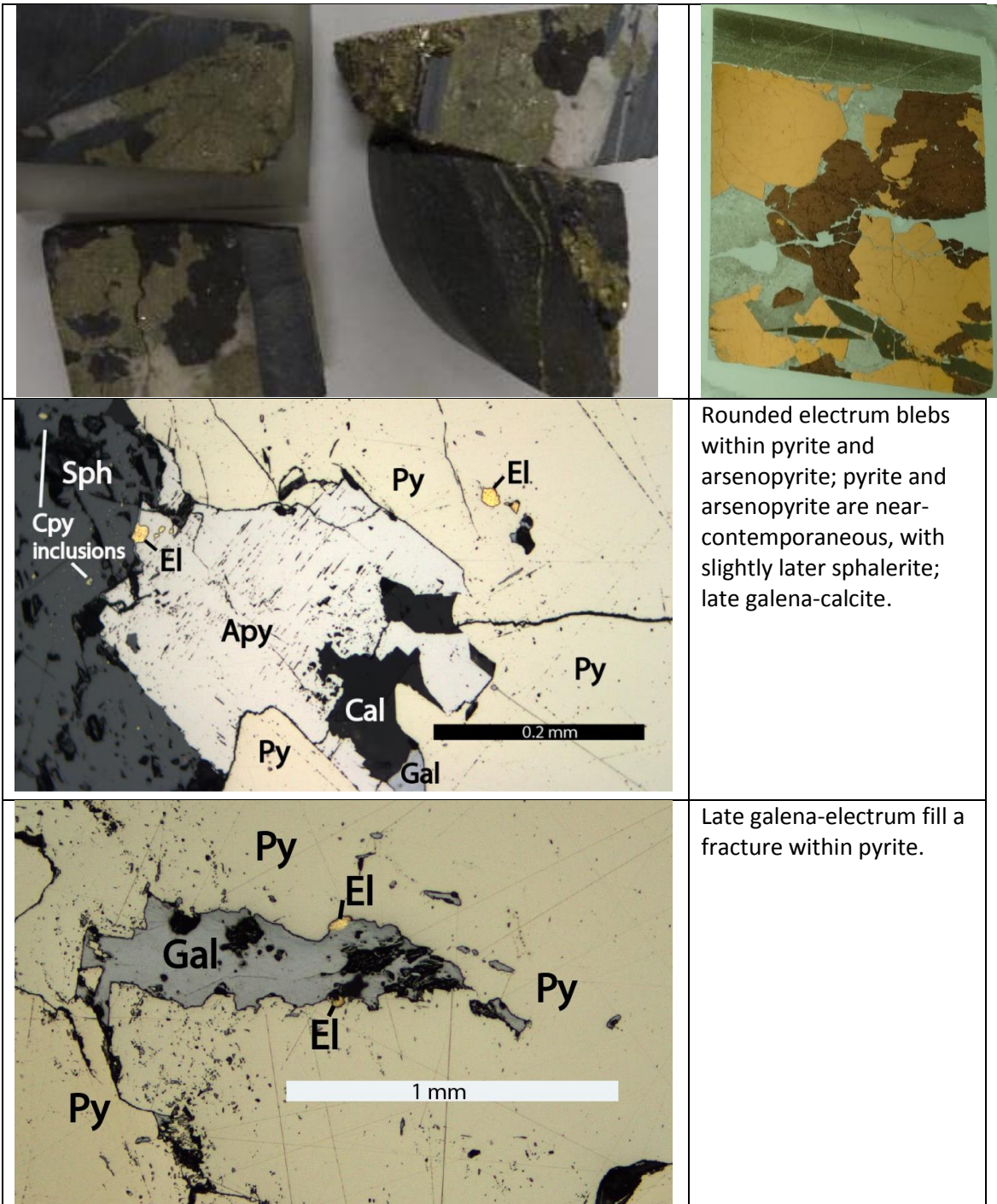
MINERAL	MODE	SIZE (mm)	NOTES
Pyrite	25-35%	.1-3.2	Pyrite makes up most of the sulfide vein; subhedral pyrite is disseminated in the siltstone host
Sphalerite	10-20%	.5-3.8	Anhedral grains are intergranular with py in sulfide vein; deep red IR (internal reflectance)
Quartz	10-15%	.001-.01	Main component in siltstone; some fine, subhedral to euhedral crystals have formed along the vein edges
Calcite	10-15%	.01-2	Calcite is a fine and minor alteration mineral which overprints the matrix; it is also part of the vein mineralogy
Carbon	2-5%	.001	Very fine carbon makes up a portion of the siltstone host
Galena	2-5%	.01-.4	Fine anhedral masses of galena fill fractures within py and sph; often formed with electrum
Arsenopyrite	2-4%	.1-.9	Minor phase, with euhedral to subhedral grains located along the edges of pyrite
Chalcopyrite	≤1%	.01	Fine inclusions within sphalerite
Electrum	≤1%	.03	Late, rounded blebs included within pyrite and arsenopyrite; fracture filling electrum is also strongly associated with galena

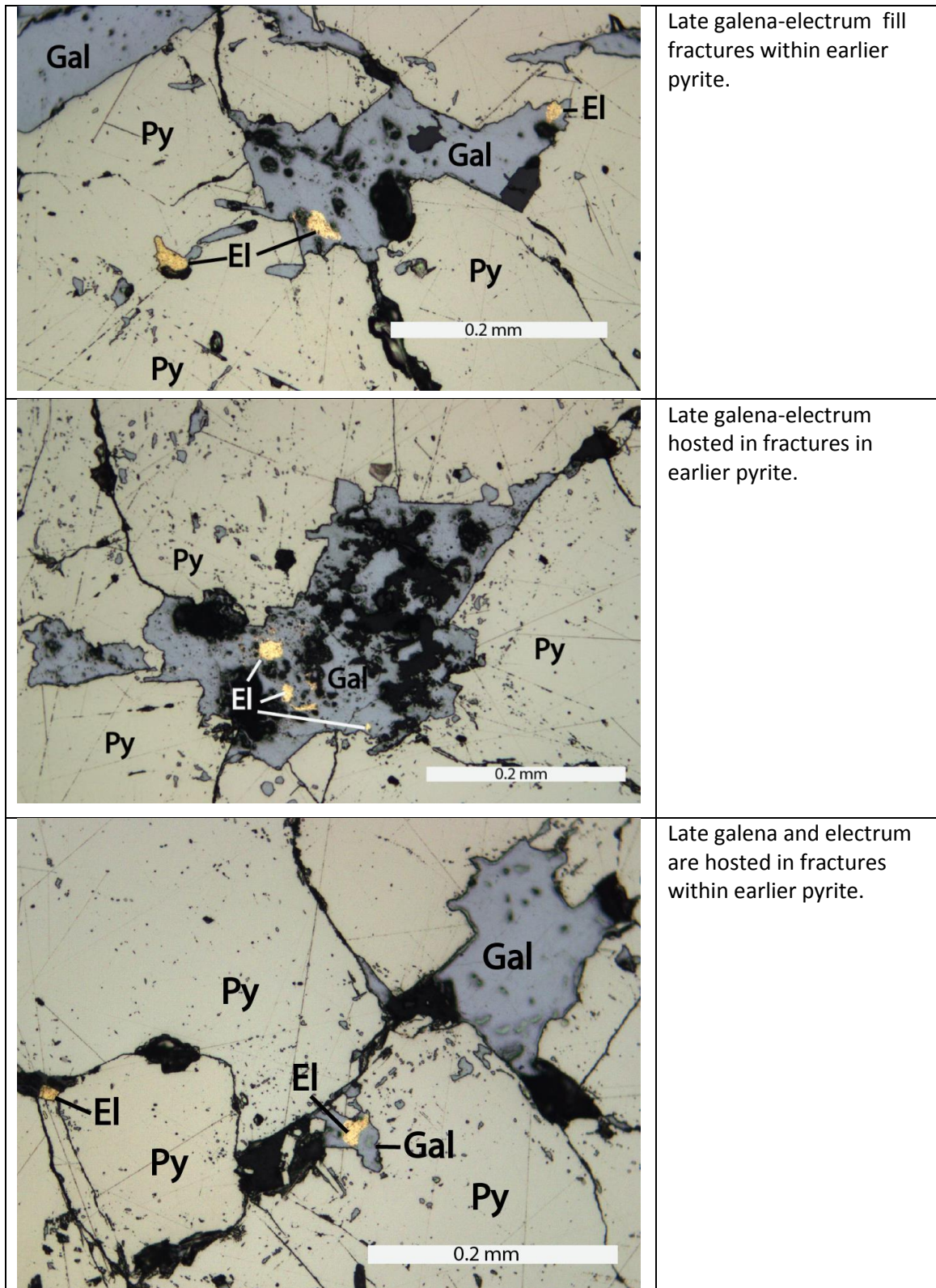
**Alteration:**

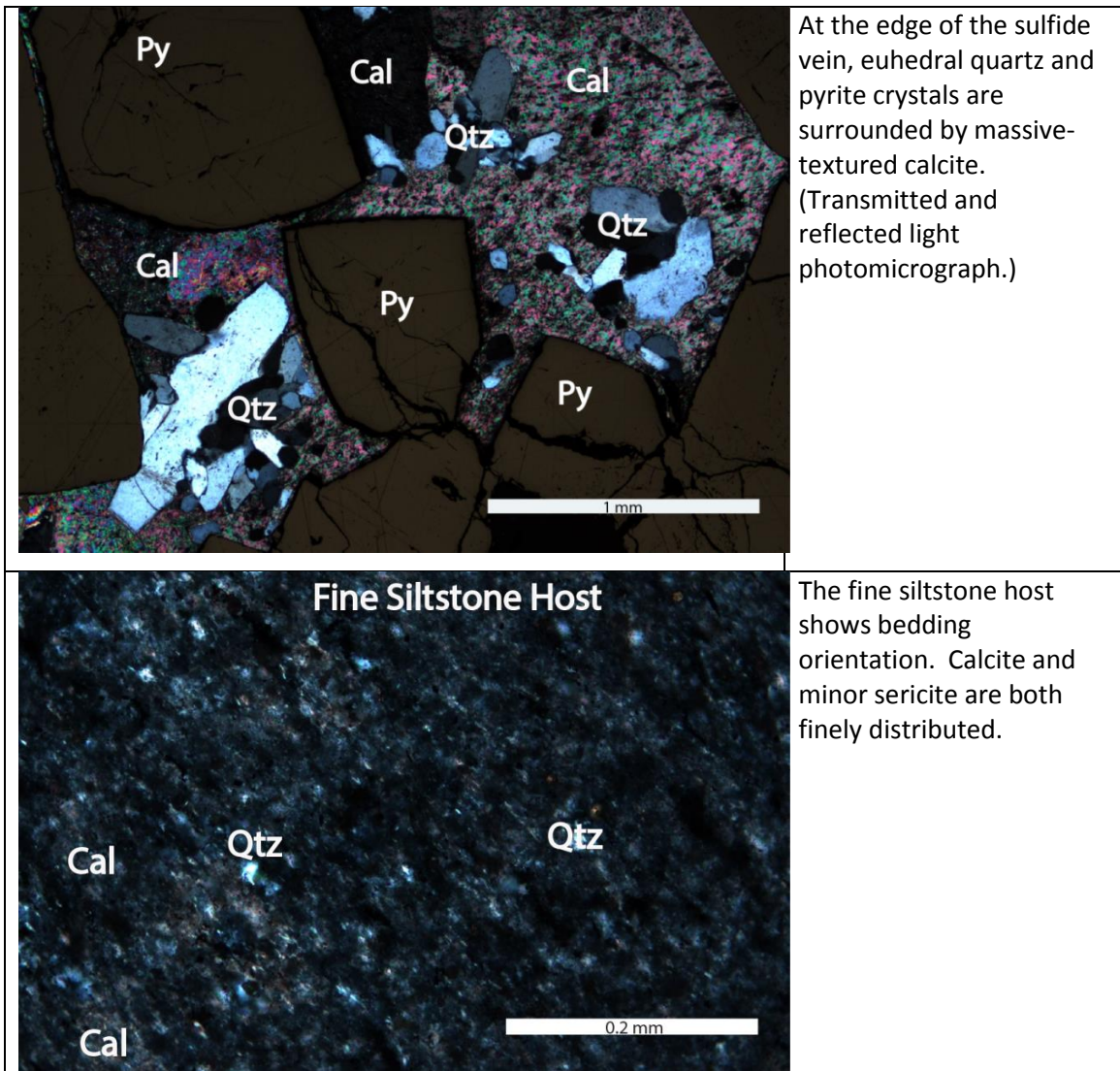
Minor calcite overprints the siltstone host, and is disseminated in the sample along bedding.

**Veins:**

A pyrite-sphalerite-calcite-arsenopyrite vein with later chalcopyrite-galena-electrum. The vein has clean edges, and cuts across the siltstone bedding.







At the edge of the sulfide vein, euhedral quartz and pyrite crystals are surrounded by massive-textured calcite. (Transmitted and reflected light photomicrograph.)

### Fine Siltstone Host

The fine siltstone host shows bedding orientation. Calcite and minor sericite are both finely distributed.

## MANTOS MINERALIZATION

**Sample #:** 1CR07 **Hole** 345/529.4m

**Rock Type:** Manto replacement of siltstone/ sandstone within the Caracol Formation.

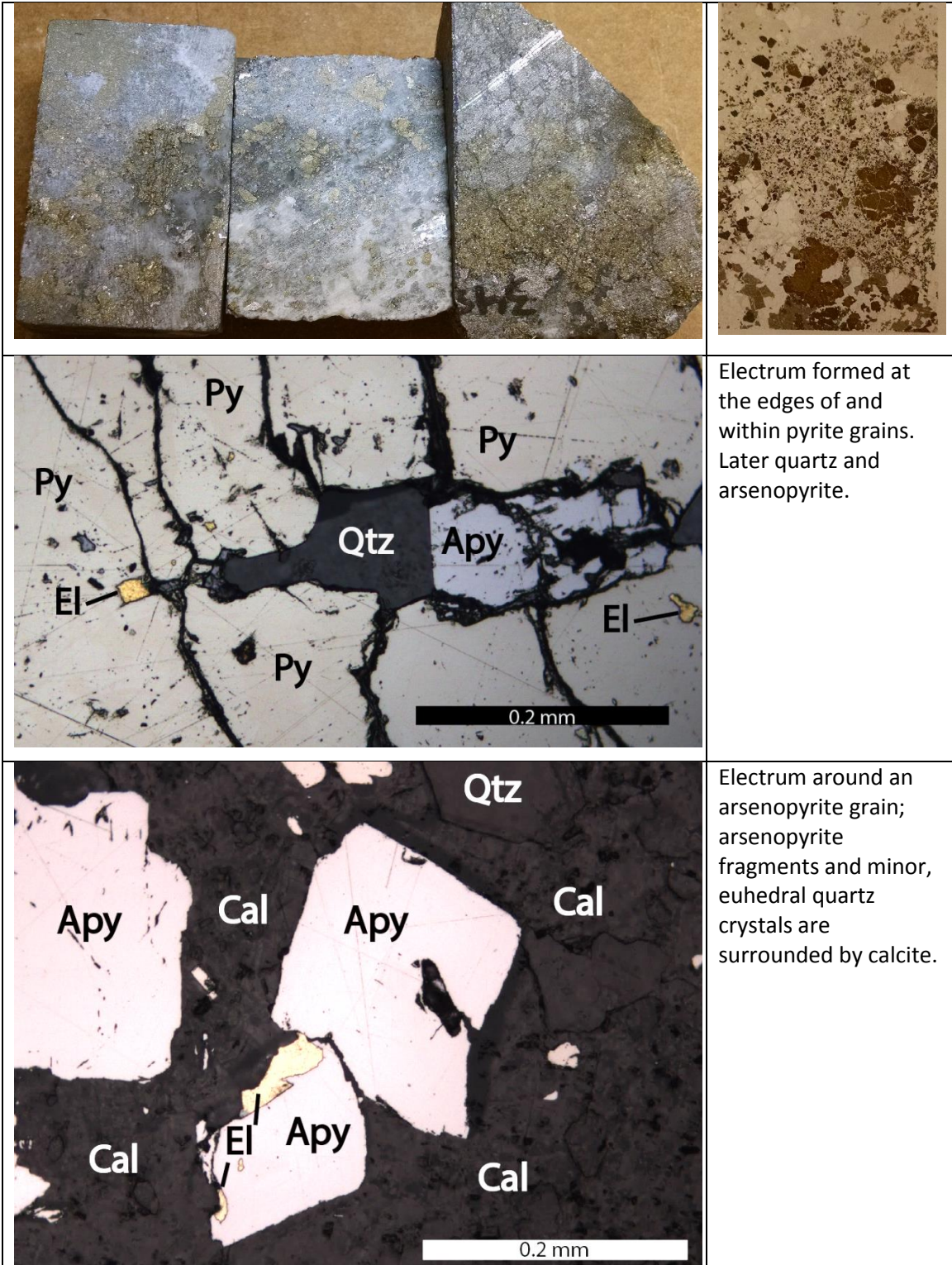
**Sample Description:** Relatively high grade manto within the Caracol Formation. Angular fragments of pyrite and arsenopyrite are hosted in a quartz-calcite matrix. The quartz formed large, subhedral, interlocked grains. A few grains of electrum, associated with galena, formed along the edges of arsenopyrite or pyrite grains hosted in calcite.

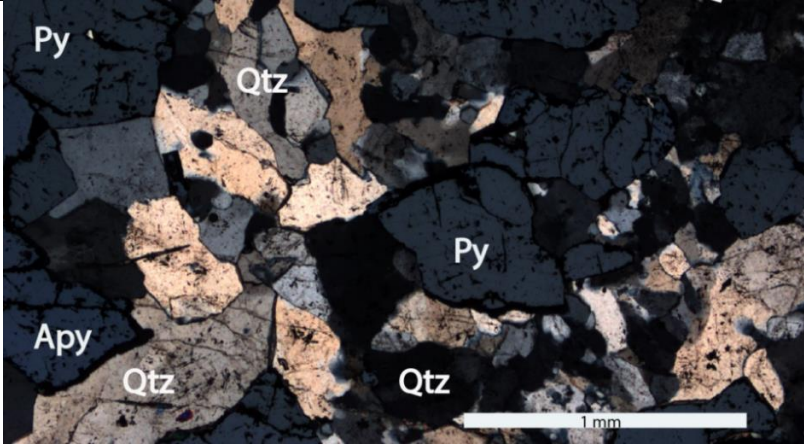
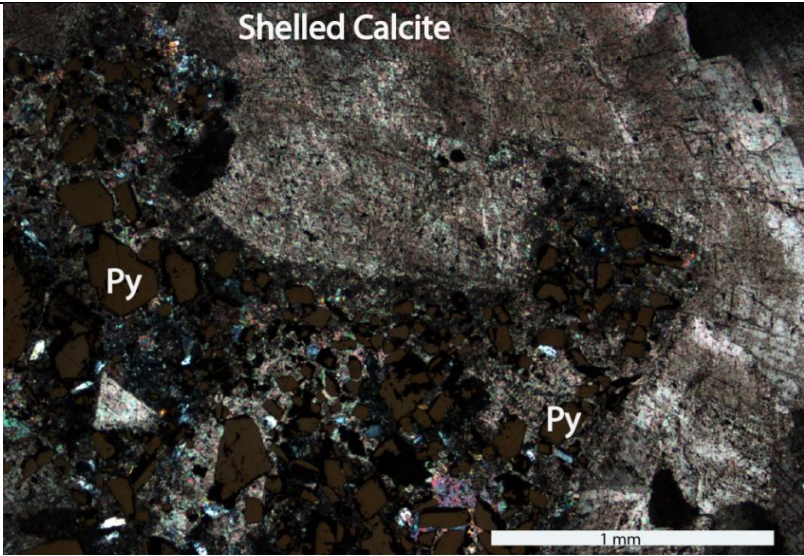
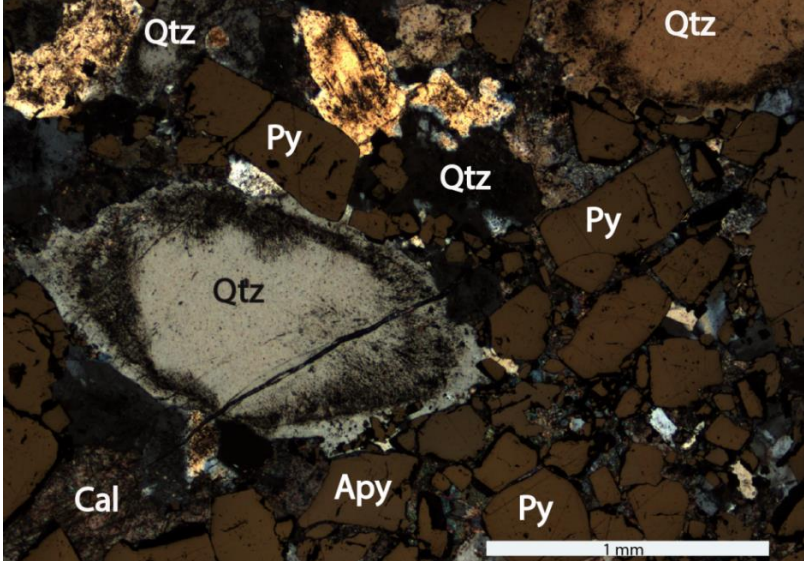
Selected Assays	
Au (ppm)	60.7
Ag (ppm)	39.2
As (ppm)	20000

### Overall Mineralogy:

MINERAL	MODE	SIZE (mm)	NOTES
Calcite	50-60%	.01-5	Coarse, largely anhedral grains make up most of the mantos; a rounded, shell-like texture with undulatory extinction is common
Pyrite	10-18%	.01-3.1	Anhedral to subhedral grains within the mantos; concurrent with apy
Arsenopyrite	5-12%	.01-3	Anhedral to subhedral grains within the mantos; often intermixed with pyrite
Quartz	5-10%	.01-3.4	Varies between fine, subhedral, jigsaw-textured quartz and coarser, anhedral quartz grains; the jigsaw texture is unique
Galena	≤1%	.01-.2	Anhedral galena is included within large py grains; galena is associated with electrum deposition
Sphalerite	≤1%	.01-.3	Anhedral grains; red IR; a later phase occurring between pyrite grains
Electrum	≤1%	.01-.1	Round electrum grains tend to form on the edges of pyrite or arsenopyrite grains
Chalcopyrite	≤1%	.001	Cpy formed only as very fine inclusions within sphalerite

**Alteration:** MANTO REPLACEMENT of the Caracol Formation; no host rock available for analysis in thin section.



	<p>Jigsaw-textured quartz cements pyrite grains within the mantos. (Transmitted and reflected light photomicrograph.)</p>
<p>Shelled Calcite</p> 	<p>Fine, 'shelled' calcite hosts finer pyrite grains. (Transmitted and reflected light photomicrograph.)</p>
	<p>Large quartz grains adjacent to brecciated pyrite are cemented by calcite. (Transmitted and reflected light photomicrograph.)</p>

**Sample #: 1CR08****Hole 345/533.4m**

**Rock Type:** Coarse sulfide-calcite manto ore hosted in the Caracol Formation.

**Sample Description:** Anhedral to large euhedral crystals of near-contemporaneous pyrite and arsenopyrite compose over half the sample. The matrix host is made of large subhedral to euhedral interlocked quartz grains. Calcite often surrounds euhedral quartz or other sulfides. In a few instances, the calcite cuts through the earlier quartz or sulfide grains.

Selected Assays	
Au (ppm)	40.6
Ag (ppm)	42.8
As (ppm)	20000

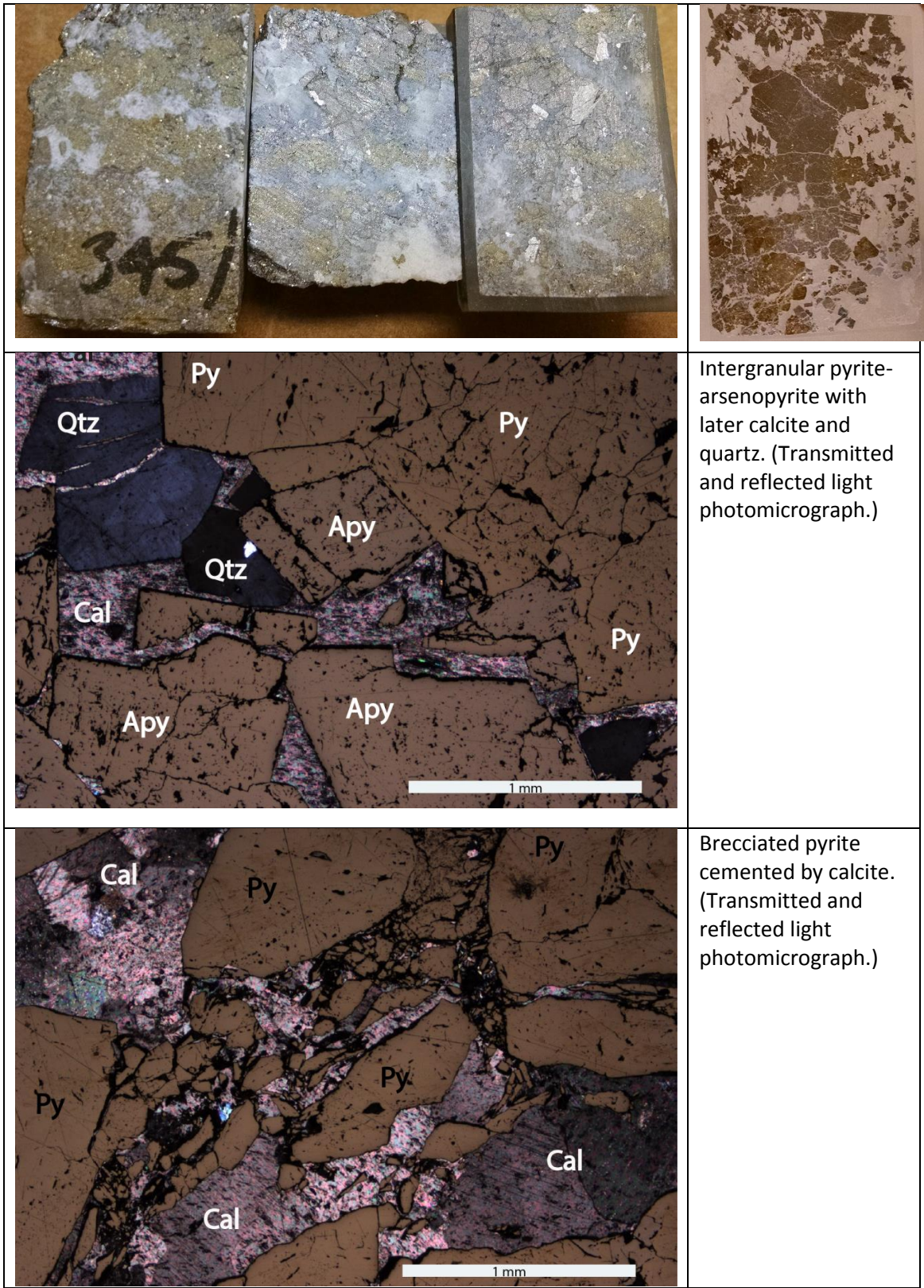
**Overall Mineralogy:**

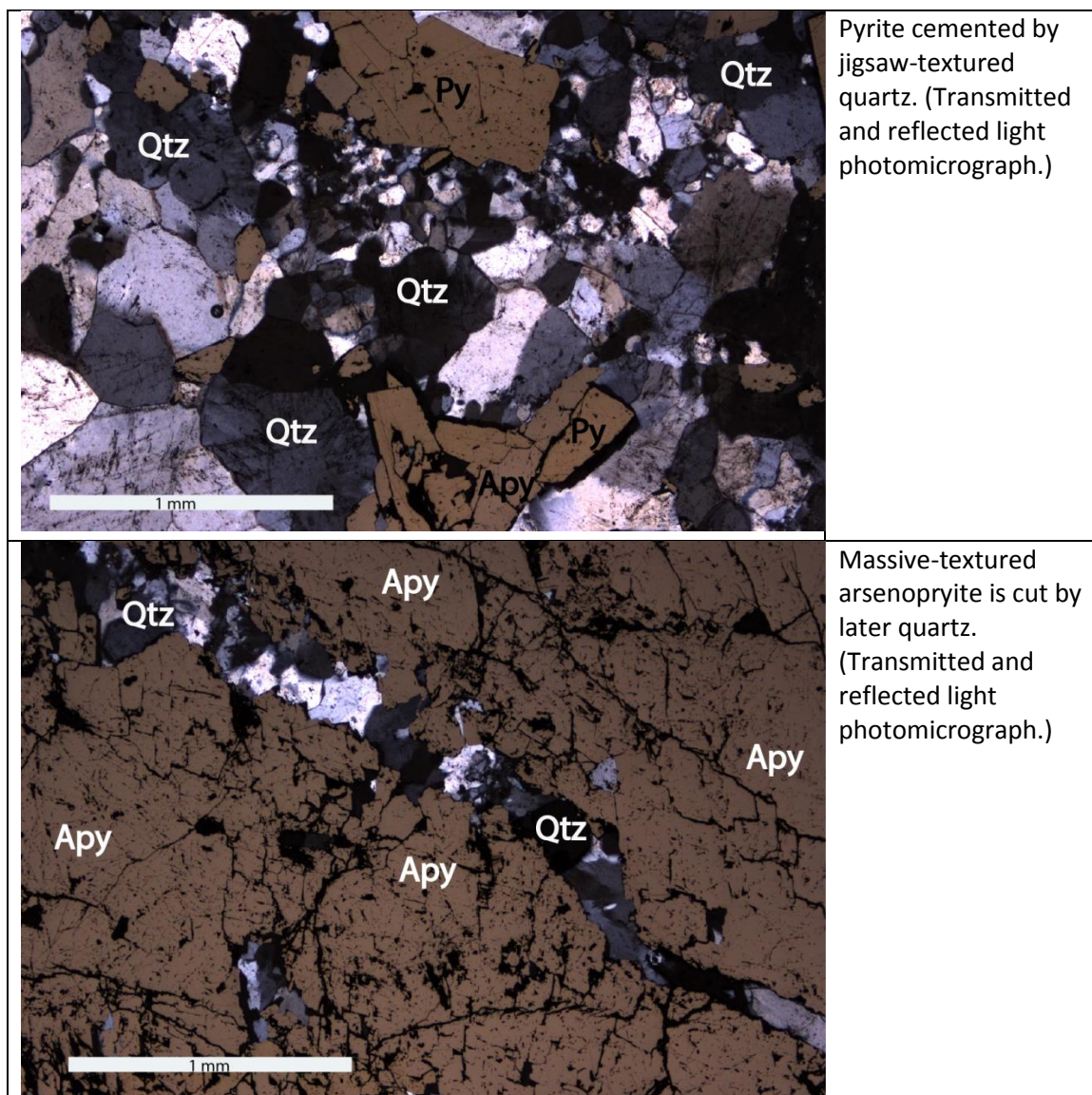
MINERAL	MODE	SIZE (mm)	NOTES
Pyrite	30-35%	.01-3	Subhedral; can form large grains; tends to have broken appearance with fine inclusions; formed concurrently or slightly before apy
Arsenopyrite	25-30%	.1-5	Anhedral to euhedral; intermixed with pyrite; apy grains can also have fine inclusions
Quartz	10-20%	.1-4	Anhedral-subhedral; fills in gaps left between sulfides; puzzle-piece texture between sulfides common; one section shows quartz intergrown with feldspar (?); can have anomalous blue extinction
Calcite	10-15%	.1-2	Coarse, interlocking grains surround quartz and cuts across the mantos in small veinlets; calcite veinlets more common in qtz-rich sections
Feldspar (?)	1-3%?	.5-3.5	Large, rounded (beat-up) grains, similar to quartz, and adjacent to coarse calcite and qtz; difficult to determine type of feldspar as grains are randomly oriented; biaxial figure evident (not flash figure)
Galena	≤1%	.1-3	Fine, late phase filled fractures through pyrite and arsenopyrite
Sphalerite	≤1%	.01-3	Anhedral, minor phase; often near the late cc veinlets

**Alteration:** MANTO REPLACEMENT of the Caracol Formation; no host rock available for analysis in thin section.

**Veins:** Fine, discontinuous and irregular calcite veins cut the manto sample.







**Sample #:** 3CR05

**Hole** 390/595.4m

**Rock Type:** Massive-textured sulfide vein/ mantos cuts through the Caracol Formation.

**Sample Description:** The sandy portion of the sample contains jigsaw-textured quartz. The cross-hatch pattern of the calcite-sericite ore stage alteration is clear, and sericite grains are strongly developed. The sulfide portion of the sample has high gold grades, with intergranular pyrite, arsenopyrite, and sphalerite cemented by quartz and calcite. Disseminated pyrite and arsenopyrite are common.

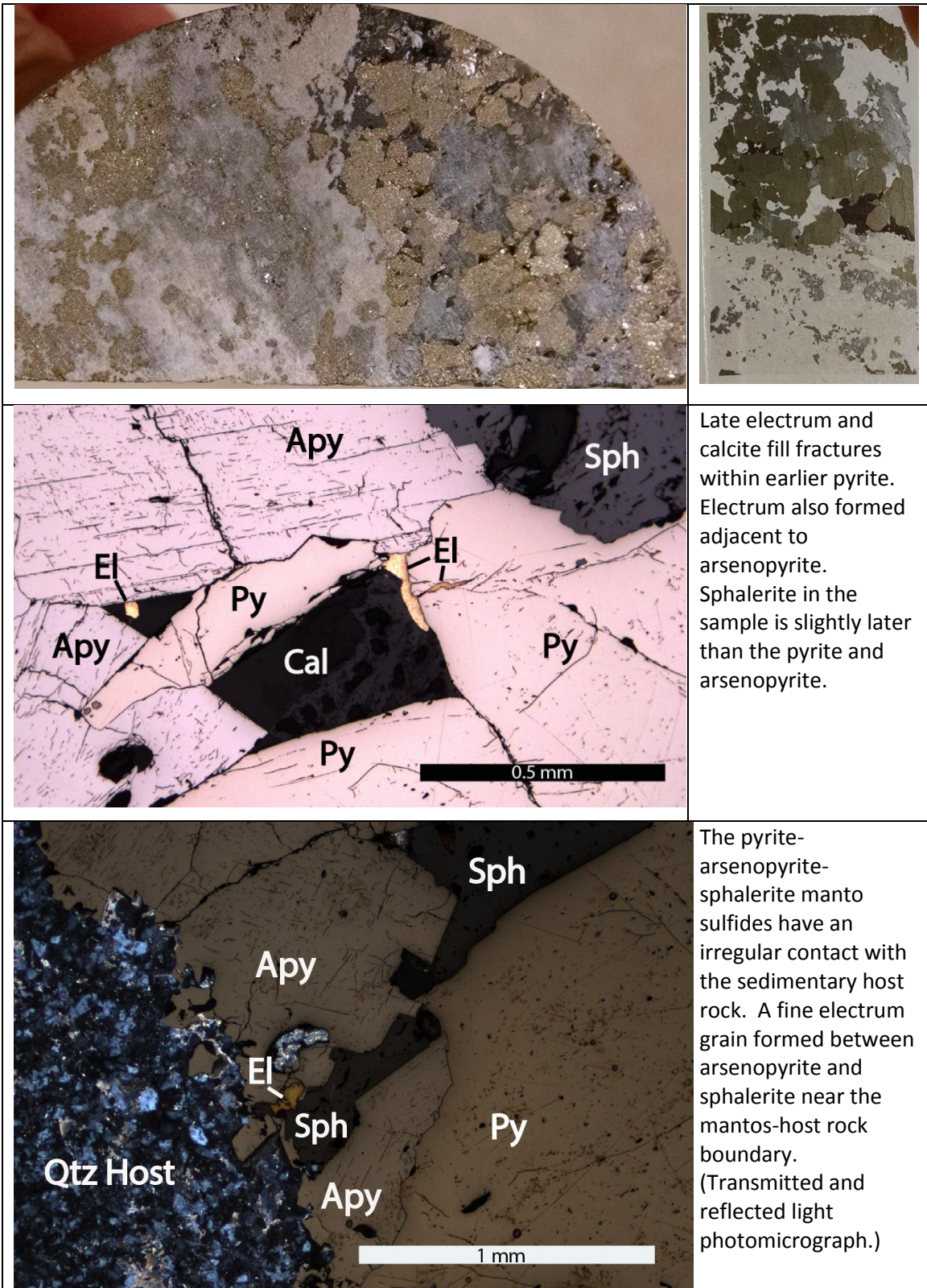
Selected Assays	
Au (ppm)	70.7
Ag (ppm)	67.7
As (ppm)	20000

**Overall Mineralogy:**

MINERAL	MODE	SIZE (mm)	NOTES
Quartz	20-30%	.01-1.8	Equigranular, jigsaw-textured quartz grains make up the host; larger quartz grains also fill spaces within the mantos
Pyrite	15-25%	.1-2.6	Subhedral pyrite is the most common sulfide in the mantos; finer, subhedral pyrite is disseminated within the host rock
Calcite	15-20%	.01-.1	Fine calcite overprints the host rock; calcite also fills spaces within the mantos section
Feldspar	5-10%	.1-6.5	Fine xtals found in small veinlets and throughout the matrix; large, coarse xtals are found within the massive sulfide (mantos) portion
Arsenopyrite	5-10%	.1-1.5	Subhedral crystals are intergrown with pyrite in the mantos; apy is also disseminated in host rock; apy may be slightly later than pyrite
Sphalerite	2-5%	.1-1.7	Anhedral grains within the mantos fill gaps between py and apy; Common near edge of mantos, forming an irregular boundary with the host rock; bright red internal reflections (IR)
Galena	1-2%	.1-.4	Minor late phase in mantos, filling fractures in earlier sulfides
Sericite	≤1%	.1	Alteration mineral associated with ore-stage sulfides; clear cross-hatch pattern in the host rock
Chalcopyrite	≤1%	.1	Cpy formed as fine inclusions in sphalerite; a few larger grains with altered rims formed between pyrite and arsenopyrite grains
Electrum	≤1%	.01-.1	Small, round el bleb found near the edges of and within pyrite and arsenopyrite grains; larger electrum grains formed close to the manto-host rock boundary

**Alteration:**

The sample was not strongly stained by sodium cobaltinitrite. The host rock appears to have been recrystallized, and fine, interlocked, jigsaw grains of quartz are common. The ore stage calcite –sericite alteration strongly overprints the host rock, and the elongate sericite crystals form a clear cross-hatch pattern. Disseminated pyrite and arsenopyrite are present.



Late electrum and calcite fill fractures within earlier pyrite. Electrum also formed adjacent to arsenopyrite. Sphalerite in the sample is slightly later than the pyrite and arsenopyrite.

The pyrite-arsenopyrite-sphalerite manto sulfides have an irregular contact with the sedimentary host rock. A fine electrum grain formed between arsenopyrite and sphalerite near the manto-host rock boundary. (Transmitted and reflected light photomicrograph.)

	<p>Calcite associated with ore-stage alteration overprints the host rock. The quartz in the host rock is equigranular and interlocked, and may have been recrystallized. (Transmitted and reflected light photomicrograph.)</p>
	<p>Equigranular, interlocked, jigsaw quartz within the host rock is associated with the ore-stage alteration, and may represent recrystallization. (Transmitted and reflected light photomicrograph.)</p>
	<p>The ore stage calcite – sericite alteration strongly overprints the host rock, and the elongate sericite grains form a clear cross-hatch pattern.</p>

## HIGH GRADE SILVER SAMPLE

**Sample #:** 1CR32

**Hole** 375/286.4m

**Rock Type:** A sphalerite-dominant vein cuts across weakly altered Caracol Formation.

**Sample Description:** A sphalerite vein cuts the Caracol Formation. A silver-mineral-bearing vein and a calcite-galena vein cut parallel to the earlier sphalerite vein. The silver-bearing minerals acanthite, pyrrargyrite, and tennantite are closely associated with galena. The siltstone host rock contains some sericite and carbonate alteration minerals.

Selected Assays	
Au (ppm)	0.552
Ag (ppm)	1580
As (ppm)	4350

### Overall Mineralogy:

MINERAL	MODE	SIZE (mm)	NOTES
Sphalerite	40-50%	.1-4	Part of a 2-5cm wide sph vein; Red-orange IR; Grains are anhedral, irregular boundaries; Some grains show zoning; pieces of sphalerite are present in calcite-dominant veins
Calcite	15-20%	.1-4.6	Common vein mineral; can have undulatory extinction; weakly overprints the host rock
Quartz	10-15%	.01-5	Euhedral grains formed within veins and are surrounded by calcite; angular quartz grains comprise the majority of the host rock; interlocking jigsaw texture in the host rock may be recrystallization
Pyrite	5-10%	.05-.1.4	Fine, subhedral pyrite is disseminated outward from the sulfide vein; Subhedral to euhedral pyrite crystals have formed throughout the silver-rich vein
Galena	5-8%	.01-1	Gal is part of a 1cm-wide calcite-galena vein as rounded to octagonal shaped xtals; abundant triangular plucks; strongly associated with the silver mineralogy (acanthite, tennantite, and pyrrargyrite)
Arsenopyrite	2%	.01-.09	Subhedral to anhedral; fine, creamy white grains within the silver- rich vein
Acanthite (light green-gray)	1-3%	.01-.1	Intimately associated with tennantite and acanthite; often intergrown with galena; Acanthite additionally formed acanthite veinlets which cut earlier sulfides; acanthite inclusions within sph are common in close proximity to the silver-rich vein; some darker to lighter anisotropy with twinning

Pyrrargyrite (Gray-Blue, with Red IR)	1-2%	.01-.06	Anhedral; blue-gray color; strong RED IR (internal reflections); strongly associated with galena and tennantite, and to a lesser degree acanthite
Tennantite (Green-Gray)	1-2%	.01-.05	Tennantite is a darker green-grey color than acanthite; strongly associated with galena, acanthite, and pyrrargyrite; isotropic
Marcasite	1-2%	.01	Fine, interlocked marcasite crystals developed at the edges of a few larger pyrite grains
Chalcopyrite	≤1%	.01-.1	Minor inclusions within sphalerite
Sericite	≤1%	.005-.01	Alteration phase, found in host rocks near quartz grains

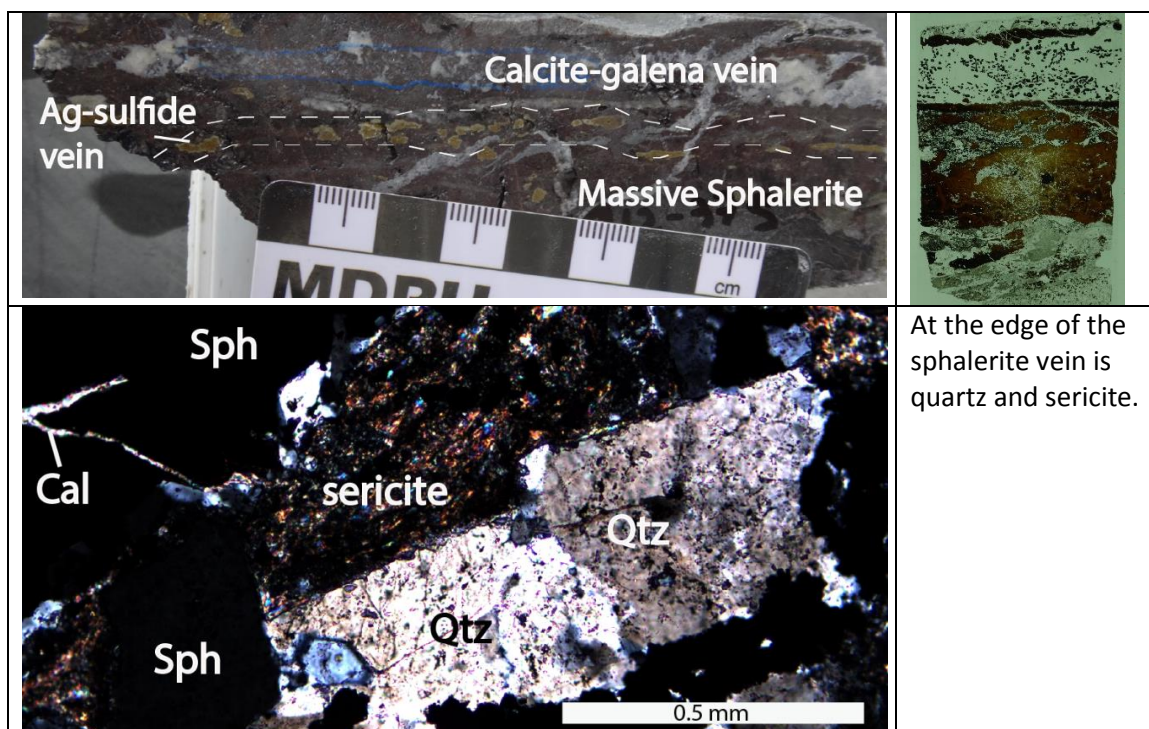
#### Alteration:

Ore stage alteration consists of calcite and sericite, with potential quartz recrystallization. The sericite in this silver rich sample is larger and more concentrated than in analyzed gold rich samples.

#### Veins:

A sphalerite vein is cut by a fine, irregular, calcite-pyrite-galena-acanthite-tennantite-pyrrargyrite-quartz-arsenopyrite vein. A separate calcite-galena vein also cuts the sph vein.

Very fine acanthite veinlets cut the sphalerite vein, but end at the calcite-galena vein.



	<p>A grain of intermixed galena-pyrargyrite-tennantite within the calcite-silver mineral vein which cuts sphalerite. (Transmitted and reflected light photomicrograph.)</p>
	<p>The calcite-pyrite-galena-silver mineral vein cuts sphalerite. The galena is associated with pyrargyrite (blue-gray color), acanthite (green-gray color) and tennantite (slightly darker color than acanthite.)</p>
	<p>A fine acanthite grain cuts through the sphalerite. Where the sphalerite looks 'dirty' there are fine acanthite inclusions. A calcite-galena-pyrargyrite vein also cuts the sphalerite.</p>



## 10 APPENDIX B: ZIRCON U-Pb AND FT DATA

### Zircon U/Pb data

Analysis Name	Preferred Age (Ma)	2 -sigma	2 +sigma	Age Type
RAD_0	74.82	3.71	3.71	206Pb/238U concordant scans
RAD_1	560.79	17.79	17.77	206Pb/238U concordant scans
RAD_2	334.27	20.39	27.44	Pbc-corrected isotopic sums
RAD_3	187.04	9.15	9.14	206Pb/238U concordant scans
RAD_4	75.76	3.69	3.68	206Pb/238U concordant scans
RAD_5	72.74	13.34	13.33	206Pb/238U concordant scans
RAD_6	90.26	8.06	8.05	206Pb/238U concordant scans
RAD_7	74.15	3.32	3.31	206Pb/238U concordant scans
RAD_8	73.84	2.94	2.94	206Pb/238U concordant scans
RAD_9	73.02	3.79	3.79	206Pb/238U concordant scans
RAD_10	79.71	2.68	2.68	206Pb/238U concordant scans
RAD_11	71.84	4.05	4.05	206Pb/238U concordant scans
RAD_12	1132.82	34.76	34.67	206Pb/238U concordant scans
RAD_13	1107.96	38.56	37.84	207Pb/235U concordant scans
RAD_14	72.93	3.23	3.23	206Pb/238U concordant scans
RAD_15	72.26	3.07	3.06	206Pb/238U concordant scans
RAD_16	72.51	3.84	3.84	206Pb/238U concordant scans
RAD_17	287.97	11.35	11.34	206Pb/238U concordant scans
RAD_18	75.50	4.36	4.36	206Pb/238U concordant scans
RAD_19	998.59	32.21	32.13	206Pb/238U concordant scans
RAD_20	69.38	3.62	3.62	206Pb/238U concordant scans
RAD_21	73.59	4.35	4.35	206Pb/238U concordant scans

## Zircon Fission Track data

Note: the 'Analysis Name' correlates to the same 'Analysis Name' used to identify the U/Pb data

Analysis Name	FT Age (Ma)	95%-CI (Ma)	95%+CI (Ma)	Area um <sup>2</sup>	U/Cation	+/- 1sig
RAD_0	11.74	6.40	14.08	3.7239E+02	0.0052	0.0009
RAD_1	37.77	14.70	24.02	5.3014E+02	0.0045	0.0008
RAD_2	55.89	23.10	39.26	3.9740E+02	0.0030	0.0005
RAD_3	56.99	22.63	37.41	5.3136E+02	0.0027	0.0005
RAD_4	56.40	22.85	38.31	4.2111E+02	0.0032	0.0006
RAD_5	81.98	32.99	54.98	5.3128E+02	0.0017	0.0003
RAD_6	56.69	20.22	31.35	5.3114E+02	0.0048	0.0008
RAD_7	23.00	9.92	17.44	5.3046E+02	0.0046	0.0008
RAD_8	61.38	22.15	34.57	3.5972E+02	0.0061	0.0010
RAD_9	78.71	26.79	40.49	5.2958E+02	0.0048	0.0008
RAD_10	74.76	29.90	49.65	5.3060E+02	0.0020	0.0003
RAD_11	114.68	38.97	58.76	5.3037E+02	0.0033	0.0006
RAD_12	145.05	59.16	99.15	5.3035E+02	0.0009	0.0002
RAD_13	116.87	45.32	73.60	5.3032E+02	0.0014	0.0002
RAD_14	76.21	26.29	40.01	5.3002E+02	0.0045	0.0008
RAD_15	67.32	23.24	35.40	5.3013E+02	0.0053	0.0009
RAD_16	72.00	24.59	37.23	5.3115E+02	0.0051	0.0009
RAD_17	82.12	29.84	46.70	5.3118E+02	0.0030	0.0005
RAD_18	60.68	24.84	41.93	3.4638E+02	0.0033	0.0006
RAD_19	52.03	19.77	31.80	5.3156E+02	0.0037	0.0006
RAD_20	89.22	33.25	52.78	4.0585E+02	0.0031	0.0005
RAD_21	98.72	39.37	65.15	4.3074E+02	0.0019	0.0003